**Showcasing research from Professor Ben B Xu's laboratory, Northumbria University, Newcastle upon Tyne, UK; Professor Jianchun Jiang's laboratory, Institute of Chemical Industry of Forest Products, Chinese Academy of Forestry, Nanjing, China; Professor Wanxi Peng's laboratory, Henan Agricultural University, Zhengzhou, China; Professor Shengbo Ge's laboratory, Nanjing Forestry University, Nanjing, China.**

A comprehensive review of covalent organic frameworks (COFs) and their derivatives in environmental pollution control

This review offers a holistic analysis and comparison of COFs and their derivatives, with a specific application field in pollution management in air, water, and soil. The challenges and prospects for large-scale preparation and application are highlighted.

## As featured in:

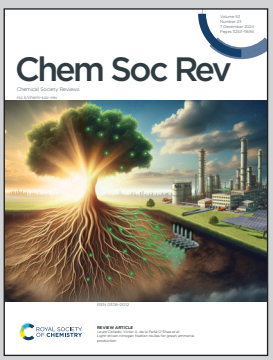


See Wanxi Peng, Runzhou Huang, Ben Bin Xu, Jianchun Jiang *et al.*, *Chem. Soc. Rev.*, 2024, **53**, 11259.

ROYAL SOCIETY OF CHEMISTRY

rsc.li/chem-soc-rev

Registered charity number: 207890

Chem Soc Rev

TUTORIAL REVIEW

View Article Online
View Journal | View Issue



Cite this: *Chem. Soc. Rev.*, 2024, 53, 11259

# A comprehensive review of covalent organic frameworks (COFs) and their derivatives in environmental pollution control†

Shengbo Ge,‡[a] Kexin Wei,‡[a] Wanxi Peng,*[b] Runzhou Huang,*[a] Esther Akinlabi,[c] Hongyan Xia,[d] Muhammad Wakil Shahzad,[c] Xuehua Zhang,[e] Ben Bin Xu *[c] and Jianchun Jiang*[f]

Covalent organic frameworks (COFs) have gained considerable attention due to their design possibilities as the molecular organic building blocks that can stack in an atomically precise spatial arrangement. Since the inception of COFs in 2005, there has been a continuous expansion in the product range of COFs and their derivatives. This expansion has led to the evolution of three-dimensional structures and various synthetic routes, propelling the field towards large-scale preparation of COFs and their derivatives. This review will offer a holistic analysis and comparison of the spatial structure and synthesis techniques of COFs and their derivatives. The conventional methods of COF synthesis (*i.e.*, ultrasonic chemical, microwave, and solvothermal) are discussed alongside the synthesis strategies of new COFs and their derivatives. Furthermore, the applications of COFs and their derived materials are demonstrated in air, water, and soil pollution management such as gas capture, catalytic conversion, adsorption, and pollutant removal. Finally, this review highlights the current challenges and prospects for large-scale preparation and application of new COFs and the derived materials. In line with the United Nations Sustainable Development Goals (SDGs) and the needs of digital-enabled technologies (AI and machine learning), this review will encompass the future technical trends for COFs in environmental pollution control.

Received 31st May 2024

DOI: 10.1039/d4cs00521j

rsc.li/chem-soc-rev



**Key learning points**

(1) This review summarizes the research status of COFs and their derived materials in the field of environmental pollution control, which has never been summarized in detail. The application of COFs and derived materials in environmental pollution control was elaborated from three aspects of pollution.
(2) It emphasizes the significance of AI and machine learning for COF research in the context of the rapid development of digitalization and IT.
(3) Not only does it emphasize the strong research potential of COFs in the field of sustainable environment, but it also points out the future development direction of COFs, combining the UN SDG strategy and global policy development.

[a] *Co-Innovation Center of Efficient Processing and Utilization of Forest Resources, College of Materials Science and Engineering, Nanjing Forestry University, Nanjing 210037, China. E-mail: runzhouhuang@njfu.edu.cn*
[b] *School of Forestry, Henan Agricultural University, Zhengzhou 450002, China. E-mail: pengwanxi@163.com*
[c] *Department of Mechanical and Construction Engineering, Northumbria University, Newcastle upon Tyne, NE1 8ST, UK. E-mail: ben.xu@northumbria.ac.uk*
[d] *Department of Applied Sciences, Northumbria University, Newcastle upon Tyne, NE1 8ST, UK*
[e] *Department of Chemical and Materials Engineering, University of Alberta, Edmonton, Alberta, T6G 1H9, Canada*
[f] *Key Lab of Biomass Energy and Material of Jiangsu Province, Jiangsu Co-Innovation Center of Efficient Processing and Utilization of Forest Resources, Institute of Chemical Industry of Forest Products, Chinese Academy of Forestry, Nanjing 210042, China. E-mail: jiangjc@icifp.cn*

† Electronic supplementary information (ESI) available. See DOI: 10.1039/d4cs00521j

‡ These authors contributed equally to this work and act as co-first authors.

## 1. Introduction

Covalent organic frameworks (COFs), a class of crystalline porous polymers consisting of highly ordered organic units,[1] have attracted significant interest owing to their precise spatial assembly at the atomic level.[2] The versatile structural design of this material makes it highly sought after for application as conductive components,[3,4] and in photocatalysis,[5] energy storage,[6,7] the biomedical field,[8] and others. The current focus on flexible electronic devices,[9,10] gas storage,[11] adsorption,[12] and membrane materials[13] has promoted designability and functionality. COFs have been applied in environmental governance because of their porous nature, low skeleton density,[14] open pore structures,[15] and structural trimmability.[16] As new materials for preventing and controlling environmental

pollution, the future development of COFs and their derivatives has important strategic significance for addressing global environmental pollution and environmental change[17–20] and protecting human health.[21–24]

Normally, the pollutants in the environment can be divided into the atmospheric,[25] water system,[26] and soil or earth system pollutants.[27] Fig. 1 compares the performance of COFs and existing materials in environmental pollution control from four dimensions: sustainability of raw materials, environmental impact of the synthesis processes, recyclability of materials, and biodegradability. It can be seen that COFs have excellent performance and great development prospects in the field of environmental pollution control. Atmospheric pollutants mainly include gaseous and small particle pollutants.[28,29] Nanomaterials and proton exchange membranes (PEMs) have gained significant popularity in the gas capture because of their effectiveness and efficiency.[30–32] It was also reported that two-dimensional transition metal oxides could be employed for catalytic elimination of atmospheric pollutants.[33,34] For elimination of atmospheric pollutants, COFs exhibit several advantages such as low density,[35] strong chemical stability,[36] and high specific surface area.[37] Additionally, the combination of COFs with fluorescent probes allows for precise pollutant detection.[38,39]

There are many factors that affect the water environment, among which antibiotics, perfluorinated compounds (PFASs) and microplastics are the most widely studied.[40,41] UVA-LED $TiO_2$ photocatalysis of antibiotics,[42] MOF adsorption of PFASs,[43] and nanomaterial adsorption of trace pollutants in water,[44] are the important methods reported for removing pollutants, and the latest research shows that nanocomposite membranes can be used to remove heavy metals from water completely.[45–47] By functionalizing COFs with a carboxyl group or glutathione, the adsorption efficiency and detection accuracy of water pollutants can be maintained at a high level.[48,49] Photocatalytic properties can be achieved in COFs by structural design, achieving sustainable and energy-saving materials for decomposing harmful substances in water.

**Shengbo Ge**

*Shengbo Ge is an associate professor at College of Materials Science and Engineering, Nanjing Forestry University. He received his PhD in forestry engineering from Central South University of Forestry and Technology (2020). His research focuses on micro-nano structure regulation and recombination of wood cells, advanced biomass composite materials, and green and sustainable energy. He has published more than 100 SCI papers.*

**Wanxi Peng**

*Wanxi Peng is a professor at College of Forestry, Henan Agricultural University. He received his PhD in agricultural mechanization engineering from South China Agricultural University (2006). His research focuses on forest biomass resource utilization, forestry engineering, and wood-based panel engineering. He has published more than 200 SCI papers.*

**Runzhou Huang**

*Runzhou Huang is a professor in College of Materials Science and Engineering at the Nanjing Forestry University. He obtained his PhD in bio-based composites from Nanjing Forestry University in 2012. The research in his group focuses on the nano-cellulose and its applications, lost circulation control materials development and natural fiber reinforced polymer composites.*

**Xuehua Zhang**

*Professor Xuehua Zhang completed her PhD in Biomedical Engineering from Shanghai Jiao Tong University. She first worked as an Endeavour Research Fellow in the Department of Applied Math, Australian National University in Canberra (capital of Australia). She was then awarded with an Australian Research Council (ARC) Postdoctoral Fellowship in her early career, and later with the highly prestigious ARC Future Fellowship. From 2017 to present, she was a Professor and Canada Research Chair (Tier 1) at the Department of Chemical and Materials Engineering, University of Alberta.*

 

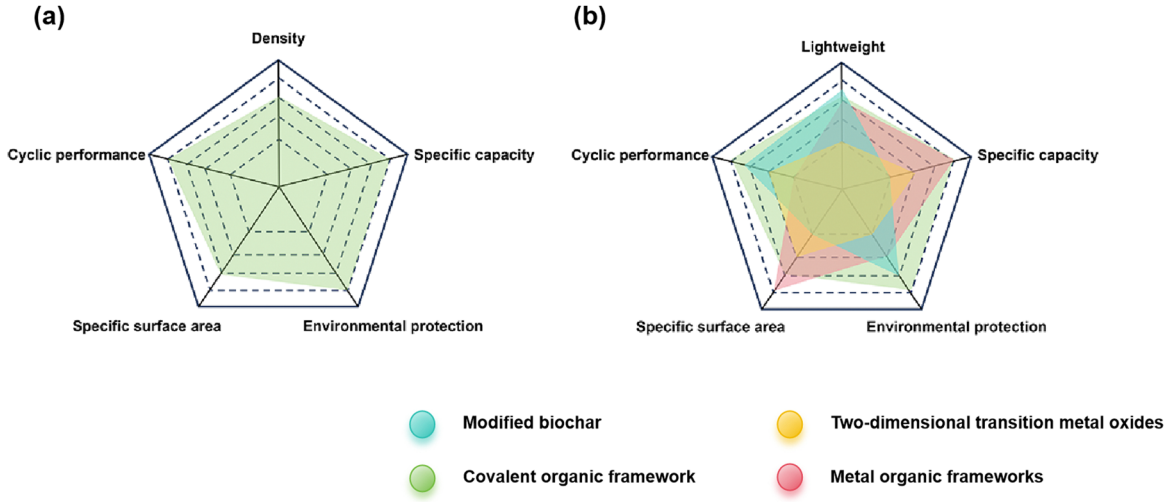


Fig. 1 (a) COF performance diagram. (b) Performance comparison between COFs and current materials in environmental pollution control.

Heavy metals and metalloids are the primary contaminants in soil/earth systems.[50] Researchers usually employed modified biochar or carbon with strong pollutant adsorption capabilities.[51–53] Thermal desorption is another method to remediate adulterated soil,[54] with exhaust gas often recirculated within the treatment system.[55,56] Non-thermal plasma technology has been employed to remediate soil contaminated by non-aqueous phase liquids.[57–59] COFs generally exhibit excellent recyclability and can be regenerated with minimal performance loss. COFs are usually constructed from biocompatible and non-toxic building blocks, reducing the risk of secondary contamination and making COFs safe for use in soil environments, ensuring that remediation efforts do not introduce additional pollutants, thereby maintaining soil quality for agricultural and ecological purposes.

COFs in environmental governance have spurred an increasing number of reviews in this domain (Fig. 2). This review differs from existing literature in that it comprehensively explores the COF design principles and synthetic pathways, and by studying in detail the intrinsic spatial structure and bonding type of COFs, it provides researchers with the key fundamental understanding necessary to advance COF materials from scratch. This review highlights the transformative potential of artificial intelligence (AI) and machine learning

**Ben Bin Xu**

*Ben Bin Xu (FRSC, FIMMM, FRSA, FSCI) is a Professor (Chair) of Materials and Energy at Northumbria University, UK. Ben's research interests cover materials, surface, sustainability, energy, biomedical engineering and micro-engineering. He has published 260+ journal articles (h = 59), 10 books/chapters, 7 patents, given 100+ invited talks and won multiple awards (Stanford/Elsevier World Top 2% Scientist (2024), AIChE Excellence in Research-Mid-Career Investigator Award in the 'composites' area (2023), 2016 Young investigator award from the International Polymer Networks Group, etc.). Ben chairs the Materials Characterization & Properties Group in the IoM3 and the Composites area in the AICHE (US).*

**Jianchun Jiang**

*Prof. Jianchun Jiang is an expert of forestry engineering, and honored as an academician of the Chinese Academy of Engineering. He served as chairman of the Bio-based Materials and Industry Technology Innovation Strategic Alliance, and vice chairman of the Forest Chemistry branch of the Chinese Society of Forestry and Biomass Energy and Industry Technology Innovation Strategic Alliance. Prof. Jiang's research interests focus on fundamental research and industrialization through thermochemical conversion of biomass. Prof. Jiang's research achievements have been widely introduced and applied in both China and foreign countries, including Japan, Italy, etc. He has won the award of National Scientific and Technological Progress of China four times, respectively in 2006, 2009, 2013, 2016.*

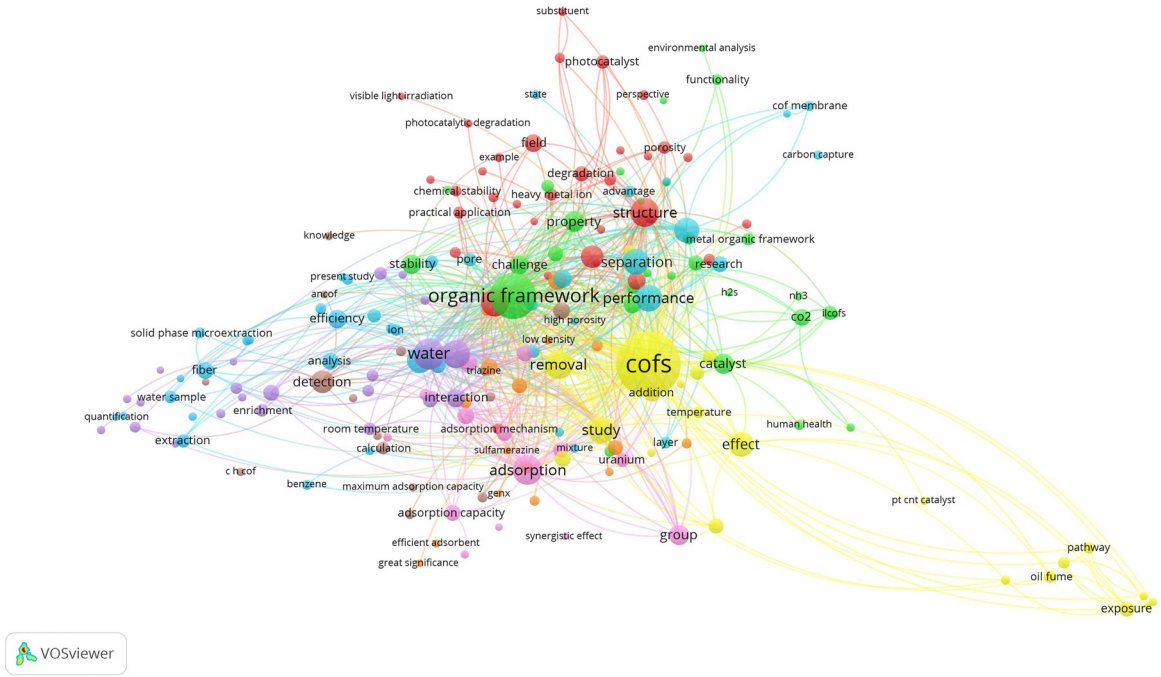


Fig. 2 Keywords of research papers related to environmental pollution/COFs in the past five years.

(ML) in COF research. In the context of the rapid development of the internet and digital technologies, AI and ML are positioned as indispensable tools for accelerating discovery, optimizing synthetic processes, and predicting the performance of COFs under various environmental conditions. This integration of AI and ML enhances the efficiency and precision of COF research and opens up new avenues for innovation in materials science. Moreover, this review conducts a rigorous life cycle assessment (LCA) of COFs, offering insights into their environmental impact from synthesis to application. This LCA evaluation is pivotal for understanding the sustainability of COFs and guiding researchers and policymakers towards more environmentally friendly practices. The analysis aligns the future development of COFs with the sustainable development policies of different countries and organizations, underscoring the global imperative for sustainable innovation.

In synthesizing these perspectives, this review serves as a crucial resource for researchers aiming to harness the full potential of COFs in environmental governance. It highlights the importance of interdisciplinary approaches, combining advanced materials science with cutting-edge AI technologies to address the pressing environmental challenges of our time.

## 2. Synthesis of COFs and derivatives

### 2.1. The history and evolution of COFs

Fig. 3 tabulates the synthetic strategies previously utilized to obtain COFs. In 2005, Yaghi *et al.* first proposed the design strategy and implementation for synthesising microporous and mesoporous crystal COFs.[60] In 2007, Yaghi's team synthesized a three-dimensional covalent organic framework (3D COF) by targeting two networks based on tetrahedral and triangular nodes: bor and ctn. The findings mark important progress in the laboratory synthesis of COFs.[61] In the early 2010s, researchers began to expand structural diversity in COFs and explore the potential of COFs to be applied in gas adsorption, catalysis, separation, and other fields.

Zou *et al.* developed a two-step doping method to enhance the hydrogen storage capacity of COFs for application in fuel cell vehicles.[63] Ritchie *et al.* utilized microwave heating and a conventional solvothermal approach to synthesize COFs,[70] with a high specific surface area for storage purposes. Nagai *et al.* synthesized COFs using additional azide building blocks[64] to allow more possible shapes and structures. The designable azide units were fixed to the COF walls, offering many active sites for the reaction.

The aqueous phase synthesis method optimizes the reaction path, improves the synthesis efficiency, and solves the environmental pollution problem caused by organic solvents. In 2012, a breakthrough in synthesizing COFs in the aqueous phase was realized in the biomedical field.[65] In 2017, COFs were applied to electronic devices, such as supercapacitors, thus expanding the application fields of COFs. In a recent study, Sick *et al.* used COFs to form polyimide sheets through covalent bonds as a new type of photoelectrode.[66] Chandra *et al.* synthesized two redox-active COFs [TpBD-$(OH)_2$ and TpPa-$(OH)_2$] with a high surface area and extended π-conjugated structures. These COFs exhibit excellent specific capacitance and retain 88% of their capacitance after 10 000 cycles, making them highly desirable in supercapacitors.[67]

### 2.2. Chemical structure and configuration of COFs

The spatial structure and bonding type of COFs depend on the specific building blocks and reaction conditions.[74–76] Fig. 4 details the topology of different 2D and 3D COF combinations.

 

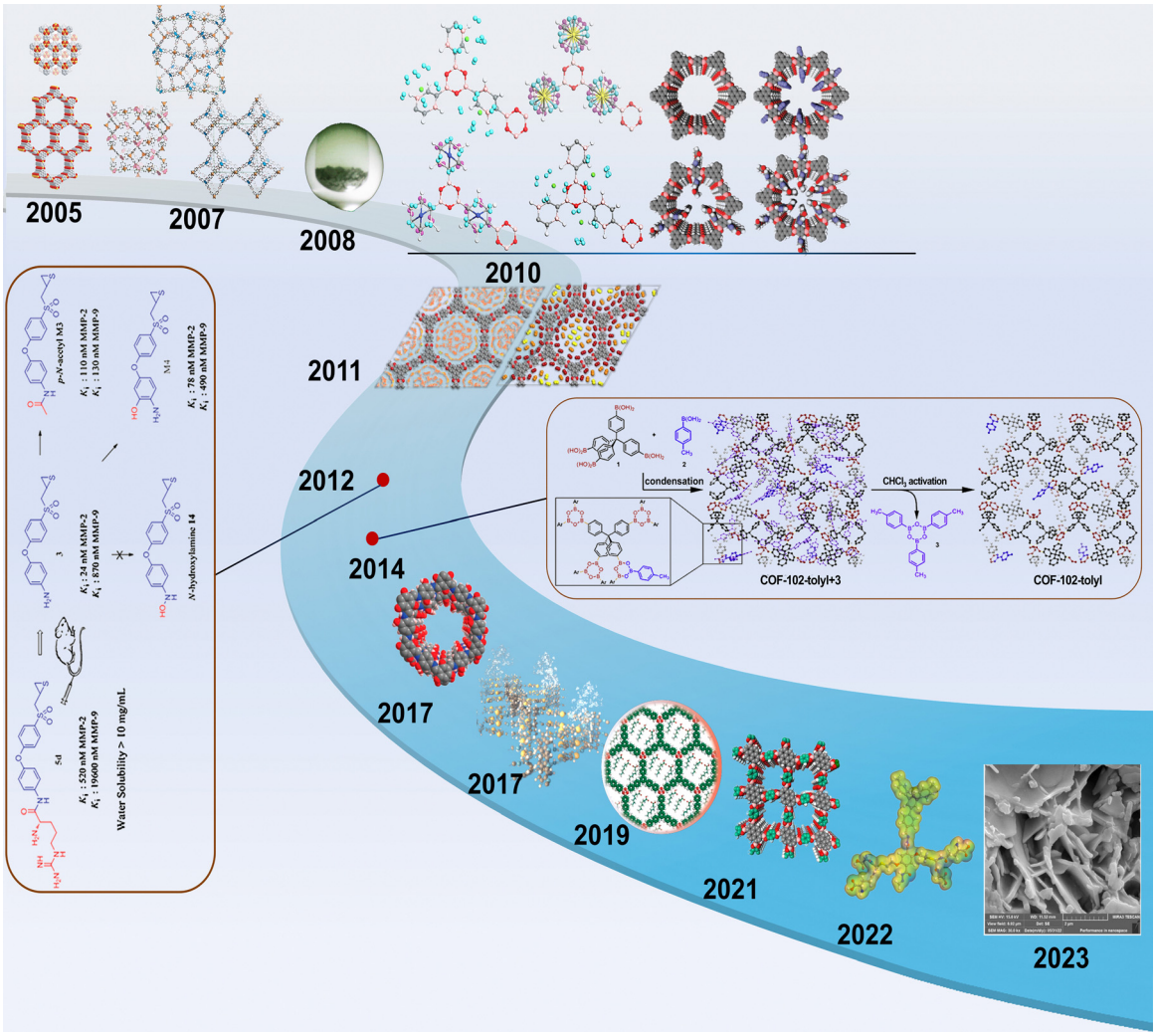


Fig. 3 The evolution of COF synthesis. Reproduced from ref. 60 and 61 with permission from AAAS, Copyright 2005 and Copyright 2007. Reproduced from ref. 62–69 with permission from the American Chemical Society, Copyright 2009, Copyright 2010, Copyright 2011, Copyright 2011, Copyright 2017, Copyright 2017, Copyright 2019 and Copyright 2021. Reproduced from ref. 70–73 with permission from Elsevier, Copyright 2010, Copyright 2013, and Copyright 2022 and 2023.

**2.2.1. Spatial structure of COFs.** The unique porous structure of COFs is determined by their topology. COFs can be categorized into two types based on the size of their building units: two-dimensional (2D) and three-dimensional (3D) where both feature periodic and ordered arrangements.[79] The building units in 2D COFs are planar and connected by covalent bonds to form a lattice-like structure. Meanwhile, certain porous properties can also exist perpendicular to the plane. On the other hand, 3D COFs have a spatial structure and building units are formed through 3D connections.[80,81]

2D COFs can be designed using various topological structures by choosing various building units and adjusting their connection. The common types of 2D COF spatial structures include hexagonal, tetragonal, rhombus, star-pore, trigonal, and kagome.[82]

Hexagonal COFs are the simplest structure, consisting of six structural units connected by covalent bonds, and mainly adopts the $[C_3 + C_2]$ topological structure.[78] Tetragonal COFs usually comprise four covalently linked building blocks arranged in a square on a plane.[83] Rhombohedral COFs are usually prepared with a $[C_2 + C_2]$ topology.[84] Star-pore COFs are crystalline porous materials with a 2D topology created by π-conjugated building units connected by covalent bonds. Feng *et al.* created a star-pore COF based on the $C_3$ symmetric molecule of a phenanthrene ring trimer as the building block. Yang *et al.* constructed an ordered mesoporous two-dimensional COF using a unique overlapping stacking pattern.[85] The maximum utilization of COF pores improved the gas storage and separation capabilities of COFs.

Triangular COFs can be prepared *via* $C_3$-symmetric or $C_6$-symmetric connections.[86] Kagome lattice structures are often designed using $[C_3 + C_2]$ or $[C_2 + C_2]$ diagrams.[87] With the realization of $C_2$-symmetric connectors and $C_2$-symmetric TPE

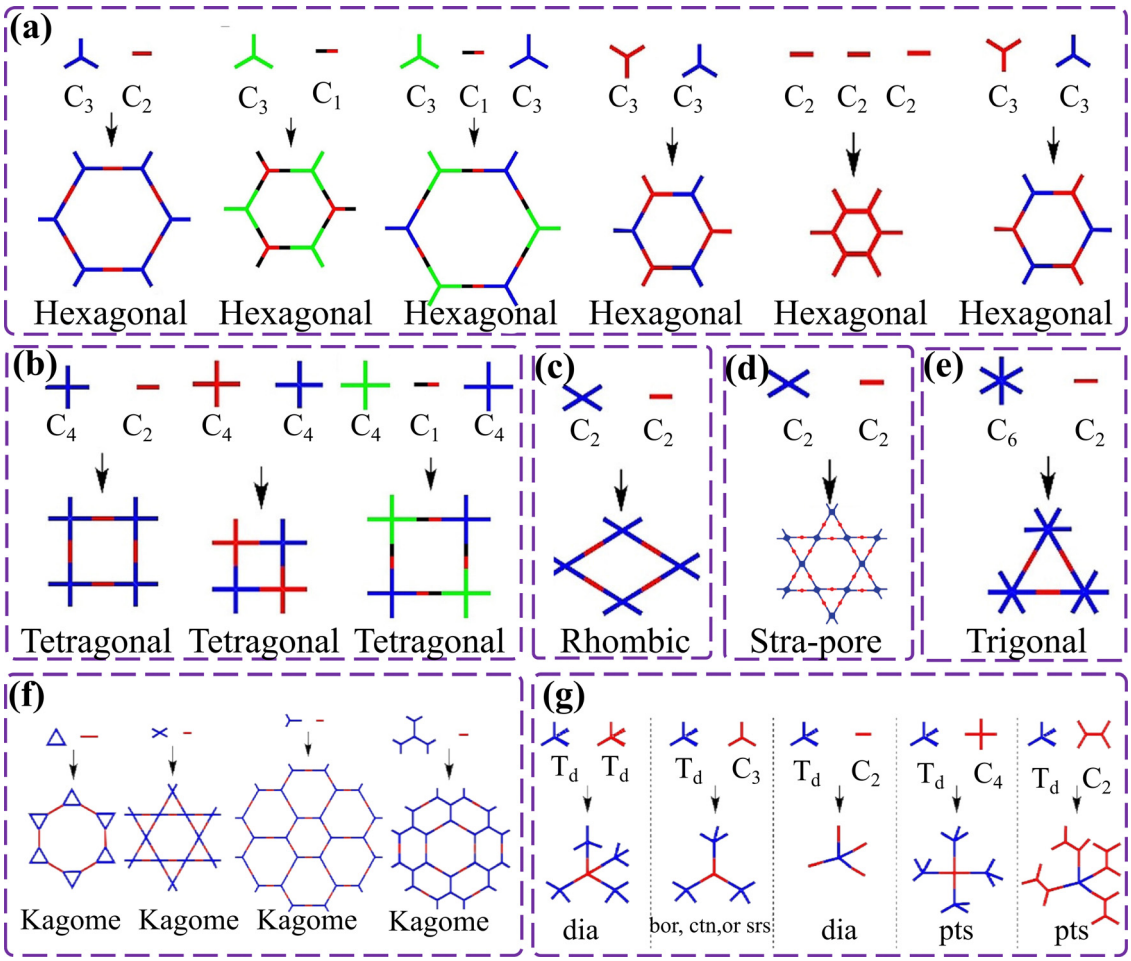


Fig. 4 Topological structure diagram of various COFs. (a) Hexagonal COFs, (b) tetragonal COFs, (c) rhombic COFs, and (d) star-pore COFs. (e) Trigonal COFs, (f) Kagome COFs, and (g) 3D COFs. Reproduced from ref. 77 (Fig. 4a–c and e–g) and ref. 78 (Fig. 4d) with permission from Wiley, Copyright 2019 and Copyright 2018.

junctions, kagome structures are often found in imine-linked COFs and boronate-linked COFs.[88]

3D COFs mainly include topological structures such as [$T_d$ + $T_d$], [$T_d$ + $C_2$], [$T_d$ + $C_3$], [$T_d$ + $C_4$] and [$C_2$ + $C_3$].[77] Lin *et al.* applied square (2D-$C_4$) and tetrahedral (3D-$T_d$) to connect to 3D porphyrin-based COFs through a [4 + 4] imine condensation reaction.[89] Xiao *et al.* constructed a 3D COF with a 2D hexachlorobenzene network using [3 + 2] imine condensation.[90] Zhu Jun *et al.* synthesized 3D-CageCOF-1 with a [6 + 2] method, showing high $CO_2$ absorption.[91] Li *et al.* created JUC-568 with a [6 + 3] method, showing porosity and $CO_2/CH_4$ adsorption rates of 98/48 $cm^3\ g^{-1}$.[92] Li *et al.* used the [6 + 4] configuration method to form a stp topology and constructed JUC-564 based on 6-linked triphenylethylene monomers.[93] Li *et al.* used the [6 + 4] configuration method to form a hea topology to synthesize 3D-hea-COF, which showed permanent porosity and an ultra-high specific surface area, and exhibited good adsorption performance for $H_2$, $CO_2$ and $CH_4$.[94] Xu *et al.* developed 3D she-net COFs with [6 + 4] methods for effective $CO_2$ reduction.[95] Liu *et al.* synthesized JUC-621 with a qtz topology for dye and iodine adsorption.[96] Jin *et al.* used a bottom-up [8 + 2] construction method to design NKCOF-21 with a bcu topology, which can efficiently and selectively remove ethane from ethylene/ethane mixtures, with an ethylene purification rate of up to 99.9%.[97] Liu *et al.* formed a scu topology with [8 + 4], synthesizing 3D COFs for application as effective small molecule storage and battery materials.[98]

**2.2.2. Chemical bonding in COFs.** Common bonding types in COFs include boroxine and borate esters, imine bonds, hydrazone and azine bonds, and C=C bonds.[99] Boroxine and borate esters are valued in coordination chemistry, organic synthesis, and materials science due to their unique boron–oxygen bonds. In 2007, Yaghi *et al.* synthesised the first COF material through the self-condensation of boric acid, which led to the formation of a boroxine ring.[61] Brucks *et al.* introduced monofunctional arylboronic acids into 3D COFs,[71] which improved the order and porosity of COFs. Hamzehpoor *et al.* proposed a new synthesis method for boron-containing COFs by adding molecular oxygen, addressing the solubility issue of boric acid precursors in water.[69]

Imine bonds formed between ketone or aldehyde and amine groups exhibit higher stability than boron-oxygen bonds. The

 

first COF material using imine bonds features five independent diamond skeletons, offering excellent thermal stability and porosity, withstanding temperatures up to 490 °C.[100] On this basis, Fang *et al.* applied amine linkers to synthesise two 3D microporous alkali functionalized COFs,[101] with pore widths of 8.1–8.3 Å as novel adsorbents. Imine bonds have become a popular linking motif due to their moisture resistance.[102–104] The construction of a conjugated π–π system around the COF sheet makes imine bonds particularly attractive in COFs.[105] Currently, imine bonds are the main bonding strategy adopted in COFs.[106]

Hydrazone bonds can be initiated between aldehydes or ketones and amino groups or their derivatives by connecting nitrogen and carbon atoms.[107,108] Dalapati *et al.* obtained rhombohedral COFs using a solvothermal method,[109] which have AA stacking arrangements and very small pore sizes of only 2 nm, which can be used to accurately detect the picric acid content and effectively reduce the risk of explosion.[110,111]

Recently, azine bonds have gained wide recognition in synthesising new porous organic materials known as covalent triazine framework materials (CTFs). Liu *et al.* synthesized highly crystalline CTFs using aldehyde monomers with bespoken thermal stability and improved photocatalytic performance.[112] Another development is the hybrid ketoenamine and hydrazone structure promoted by Mitra *et al.*, which has good thermal stability.[113]

Studies show that C=C bonds have stronger binding capacities than single bonds. The use of $sp^2$ hybridized carbon-based conjugated bonds in COFs produces highly desirable nanostructured materials. Jin *et al.* developed a novel 2D crystalline COF composed entirely of $sp^2$ carbons, with C=C bonds extending along the *x* and *y* directions, exhibiting excellent electrical conductivity.[114] Shi *et al.* synthesized 2D COFs with $sp^2$ carbon-conjugated porphyrin (Por-$sp^2$c-COF) using a photochemical method, achieving excellent chemical stability.[115] The application of C=C bonds has extended to 3D COFs,[116,117] with Yang *et al.* synthesizing two 3D crystalline COFs with an epitaxially stacked layered structure, achieving enhanced crystallinity and anisotropy.[118]

### 2.3. The synthesis methods of COFs and their derivatives

**2.3.1. COF synthesis methods.** The synthesis of COFs is highly dependent on various application scenarios. Although solvothermal methods are widely used, with the continuous deepening of research, water-mediated synthesis, ionic liquid-mediated synthesis, and low-melting-point solvent-mediated synthesis have attracted widespread attention from researchers due to their unique advantages.[119,120] This section provides an overview of the synthetic methods of COFs and their derivatives.

*2.3.1.1. Solvothermal methods.* Solvothermal reactions use high-temperature organic solvents to promote the formation of COFs.[121] It is crucial to select suitable organic precursors, which usually contain reactive groups and are soluble in solvents such as *N*-methylpyrrolidone and *N*,*N*-dimethylformamide. The precursors undergo condensation reactions in the solvent, resulting in the polymerization of the monomers and the formation of COF structures. After cooling, the COF crystals are extracted by separation and washing.[122,123] Experiments have shown that COF crystals grow better at high temperatures and in organic solvents. The solvent type, pressure, reaction temperature, and catalyst significantly affect COF crystal growth.

Xiong *et al.* used tris(4-aminophenyl)amine as the main building block to synthesize two electrochromic materials,[124] by conducting a Schiff base condensation reaction. The COFs were connected by imine bonds (Fig. 5a and c). By reducing different structural units, the electrochromic materials had richer colours and exhibited more novel performance. Su *et al.* created a multilayer COF with bifunctional groups (D-COF) using melamine and terephthalaldehyde, with imine groups inhibiting dissolution and amide groups providing active sites, making it a strong anode material (Fig. 5b).[125]

Solvothermal methods usually involve the polymerization of monomers and the crystallization of the skeleton simultaneously, making it arduous to achieve high crystallinity and balance the process of COFs. Han *et al.* developed a two-step solvothermal strategy by separating polycondensation and crystallization to improve the crystallinity with dimethylacetamide as a solvent.[127] Despite being traditional, solvothermal methods are costly and energy-intensive, which prompts the search for greener synthesis methods.

*2.3.1.2. Microwave-assisted synthesis.* The microwave-assisted reaction is a new method in organic molecule synthesis,[128,129] to increase the reaction rate, improve product purity, and bring more designability to the crystal structure.[130] Microwave-assisted synthesis has become an effective method for synthesising COFs, and this green chemistry approach can greatly reduce reaction time and energy consumption. Neil *et al.* first proposed a method for synthesizing COFs assisted by a microwave reactor.[62]

In the last few years, microwave-assisted synthesis methods have been widely applied in synthesising other types of COFs. Zhang *et al.* reported a strategy for preparing a CTF/$Fe_2O_3$ composite material using $ZnCl_2$ as a catalyst and reaction medium in a microwave reactor (Fig. 5d).[126] This magnetic porous covalent triazine-based framework composite material can absorb dyes in water and is expected to become a new material for water environment management. Ji *et al.* mixed two COF monomers with mesitylene, namely 1,4-dioxane and triethylamine,[131] and microwave-heated for 30 min at 70 °C. This process created a dark brown precipitate which was subsequently cooled and washed to obtain TH-COF. This novel material can extract and detect the PFAS content in water, making it a promising environmental treatment material.

*2.3.1.3. Mechanochemical synthesis method.* Mechanochemical synthesis uses mechanical force to stimulate chemical reactions. Unlike the solvothermal methods, mechanochemical synthesis does not rely on high-temperature organic solvents,

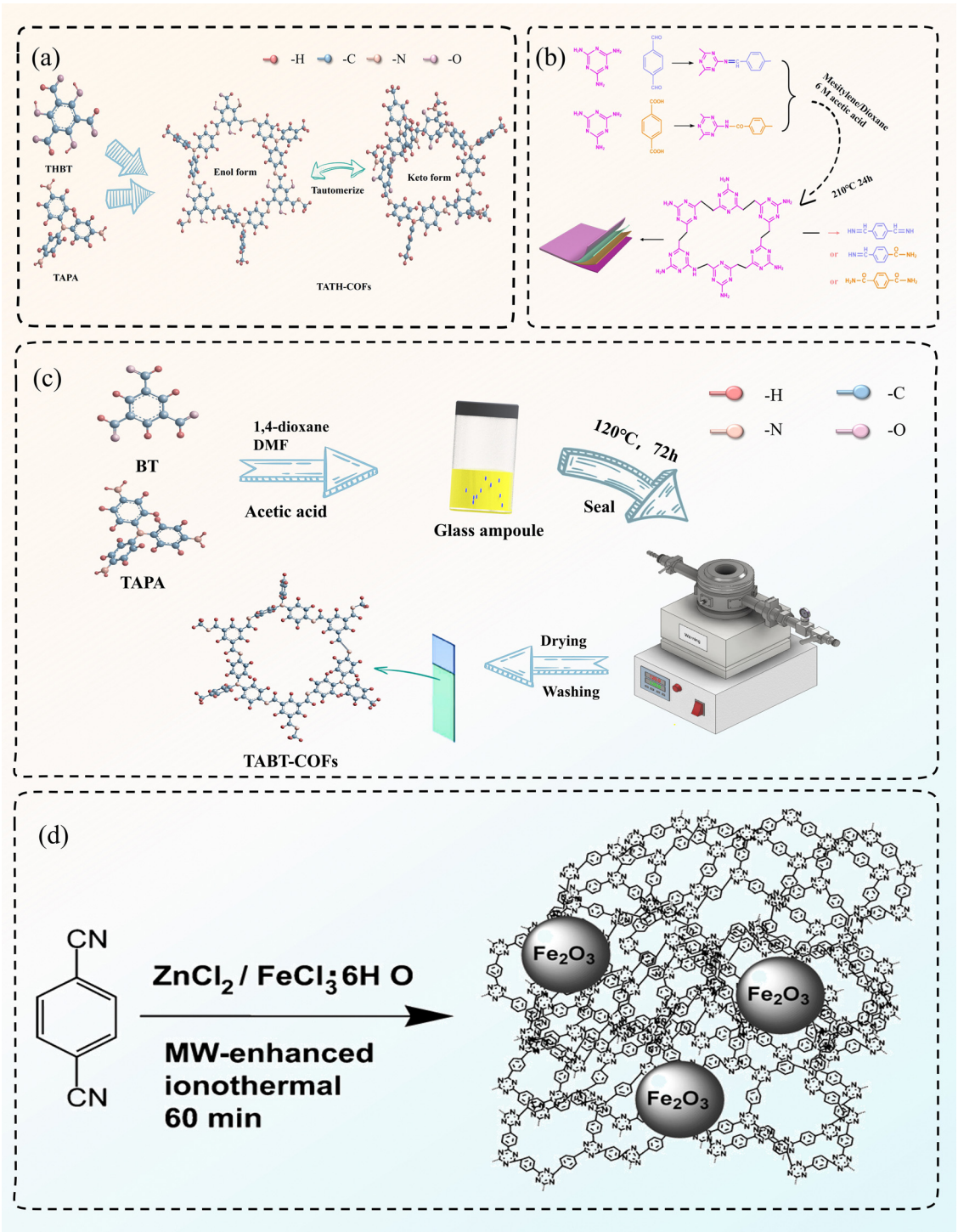


Fig. 5 Synthesis method of COF materials. (a) Synthesis method of TABT-COF. (b) Schematic diagram of the route to synthesize COFs through bifunctional groups. (c) Synthesis method of TATH-COF. (d) Microwave-enhanced high-temperature ionization strategy to yield a CTF/$Fe_2O_3$ composite. Reproduced with permission from ref. 126 (Fig. 5d), Copyright 2011 Elsevier.

thereby reducing the energy consumption of the reaction.[132,133] Biswal *et al.* synthesized network-like COFs with excellent chemical and thermal stability through room temperature solvent-free mechanochemical milling.[134] These COFs exhibit graphene-like layers with strong environmental adaptability, maintaining good morphology in boiling water, strong alkali and acid. Yang *et al.* realized an accurate production of ultra-thin 2D/2D covalent organic nanosheets (CON) heterojunctions *via* a mechanochemical strategy (Fig. 6a).[135] Compared to pure COF materials, the photocatalytic conversion efficiency of

 

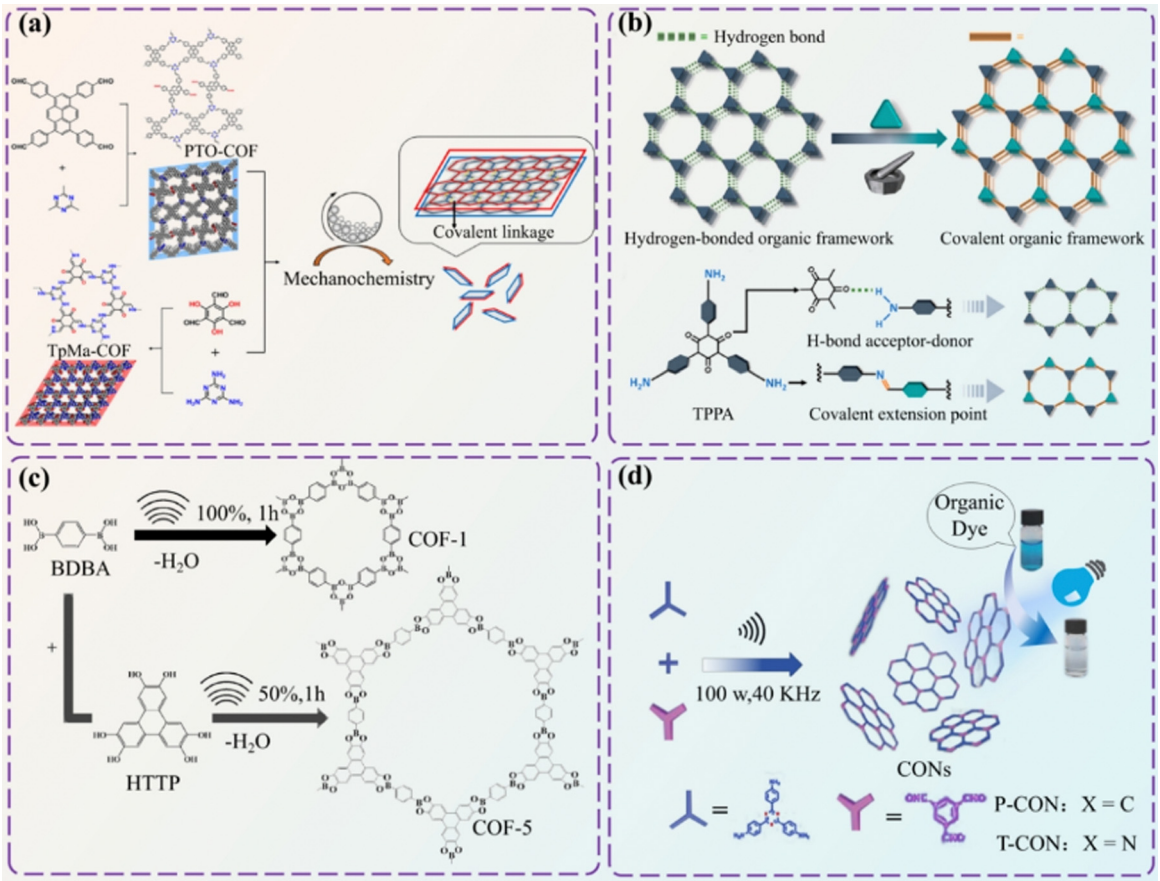


Fig. 6 Synthesis method of COF materials. (a) Schematic diagram of heterogeneous combination into 2D/2D TpMa/PTO CON using a mechanochemical strategy. (b) Schematic diagram of conversion of HOF into COFs using a mechanochemical strategy. (c) Synthesis of COF-1 and COF-5 *via* a sonochemical route. (d) Sonochemical synthesis of $NH_4$2D CON and its use as a high-performance photocatalyst for dye degradation. Reproduced from ref. 135 (Fig. 6a) and ref. 137 (Fig. 6b) with permission from the American Chemical Society, Copyright 2021 and Copyright 2023. Reproduced from ref. 138 (Fig. 6c) and ref. 139 (Fig. 6d) with permission from The Royal Society of Chemistry, Copyright 2012 and 2022.

CONs increased by 190%, thereby significantly improving the photo charge generation and separation capabilities. Guo *et al.* prepared flower-like TpBD nanosheets using a mechanochemical method.[136] The product effectively removed uranium (U(VI)) through chemical adsorption and inner sphere surface complexation, demonstrating promising environmental purification application.

In addition, researchers also used the structural connections between organic frameworks to convert organic frameworks into COFs. Hu *et al.* implemented a mechanochemical method to transform the hydrogen-bonded organic framework (HOF) into COFs (Fig. 6b).[137] The resulting COFs were large-channel 2D COFs that possessed excellent chemical stability, light absorption, and photocatalytic hydrogen evolution performance. Fan *et al.* utilized an innovative mechanochemical technique to transform the CTF-1 from its original staggered AB stacking mode to an overlapping AA stacking mode.[140] This significantly improved the crystallinity, quality, and porosity of the material, which remained permanent and ordered under ambient conditions.

*2.3.1.4. Ultrasonic chemical method.* The ultrasonic chemical method uses the mechanical vibration of ultrasonic waves to promote chemical reactions,[141] which can quickly form high-quality COF crystals. However, it may affect the crystallinity and product structure of COFs. Therefore, if large-scale production is to be achieved in the future, optimizing the reaction settings is essential.[142]

Yang *et al.* used the sonochemical strategy for the first time to yield COFs with remarkable textural characteristics (Fig. 6c).[138] Larger specific surface area provides more sites for active sites, which is more in line with the needs of functionalized COFs. Ultrasonic waves have also been found to be effective in breaking down the spatial structure of organic frameworks. For instance, the non-covalent interactions between 2D COF layers can be destroyed using ultrasonic waves, forming covalent organic nanosheets (CONs). Gan *et al.* reported a one-pot sequential condensation-stripping strategy to condense the monomers under ultrasonic treatment to fabricate ultrathin CONs (Fig. 6d).[139] The obtained ultra-thin CONs exhibited many active sites that can facilitate chemical reactions or be customized to perform additional functions.

*2.3.1.5. Photochemical method.* Photochemical synthesis allows precise reaction control by adjusting the colouration

and intensity of light in real-time under gentle conditions. However, due to the high cost of photons, they are not currently the primary choice for industrial COF production.[143]

Kim *et al.* utilized a photochemical method to synthesize a uniform-sized "sea urchin-like" COF-5 (UV-COF-5, Fig. 7a).[144] The synthesis yield (75%) and rate (48 times) of this method are higher than those of traditional methods. In another study, Kim *et al.* used a one-pot method to rapidly produce large-area, controllable 2D Lp-pi-COF films on the water surface *via* light-assisted imine condensation (Fig. 7b).[145] These atomically thin films exhibit excellent conductivity, making them promising for humidity-responsive and light-responsive electronic devices. Wu *et al.* synthesized benzoxazole-linked COF LZU-191 under sunlight at room temperature.[146] COF LZU-191 promotes sulfide oxidation and has broad application prospects in air pollution control. Jadhav *et al.* used 2D COFs to perform light irradiation in an aprotic solvent to cause a [2+2] cycloaddition reaction, which cross-linked single-layer COFs and created new vinyl groups to construct a new 3D covalent porous crystalline solid (Fig. 7c).[147] Photochemical methods are green and mild methods for synthesizing COFs.[148] They provide a high control over the reaction conditions and can produce COFs with various structures.[149]

*2.3.1.6. Room temperature synthesis.* Room temperature synthesis is a method of synthesizing COFs at relatively low temperatures. It is crucial to employ special catalysts or precursor designs to facilitate the reaction effectively at room

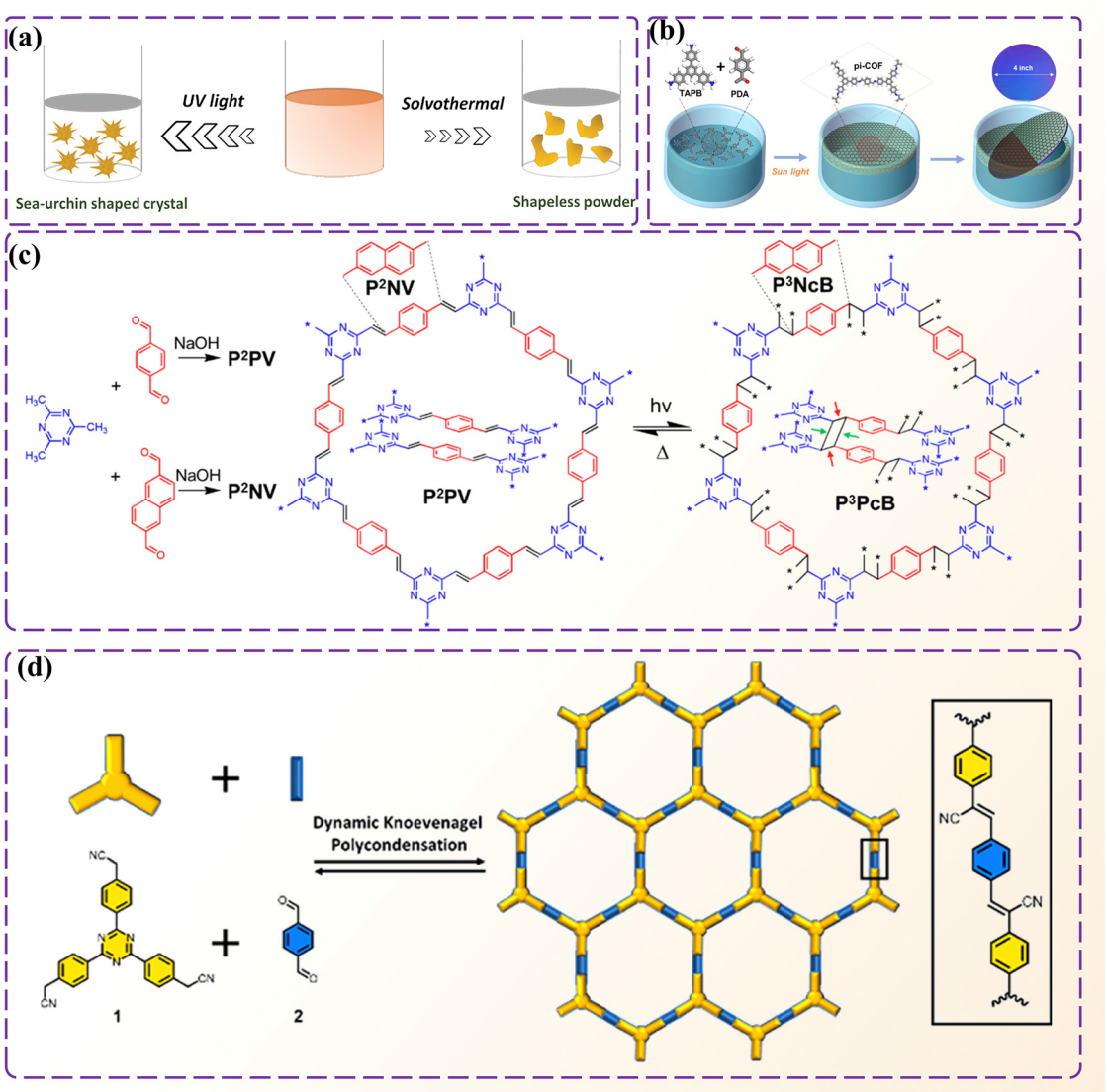


Fig. 7 Synthesis method of COF materials. (a) Comparison of the morphology of UV-COF-5 synthesized under illumination and conventional th-COF-5. (b) Schematic diagram of Lp-pi-COF synthesis *via* light-assisted imine dehydration at the water interface. (c) $P^2PV$ and $P^2NV$ COF synthesis and thermal cycle reversal under light induction. (d) Synthesis of VL-2D-SCOF-1 at room temperature. Reproduced from ref. 144 (Fig. 7a) and ref. 145 (Fig. 7b) with permission from the Royal Society of Chemistry, Copyright 2012 and 2021. Reproduced with permission from ref. 147 (Fig. 7c), Copyright 2017 Wiley. Reproduced with permission from ref. 150 (Fig. 7d), Copyright 2014 American Chemical Society.

 

temperature.[151,152] Medina *et al.* synthesized a BDT-COF with a spatial structure of AA repeated stacking enabled permanent porosity.[153] Li *et al.* obtained an ionic COF (RT-iCOF) with the highest adsorption rate for diclofenac sodium.[154] Moreover, Guo *et al.* revealed a method for aqueous-phase synthesis of ketoenamine- and imine-linked COF *via* a two-step dissolution–precipitation strategy.[155] The resulting ketamine- and imine-linked COFs exhibit impressive crystallinity and porosity, which facilitates the effective capture of iodine and uranyl. In a study by Fabozzi *et al.*, a highly extended domain of VL-2D-SCOF-1 was synthesized at room temperature (Fig. 7d).[150] This technique not only obviates the need for high-energy inputs but also eliminates the necessity for catalysts for reaction acceleration.

*2.3.1.7. Plasma-assisted synthesis.* Plasma-assisted synthesis of COFs is a cutting-edge technique involving high-voltage plasma discharge to produce COFs.[156] Plasma, a fourth state of electrically charged particles and free electrons, provides ample reactive species to initiate chemical reactions and accelerate COF synthesis. He *et al.* used liquid dielectric barrier discharge (DBD) plasma to synthesise COF-1 (Fig. 8a),[157] to regulate the spatial structure of COF-1 *via* crystal adjustments of interlayer stacking. Bora *et al.* used organic linkers NTCDA and tris(4-aminophenyl)amine to synthesize H-COF.[158] Fig. 8d shows the plasma-mediated COF functionalization at the gas–liquid interface. However, the implementation of plasma-assisted synthesis may require specialized plasma discharge equipment, which may hinder its large-scale application.

*2.3.1.8. Electric field-mediated synthesis.* The electric field-mediated method uses an external electric field to promote chemical reactions synthesising COFs.[161] Feyter *et al.* first used a directional external electric field (EEF) to control the state of covalent substances to form a self-assembled molecular network (SAMN) (Fig. 8c).[68] This network is regulated by EEF and can achieve mutual conversion with sCOF. Feyter *et al.* examined the relationship between the electric field and the reversibility of sCOF.[159] When external electric fields surround all the reaction materials, sCOF-1 gradually transforms into sCOF-2 after STM deviation. This transformation provides valuable insights into boronate-based COF formation (Fig. 8b). Rotter *et al.* used EPD technology to prepare COF films and coatings.[162] Through the innovative EPD technology, COF-5, COF-300, and BDT-ETTA COF have been prepared with impressive precision and accuracy. This technology allows for the precise control of the thickness of COF membrane materials, making it an ideal solution for use in the biomedical field. Zhang *et al.* controlled the electron dose in the electron beam and mixed the COF precursor with an organic solvent containing aqueous acetic acid as a catalyst (Fig. 8e).[160] The two-dimensional imine COF produced under a high-energy electron beam (1.5 MeV) had the highest yield and can be applied in the field of gas adsorption (Table 1).

**2.3.2. The synthesis methods of COF derivatives.** From a chemical perspective, COFs are highly customizable, offering significant porosity that presents numerous active sites for chemical groups.[163] Their skeletal and physico-chemical properties can be tailored and manipulated through blending, post-modification, and bottom-up techniques, which enhance stability and functional enrichment (Fig. 9). These methods motivate the functional design of COFs, allowing optimization to meet specific application needs.[164]

*2.3.2.1. Post-synthesis strategy.* The post-synthesis strategy effectively modifies or adds new properties to COFs by altering the synthesized framework.[165] This approach allows for enhanced material customization through techniques such as functional group insertion, metal catalysis, redox reactions, heat treatment, selection of functional monomers, and surface modification.[166,167]

Functional group insertion is typically conducted *via* nucleophilic or electron-affinity reactions to introduce desired groups into COFs. Sun *et al.* converted vinyl-functionalized mesoporous COF (COF-V) into COF-S-SH by inserting ASH groups for mercury removal (Fig. 10a).[168] Metal catalysis provides high selectivity and efficiency, enabling specific chemical transformations. Zhou *et al.* synthesized COFs through a one-step method and achieved controllable coordination of mononuclear and binuclear metal sites. The prepared COFs can be used as photocatalysts.[169] Brucks *et al.* used monofunctional boronic acid to modify COF functionality to achieve permanent porosity, long-range ordering and high functionalization density.[71]

High-temperature heat treatment can induce chemical reactions within the COF framework, altering the pore structure or chemical properties. Han *et al.* used this method to repair defects in COFs by breaking and reforming bonds.[127] The selection of appropriate monomers is crucial in synthesizing COFs. For example, triphenylamine, a non-planar molecule, can be a barrier to intermolecular aggregation. Xiong *et al.* synthesized bis(triphenylamine)-based COFs (TABT-COF and TATH-COF) with triphenylamine characteristics.[124]

*2.3.2.2. Bottom-up approach.* Bottom-up methods start with small molecules or monomers and gradually build the framework structure through synthetic chemical reactions.[171] Therefore, choosing the right monomers and solvents is crucial. Pang *et al.* constructed COFs with three various pores *via* a heterostructure hybrid connection approach (Fig. 10b).[87] These 3D COFs have numerous active sites and inherent pore structures. In order to increase the complexity of the framework structure with more active sites in 3D COFs, Xiao *et al.* practised a tangled network formed by multiple 2D layers tilted for each other *via* interleaving or tilted interpenetration,[90] which has been successfully used in synthesising many COFs.

*2.3.2.3. Blending method.* The blending method involves mixing and reacting two or more compounds. The blending method does not require expensive catalysts or high-pressure and high-temperature reaction settings.[172] This reduces costs, expands the scope of use and improves material properties. Functional materials such as metals, metal–organic frameworks, and carbon nanotubes have been synthesised by COF-based composites.[170,173,174] Magnetic COFs, combining COFs

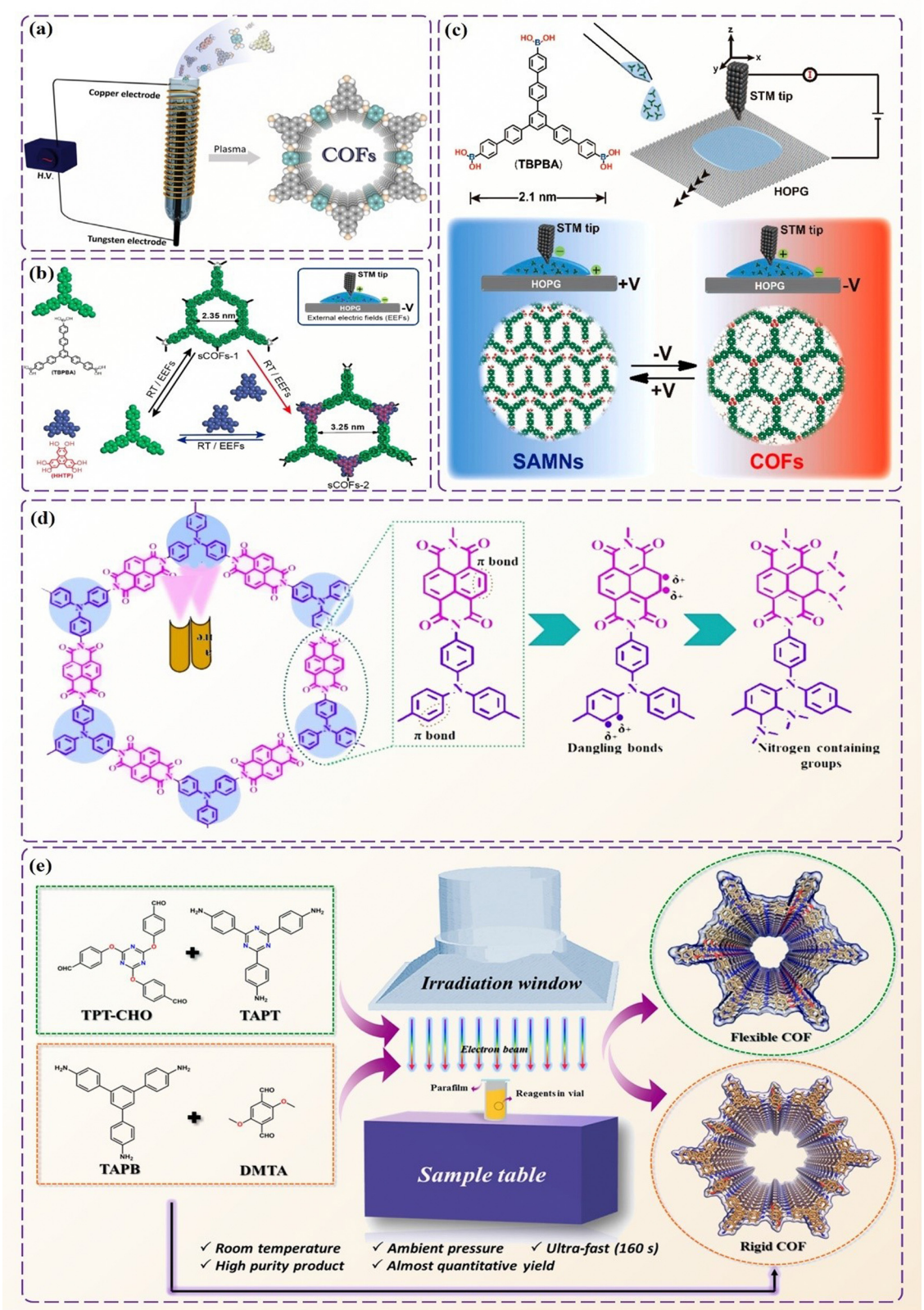


Fig. 8 Synthesis method of COF materials. (a) DBD plasma-assisted polymerization of COFs at normal pressure and low temperature. (b) Chemical structures of HHTP (left) and TBPBA plus a schematic illustration of EEF-mediated network switching between sCOF-1 and sCOF-2 (right) in SAMN. (c) Schematic diagram of electric field-induced reversible transformation between SAMN and COFs. (d) COF functionalization is mediated by plasma at the gas–liquid interface. (e) Schematic diagram of COFs synthesized by electron beam irradiation. Reproduced from ref. 157 (Fig. 8a) and ref. 158 (Fig. 8d) with permission from Wiley, Copyright 2021. Reproduced from ref. 159 (Fig. 8b), ref. 68 (Fig. 8c) and ref. 160 (Fig. 8e) with permission from the American Chemical Society, Copyright 2020, 2019 and 2020.

 

Table 1 Comparison of synthetic methods of COFs

| Synthesis method | Feature | Advantage | Disadvantage | Ref. |
|---|---|---|---|---|
| Solvothermal method | High temperature and organic solvent as reaction medium | High yield of COFs<br>Controllable crystal size and morphology<br>Large scale production | High cost<br>High energy consumption<br>Long response time | 121–123 |
| Microwave-assisted synthesis | Rapid heating of reaction mixtures using microwave energy | Simple operation<br>Short reaction time<br>Uniform reaction | High equipment cost<br>Limited penetration depth | 62 and 128–130 |
| Mechanochemical synthesis method | Uses mechanical force to stimulate chemical reactions | Environmentally friendly<br>Easy to operate | Equipment loss<br>Restricted mass production | 132 and 133 |
| Ultrasonic chemical method | Uses ultrasonic mechanical vibration to promote chemical reactions | High efficiency<br>High quality<br>No pollution | Unskilled operation<br>Lack of amplification solution | 138, 141 and 142 |
| Photochemical method | Chemical reactions under light | Environmentally friendly<br>Precise control of the reaction | High cost<br>Limits large-scale application | 143 |
| Room temperature synthesis | Chemical reactions at relatively low temperatures | Low energy consumption<br>Easy preparation | Slow reaction rate<br>Low yield<br>Limited reaction types | 151 and 152 |
| Plasma assisted synthesis | Synthesis of COFs using high-voltage plasma discharge | Fast reaction rate<br>Fewer by-products | Complex equipment<br>High cost | 156–158 |
| Electric field-mediated synthesis | Uses external electric fields to promote chemical reactions | Mild reaction conditions<br>Fast reaction rate | Electrode fouling<br>Complicated equipment<br>High cost | 161 |

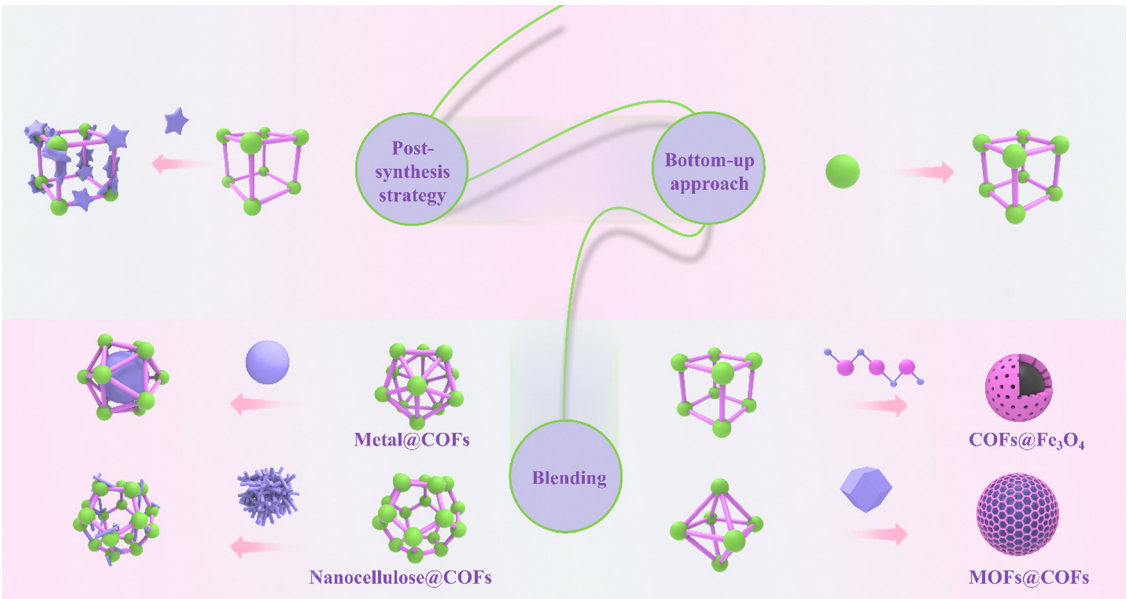


Fig. 9 Functional design method of COFs.

and magnetic nanoparticles, can adsorb heavy metal pollutants in water and soil. You *et al.* uniformly dispersed $Fe_3O_4$ nanoparticles in a mixed solution containing melamine and benzaldehyde[174] to achieve $Fe_3O_4$@COF with high saturation magnetization, high thermal stability, chemical stability and a large specific surface area (335.2 $m^2$ $g^{-1}$).

When carbon nanotubes (CNTs) are used as catalysts, they can promote electron transport within the catalyst and increase the rate of the oxygen reduction reaction. Liu *et al.* obtained a COF-based catalyst after blending CNTs (Fig. 10c),[170] which showed excellent oxygen reduction reaction performance compared with commercial Pt/C and Co-based catalysts, paving the way for the realization of efficient bifunctional electrocatalysts without pyrolysis. When MOFs are mixed with COFs, the porosity of the composite material is improved, the number of metal active sites is increased, and the adsorption and catalytic effects are enhanced. Guo *et al.* expanded the application of MOFs in biomedicine by combining the drug storage

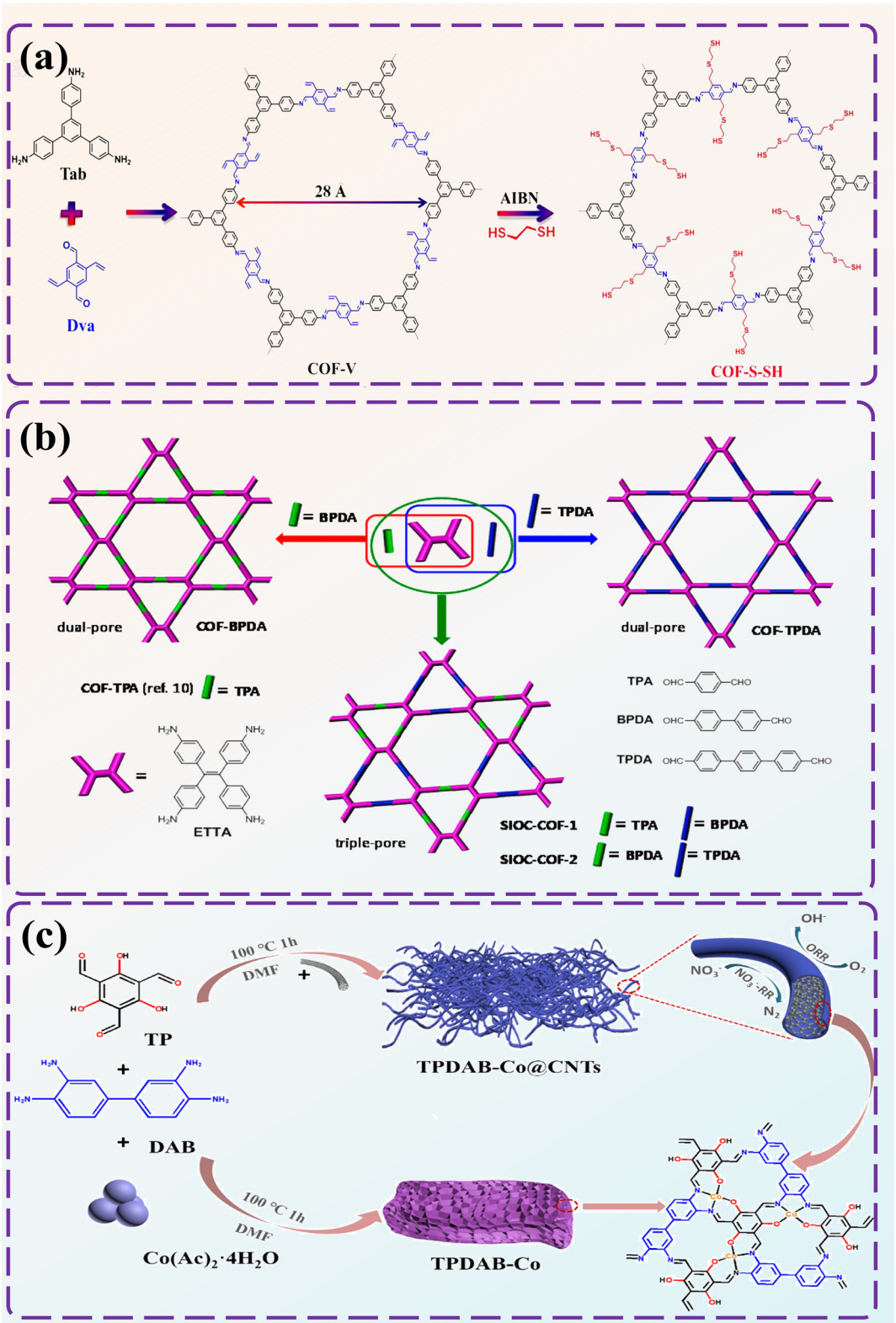


Fig. 10 Synthesis method of COF-derived materials. (a) COF-V is synthesized *via* the condensation of Dva (blue) and Tab (black), and functionalized COF-S-SH is synthesized through a thiol–ene reaction. (b) Bottom-up synthesis of dual-hole and triple-hole COFs. (c) Schematic diagram of the synthesis of TPDAB-Co and TPDAB-Co@CNT. Reproduced from ref. 168 (Fig. 10a) and ref. 87 (Fig. 10b) with permission from the American Chemical Society, Copyright 2017 and Copyright 2016. Reproduced with permission from ref. 170 (Fig. 10c) Copyright 2020 Elsevier.

 

Table 2 Comparison of synthetic methods of COF derivatives

| Synthesis method | Feature | Advantage | Category | Ref. |
|---|---|---|---|---|
| Post-synthesis strategy | Modifies or addsnew properties of COFs by changing the synthetic framework | Customized materials<br>Simple<br>High efficiency | Metal catalysis<br>Surface modification<br>Functional group insertion<br>Heat treatment | 165–169 |
| Bottom-up approach | Monomers are synthesized to build the framework | Precise control of COFs structure<br>High purity | Chemical vapor deposition<br>Molecular beam epitaxy | 171 |
| Blending method | Two or more compounds are mixed and reacted | Low cost<br>Wide application range | Mechanical blending<br>Ultrasonic mixing | 170, 172 and 173 |

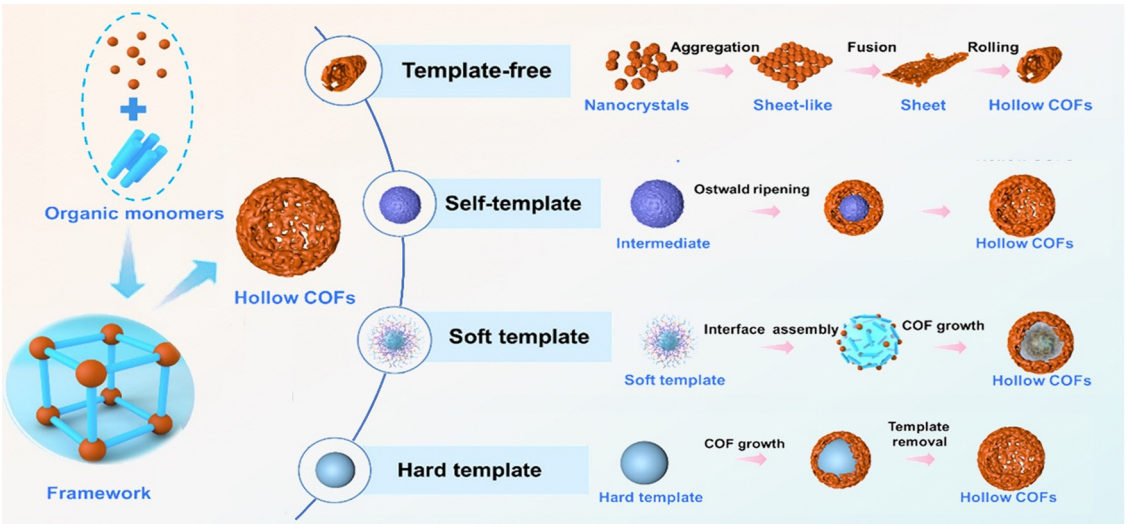


Fig. 11 Synthetic strategy of hollow COFs. Reproduced from ref. 177 with permission from American Chemical Society, Copyright 2023.

capacity of MOFs with the biological properties of COFs (Table 2).[173]

### 2.4. The unique structural COFs and their derivatives

This section presents two COFs with unique structures and functions and reviews their synthesis strategies. The first type is hollow COFs (HCOFs) with a pore structure for air pollution control; the second type is core–shell COFs with a clear hierarchical structure, good stability, and high conductivity.

**2.4.1. Synthesis of hollow COF materials.** Hollow COFs (HCOFs) differ from other COFs in their hollow structure.[175] The presence of pore structures within their framework facilitates the adsorption of molecules and gas storage.[176] Fig. 11 show four synthesis methods of hollow covalent organic frameworks: the template-free method, self-template method, soft template-assisted method, and hard template-assisted method.[177] The hard template method is typically used to create porous materials with high surface area and unique morphologies. Sun *et al.* used amino-functionalized $SiO_2$ microspheres as templates to grow $NH_2$-f-$SiO_2$@$COF_{TTA\text{-}DHTA}$,[178] which has a well-defined morphology, high crystallinity and high chemical stability.

The soft template method utilizes soluble and easily removable organic or inorganic substances as templates, allowing great control over HCOFs' structure and morphology. For instance, Tang *et al.* used n-butanol to create emulsion droplets in an aqueous solution.[179] TAPB and DMTP were raw materials produced through emulsion interfacial polymerization to produce HCOF microspheres with rich interfacial defects. The self-template method does not require external templates or guides. Instead, the material spontaneously forms the desired structure during synthesis. Kandambeth *et al.* synthesized hollow spherical COFs using a self-templating strategy, which crucially established strong π–π stacking interactions between the π systems of the organic precursor layers.[180] This method simplifies the process and reduces costs while preserving the structural integrity of the final product.

The template-free strategy produces hollow structures directly from organic building blocks without the need for predefined templates.[177] Zhou *et al.* used a rigid 3D triptycene scaffold framework to prepare COFs with a hollow spherical morphology *via* reversible B–O condensation between 1,2-diol and boronic acid (Table 3).[181]

**2.4.2. Synthesis of core–shell COF composites.** Owing to its extremely high electrical conductivity, stability, and porosity, COFs are the top material choice for the outer shell in a core–shell structure. Fig. 12c shows the application scenario of core–shell composite materials. There are four main strategies for synthesizing core–shell COF composites: coordination-induced interconnected hybrids, coating agent-assisted growth, one-pot polymerization, and seed-mediated *in situ* growth.[182]

Table 3 Comparison of synthetic methods of hollow COFs

| Synthesis method | Feature | Advantage | Disadvantage | Ref. |
|---|---|---|---|---|
| Hard template | Uses hard materials as molds or supports | Controllable shape<br>Wide range of applications | Template removal<br>High cost | 177 and 178 |
| Soft template | Uses soluble and easily removable materials as templates | Mild synthesis conditions<br>Easy removal of template | Template is unstable<br>Difficult to control | 177 and 179 |
| Self-template | No external templates or bootstrap required | Simple process<br>Environmentally friendly | Lack of structural diversity<br>Complex control | 177 and 180 |
| Template-free | Creating hollow structures from components | Structural diversity<br>Environmentally friendly | Complex optimization<br>Material-specific limitations | 177 and 181 |

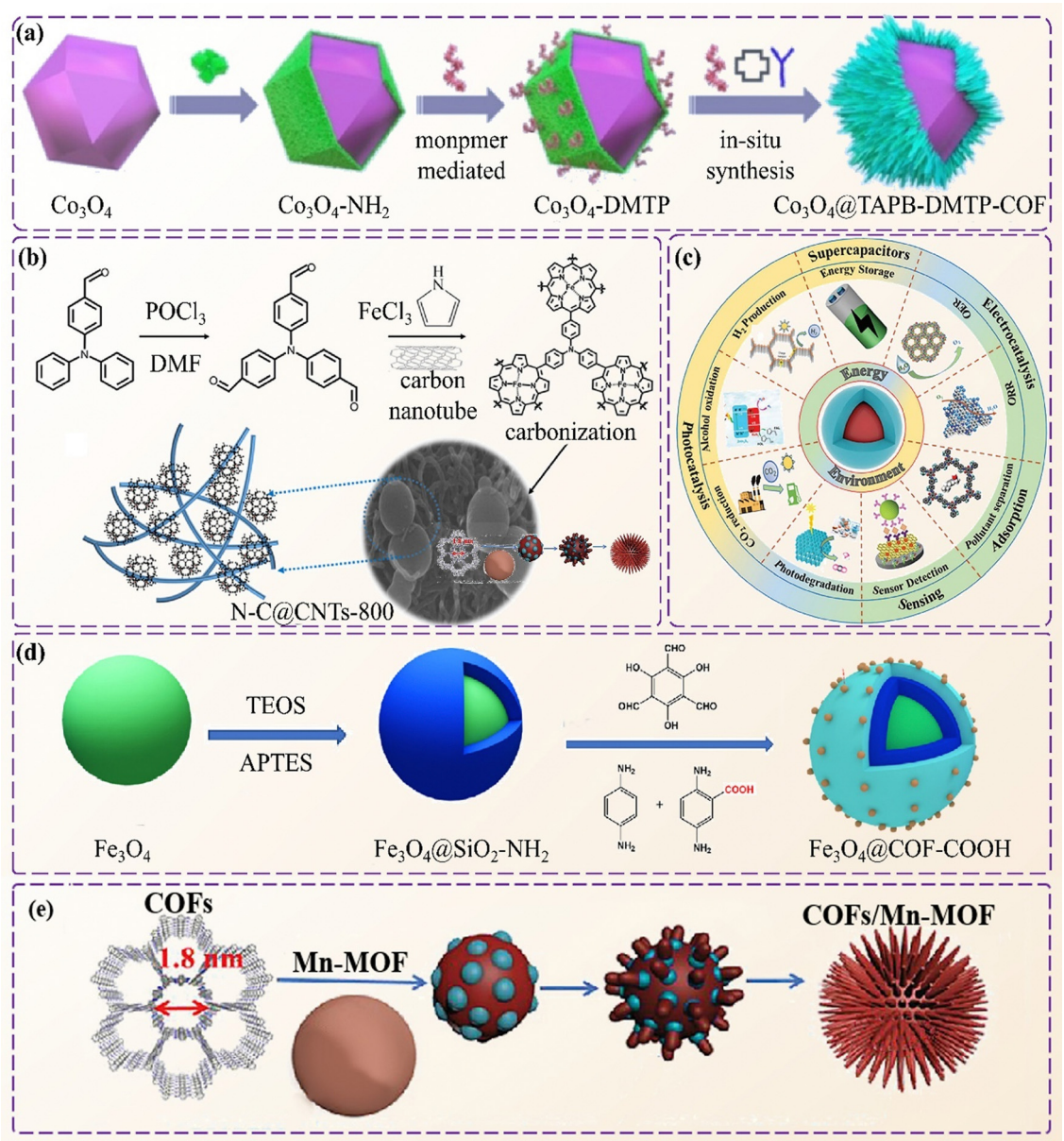


Fig. 12 Synthesis of core–shell COF composites. (a) Seed-mediated *in situ* growth method. (b) One-pot polymerization method. (c) Application of core–shell COF materials. (d) Coating agent-assisted growth method. (e) Coordination-induced interconnected hybrids. Reproduced from ref. 183 (Fig. 12a) and ref. 184 (Fig. 12d) with permission from Elsevier, Copyright 2021 and Copyright 2020. Reproduced with permission from ref. 185 (Fig. 12b), Copyright 2019 Springer. Reproduced from ref. 182 (Fig. 12c) and ref. 186 (Fig. 12e) with permission from Wiley, Copyright 2023 and Copyright 2019.

 

Table 4 Comparison of synthetic methods of core–shell COFs

| Synthesis method | Feature | Advantage | Disadvantage | Ref. |
|---|---|---|---|---|
| The seed-mediated *in situ* growth | Amino-directed monomer polymerization | High yield and uniformity<br>Scalability | Incompatible surfaces<br>Complex to generate | 182 and 183 |
| One-pot polymerization | All reactants are combined in one reaction vessel | High efficiency<br>Minimized contamination risk | Low purity of finished product<br>Reaction conditions limited | 182 and 185 |
| Coating agent-assisted growth | Applying a coating made of precursors on the substrate to promote the growth of nanostructures | Uniform growth of monomers<br>Versatility in substrate selection | Difficult to form complex structures<br>High cost | 182 and 184 |
| Coordination-induced interconnected hybrids | Formation of hybrid materials through coordination of metal ions and ligands | Tailored properties<br>Enhanced stability | Complex synthesis and design<br>High cost | 182 and 186 |

The seed-mediated *in situ* growth strategy first introduces amino groups into the substrate, which will react with organic monomers to guide the polymerization of monomers during the formation of the COF shell to form a core–shell composite material. Chen *et al.* constructed a $Co_3O_4$@TAPB-DMTP-COF composite material with a core–shell structure through a monomer-mediated *in situ* growth strategy (Fig. 12a).[183] Kong *et al.* prepared core–shell CNT@COF materials through a one-pot polymerization method (Fig. 12b),[185] where the coating agent was used as an auxiliary agent to catalyse the growth of the target material by forming a thin film on the reaction surface. Hu *et al.* prepared carboxyl functionalized nanomaterials with core–shell design through a coating agent-assisted approach (Fig. 12d),[184] to induce a new interconnected hybrid. Sun *et al.* studied a COF/Mn-MOF hybrid structure that achieved imine bonding through ligand induction.[186] The 2D layered COFs were vertically stacked and dispersed on the Mn-MOF core which produced an entire spherical design (Fig. 12e and Table 4).

# 3. Applications of COFs and their derivatives in air pollution

With the increasing air pollution, countries and international organizations have implemented various measures to reduce its impact.[187,188] COFs can efficiently remove harmful gases in atmospheric pollution,[189] where the abundant pores provide a large specific surface area and facilitate gas adsorption. In recent years, the application range of COFs has developed to include a variety of gases from $CO_2$ to volatile pollutants, $NH_3$, CO, $H_2S$, $SO_2$ and $NO_x$.[190,191]

## 3.1. $CO_2$ capture and catalytic conversion

At present, triazine-based COFs, imine-based COFs, and boron-based COFs have broad applications in $CO_2$ adsorption.[77,87,101] The pore size of COFs and the pressure at which $CO_2$ is captured are the key factors affecting the capture efficiency. Under low pressure, the $CO_2$ capture capacity of COFs is related to their pore structure; under high-pressure scenarios, the specific surface area and pore volume of COFs are the key factors determining their $CO_2$ adsorption capacity.[192,193] Additionally, 3D COF structures have been found to have a better adsorption effect on $CO_2$ than 2D COF structures. The creation of 3D COF structures, especially non-interpenetrating networks, can greatly enhance the high-pressure performance of $CO_2$ adsorption.[194,195]

In addition to the adsorption of $CO_2$, the catalytic conversion of $CO_2$ into high-value chemicals (*e.g.* MeOH, $C_2H_4$, HCOOH, and $CH_4$) represents another practical research field to alleviate the greenhouse effect. COF catalysts have been scrutinized for $CO_2$ reduction under electrocatalytic settings. Studies have demonstrated that the catalytic reduction of crystalline COFs modified with transition metal ions showed the highest efficiency.[196] Zhou *et al.* applied a one-step synthesis method to obtain a metal-salen COF with a controllable coordination environment of mononuclear and binuclear metal sites,[169] to show the highest $CO_2$ photoreduction and syngas production activity. Lu *et al.* performed TMI modification of transition metal acetate and a COF through a simple hydrothermal method to obtain a DATP COF and a DQTP COF.[196] In Fig. 13a, the DQTP COF prepared using cobalt has a high catalytic reduction efficiency for $CO_2$ and a high CO and formic acid production rate. Recently, Lu *et al.* designed a series of stable and crystalline dioxin-linked metal phthalocyanine COF with a good reactivity towards electrocatalytic $CO_2$.[197]

$CO_2$ capture and catalytic conversion are expected to be critical in mitigating climate change and realizing carbon capture and storage.[200] Researchers continue to enhance the performance of COFs to increase their efficiency in adsorbing and catalytically converting $CO_2$. Ongoing efforts in the field aim to develop COFs with improved structural stability, porosity, and tunable surface functionality.[201] These advancements will contribute to developing sustainable and effective strategies for addressing climate change and reducing greenhouse gas emission challenges.

### 3.2. Hydrogen sulfide removal

Hydrogen sulfide ($H_2S$), a poisonous gas to human health, is highly flammable and explosive even at low concentrations.

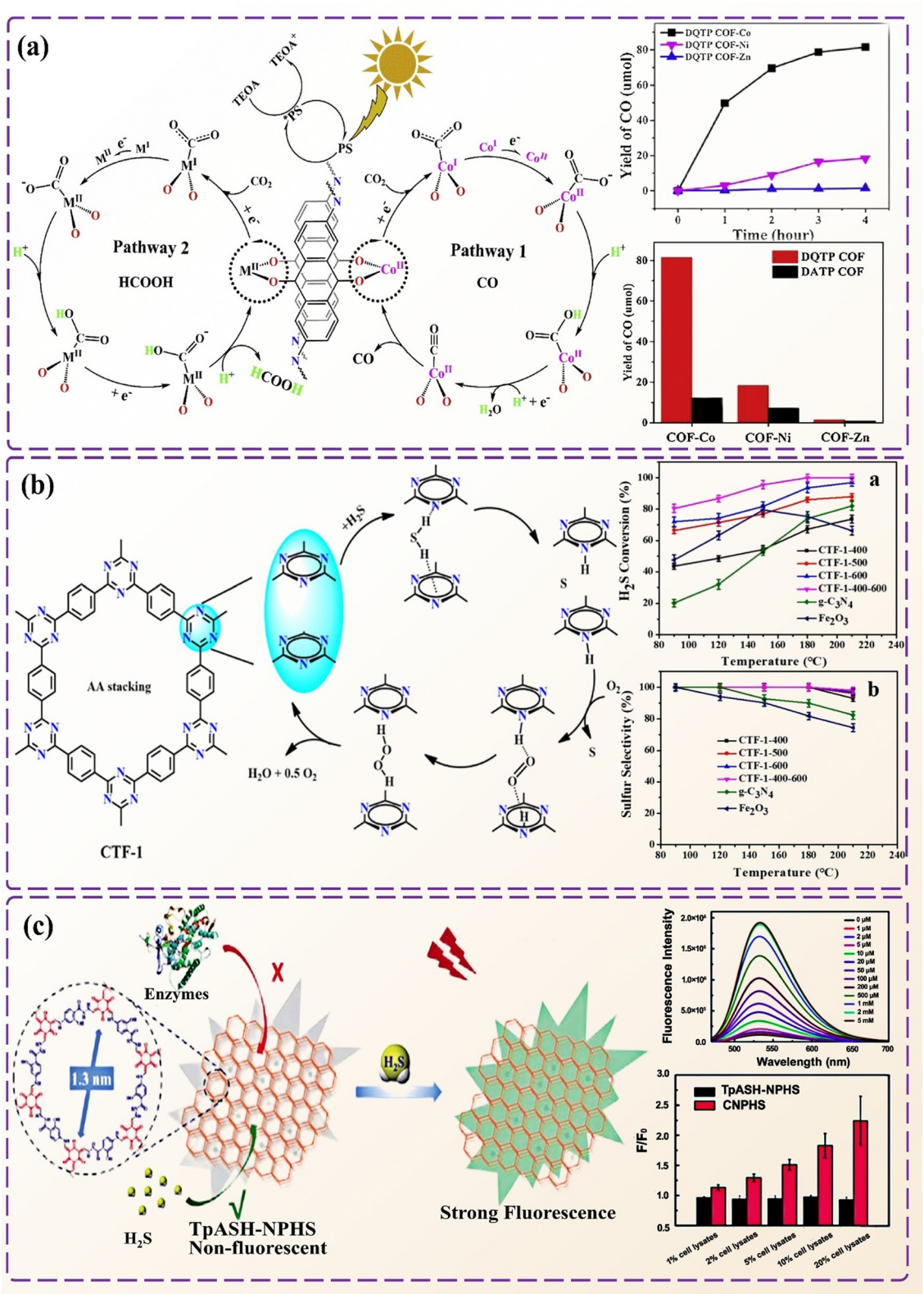


Fig. 13 Application of COFs in air pollution control. (a) The mechanism of photocatalytic reduction of $CO_2$ by DQTP COF-M and the comparison of the photocatalytic activity of DQTP COF-M for CO evolution. (b) Dissociation of $H_2S$ into S with the help of $O_2$ and the effect of reaction temperature on $H_2S$ conversion and sulfur selectivity in the double-layer A–A stacking of CTF-1-*x*. (c) COF-based nanoprobe TpASH-NPHS detects $H_2S$ levels. Reproduced with permission from ref. 196 (Fig. 13a), Copyright 2019 Elsevier. Reproduced with permission from ref. 198 (Fig. 13b), Copyright 2021 American Chemical Society. Reproduced with permission from ref. 199 (Fig. 13c), Copyright 2018 The Royal Society of Chemistry.

 

Wu *et al.* prepared a porous COF LZU-191 using a photochemical method.[146] The presence of benzene rings allows it to combine with sulfides, improve the adsorption rate of $H_2S$, and show excellent catalytic activity for visible-light-driven oxidation of sulfides to sulfoxides under mild conditions. Peng *et al.* prepared a series of covalent triazine skeletons to form a polyaryl triazine network,[198] which has abundant pores and a large specific surface area and can effectively and selectively oxidize $H_2S$ to elemental S (Fig. 13b).

COFs are also utilized to detect the $H_2S$ content in the air. Wang *et al.* prepared TpASH using the PTSA salt of 4-aminosalicylicylhydrazide (ASH) and 1,3,5-triformylphloroglucinol (Tp).[199] Two-photon fluorescent COF nanoprobes (TpASH-NPHS) were prepared by combining TpASH with fluorescent probes (Fig. 13c). TpASH-NPHS has excellent stability and biological imaging capabilities associated with high detection accuracy of $H_2S$. White *et al.* used 2D COFs as a template to create porous graphene-COF composites.[202] The porous structure of the graphene-COF composite served as an active site for chemical reactions, which enhanced the Raman signal of graphene and allowed for more accurate $H_2S$ content monitoring. The sensitivity of this composite material was comparable to that of the current state-of-the-art $H_2S$ meters, making it a promising option for gas sensing applications.

### 3.3. $NH_3$ removal

Ammonia ($NH_3$) is a known hazardous substance threatening human health and the environment. Various adsorbents have been studied to improve $NH_3$ absorption including carbon, zeolites, and COFs.[203,204]

Geng *et al.* proved that boronic acid ester-linked COFs represent an effective adsorbent for $NH_3$ capture due to a strong Lewis acid–base interaction between boric acid and the nitrogen bond in ammonia.[82] Yang *et al.* produced a series of $[HOOC]_X$-COF ($X$ = 0, 17, 33, 50 and 100) using various ratios of *p*-phenylenediamine (PA-1), triformylphloroglucinol (TFP), and 2,5-diaminobenzoic acid (DAA).[205] The $[HOOC]_{17}$-COF showed the highest porosity, the largest specific surface area, and the highest adsorption efficiency for $NH_3$. Fig. 14a shows the $NH_3$ adsorption and desorption process of $[HOOC]_{17}$-COF and the adsorption capacity of $NH_3$.

### 3.4. Volatile pollutant removal

Organic compounds that readily vaporize at normal room temperature are known as volatile organic pollutants (VOPs), which are significant contributors to atmospheric pollution and can lead to the formation of detrimental substances such as photochemical smog, secondary organic aerosols, and ozone.[209,210] Guo *et al.* synthesized a series of dpCOF-$X$ ($X$ = 1, 2, 3, 4, 5, 6, and 7).[169] The capture ability of uranyl ions can be improved by providing active sites. He *et al.* constructed a 2D dual-porous COF (SCU-COF-2) by introducing 2,20-bipyridyl groups by capturing organic iodide through methylation reaction and electron pair effect (Fig. 14b).[207] The absorption capacity of SCU-COF-2 for iodine gas reaches 6 g $g^{-1}$.

Acetylene might catalytically inhibit the production of ethylene and polyethylene. Jiang *et al.* prepared PAF-110 by imidization of the precursor.[206] The product exhibits high thermal and structural stability in which acetylene can be selectively separated from ethylene (Fig. 14c). Overall, the findings may inspire future work on the design optimization of porous organic materials to enhance the gas separation efficiency.

### 3.5. $NO_x$ and $SO_x$ removal

The emissions of nitrogen oxides ($NO_x$) and sulfur oxides ($SO_x$), mostly caused by the combustion of fossil fuels and industrial processes, pose significant threats to the environment and human health.[211–214]

Wang *et al.* developed a COF-105 that has a positive charge of metal atoms,[215] which allows $SO_2$ gas molecules to be adsorbed on the metal-doped covalent organic framework. Lee *et al.* prepared imide functionalized COF (PI-COF) as an $SO_2$ adsorbent with high mesoporosity and large surface area to reach an adsorption capacity of $SO_2$ at 6.3 mmol $g^{-1}$ (Fig. 14d).[208] Additionally, the $SO_2$ capacity of the material does not significantly decrease even after undergoing five adsorption–desorption cycles, indicating that the material is suitable for reuse. In order to better test the content of pollutants in the atmosphere, Meng *et al.* synthesized a new type of intrinsically conductive 2D COF (COF-DC-8) with a bulk conductivity of $2.51 \times 10^{-3}$ S $m^{-1}$ and a remarkable resistance to several atmospheric pollutants such as NO, $NO_2$, $H_2S$, and $SO_2$ (Table 5).[216]

## 4. Applications of COFs and their derivatives in the water treatment

Water pollution causes a significant concern as it harms the natural environment and impacts human health and sustainable social and economic development.[217,218] In this section, the role of COFs in five aspects will be elaborated including seawater desalination, dye adsorption, heavy metal adsorption, removal of organic matter, and removal of drugs in water.[219–221]

### 4.1. Desalination

Desalination aligns with the United Nations Sustainable Development Goals (SDGs) to support sustainable water management and provide clean water globally. Among the various techniques,[222] COFs have emerged as a promising filter membrane material in seawater desalination. Recently, Zhang *et al.* synthesized a series of 2D COFs as filtration membranes in seawater desalination.[223] Different hydrophilic groups were grafted onto COFs to study the effects of pore size and the number of hydrophilic groups on desalination efficiency. Fig. 15a shows the membrane desalination simulation system.

Nanofiltration membranes (NFs) exhibit characteristics of low water flux and high ion rejection rates. Liu *et al.* prepared a highly stable IISERP-COOH-COF-1 membrane with high ion rejection and water flux.[224] Subject to carboxyl functionalization to reduce pore size, it demonstrates highly selective water

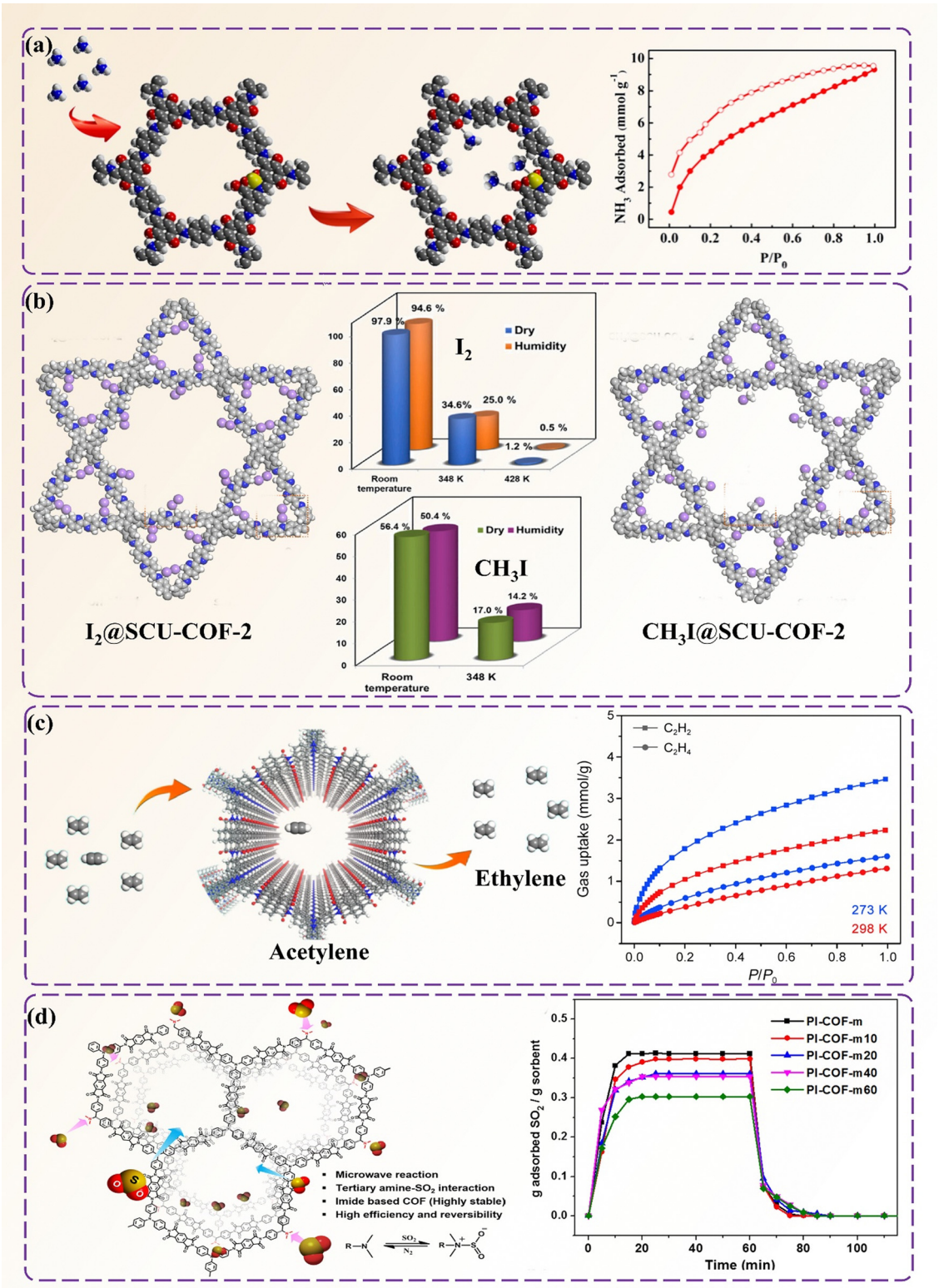


Fig. 14 Application of COFs in air pollution control. (a) $[HOOC]_{17}$-COF adsorption and desorption process of $NH_3$ and its adsorption capacity for $NH_3$. (b) Adsorption diagram and adsorption effect diagram of $I_2$ and $CH_3I$ on SCU-COF-2. (c) Selective acetylene adsorption by crystalline polyimide porous organic framework materials and ethylene and acetylene adsorption isotherms at different temperatures. (d) Functionalized PI-COF for $SO_2$ adsorption and the adsorption effect of PI-COF with different functionalization degrees on $SO_2$. Reproduced from ref. 205 (Fig. 14a) and ref. 206 (Fig. 14c) with permission from the American Chemical Society, Copyright 2018 and 2021. Reproduced with permission from ref. 207 (Fig. 14b), Copyright 2020 Elsevier. Reproduced with permission from ref. 208 (Fig. 14d), Copyright 2017 Springer.

 

Table 5 Application of COFs in air pollution control

| Type | Synthesis method | Application | Feature | Efficiency | Ref. |
|---|---|---|---|---|---|
| M(salen)-COFs | Solvothermal method | Photocatalytic $CO_2$ reduction to syngas | Binuclear metal site | $H_2$ production 11.31 mmol $g^{-1}$ $h^{-1}$ | 169 |
| DQTP COF-Co | Ultrasonic chemical method | Heterogeneous photocatalytic reduction of $CO_2$ | Transition metal ion modification | Produces formic acid 152.5 μmol $h^{-1}$ $g^{-1}$ | 196 |
| NiPc/CoPc-TFPN COF | Solvothermal method | Electrocatalytic reduction of $CO_2$ | The dioxin connection | $FE_{CO} \approx 100\%$ | 197 |
| COF LZU-191 | Photochemical method | Adsorbs $H_2S$ and catalyzes the oxidation of sulfide to sulfoxide | There are electron-withdrawing and electron-donating groups on the phenyl ring | Sulfide conversion efficiency 60–68% | 146 |
| CTF-1-*x* | Plasma induced synthesis | 100% $H_2S$ is oxidized to sulfur | Tunable structural bases characteristic of graphitic nitrogen | 100% $H_2S$ conversion | 198 |
| TpASH-NPHS | Blending method | $H_2S$ content monitoring | Flake structure Possessing phenolic hydroxyl groups | Accurate detection without causing damage | 199 |
| Porous graphene-COFs composite | Self-template method | $H_2S$ content monitoring | Metal particle imaging | The calculated detection limit of $H_2S$ is 3 ppb | 202 |
| [HOOC]X-COF | Solvothermal method | Absorption of ammonia | Open metal sites Carboxyl functional groups | The adsorption capacity for $NH_3$ is 19.8 mmol $g^{-1}$ | 205 |
| SCU-COF-2 | Room temperature synthesis | Iodine absorption | Introduction of bipyridine groups | Absorption capacity of 6.0 g $g^{-1}$ for iodine gas | 207 |
| PAF-110 | Blending method | Selective adsorption of acetylene from ethylene | The total pore volume is 0.59 $cm^3$ $g^{-1}$ | The acetylene/ethylene adsorption selectivity is 4.5 | 206 |
| COF-105 | Hard tem-plate-assisted method | $SO_2$ Adsorbent | Transition state Sc metal doping | Enhanced interaction between COF and $SO_2$ | 215 |
| PI-COF | Microwave-assisted synthesis | $SO_2$ Adsorbent | Specific surface area up to 1003 $m^2$ $g^{-1}$ | $SO_2$ adsorption capacity reaches 6.3 mmol $g^{-1}$ | 208 |
| COF-DC-8 | Room temperature synthesis | Monitor $NH_3$, $H_2S$, NO and $NO_2$ levels | The surface area is 360 $m^2$ $g^{-1}$ and the pore size is 1.7 nm. | The detection limit for various reducing and oxidizing gases is ppb | 216 |

permeation, effectively excluding ions. Fig. 15b shows that the IISERP-COOH-COF-1 membrane has an ion rejection rate of up to 95%, efficiently desalinating seawater. Zhao *et al.* prepared COF DT-Ex membranes with excellent antifouling and anti-wetting properties for seawater desalination.[226] The seawater filtration rate of COF DT-Ex membranes was more than three times higher than that of existing distillation membranes.

Currently, the use of COFs as filter membranes is limited by harsh synthesis conditions and COF agglomeration.[227] Li *et al.* fabricated a membrane-like thin-film composite membrane for reverse osmosis.[225] As an intermediate layer, COFs provide a stable spatial structure for the membrane, forming a more ordered polyamide separation layer and enhancing the seawater permeability of the membrane (Fig. 15c). Compared to conventional membranes, the COF intermediate layer-reverse osmosis membrane exhibits a 33% increase in seawater permeability, leading to a higher ion rejection rate.

### 4.2. Dye adsorption

Around $7 \times 10^5$ tons of dyes are produced annually for packaging, cosmetics, and textiles, with 10–15% spilling into the water system.[228] COFs can separate these dyes due to their 3–100 nm intrinsic pore sizes.[229] The primary COF-based dye removal methods are membrane technology, which excludes dyes based on the pore size,[230] and the use of COF particles to adsorb dye molecules through charge and size selectivity.[231]

Wang *et al.* used liquid–liquid interfacial polymerization to prepare ABC-structured COF membranes for dye separation, achieving a stable interception rate of 97.57%.[152]. This method showed superior dye adsorption performance and good chemical stability compared to AA-stacked products (Fig. 16a). Wu *et al.* prepared COF hybrid membranes *in situ* with acetic acid, resulting in higher water flux and dye rejection rates (Fig. 16b).[230] Zhang *et al.* developed a core–shell adsorbent by coating carboxyl-functionalized COFs on $Fe_3O_4$ nanoparticles for dye adsorption.[126] In another study, Yang Li *et al.* synthesized a carboxyl-functionalized COF (TzDBd) using a solvothermal method, and assessed its adsorption capacity with bright green (BG) and crystal violet (CV) dyes.[232] Fig. 16c shows that CV/BG is adsorbed through π–π and electrostatic interactions. The carboxyl COF had ultra-fast kinetics, large adsorption capacity, and good reusability.

Cationic dyes are some of the most hazardous dyes. Several attempts have been made to remove these dyes from water.[233,234] Firoozi *et al.* obtained a hybrid material MOF-5/COF (M5C) by hybridizing MOF-5 with a COF.[231] The material has a regular size structure and can quickly remove auramine O (AO) and rhodamine B (RB) cationic dyes through electrostatic interaction, hydrogen bonding and Lewis acid–base interaction.

In a recent study, Liu *et al.* reported the synthesis of a novel COF (COF-TPDD-COOH) that is highly crystalline, fluorescent, and functionalized with glutathione.[72] The unique property of this COF material is that it not only absorbs cationic dyes but also facilitates their monitoring in water. The introduction of glutathione enhances the hydrophilicity, dispersion, and

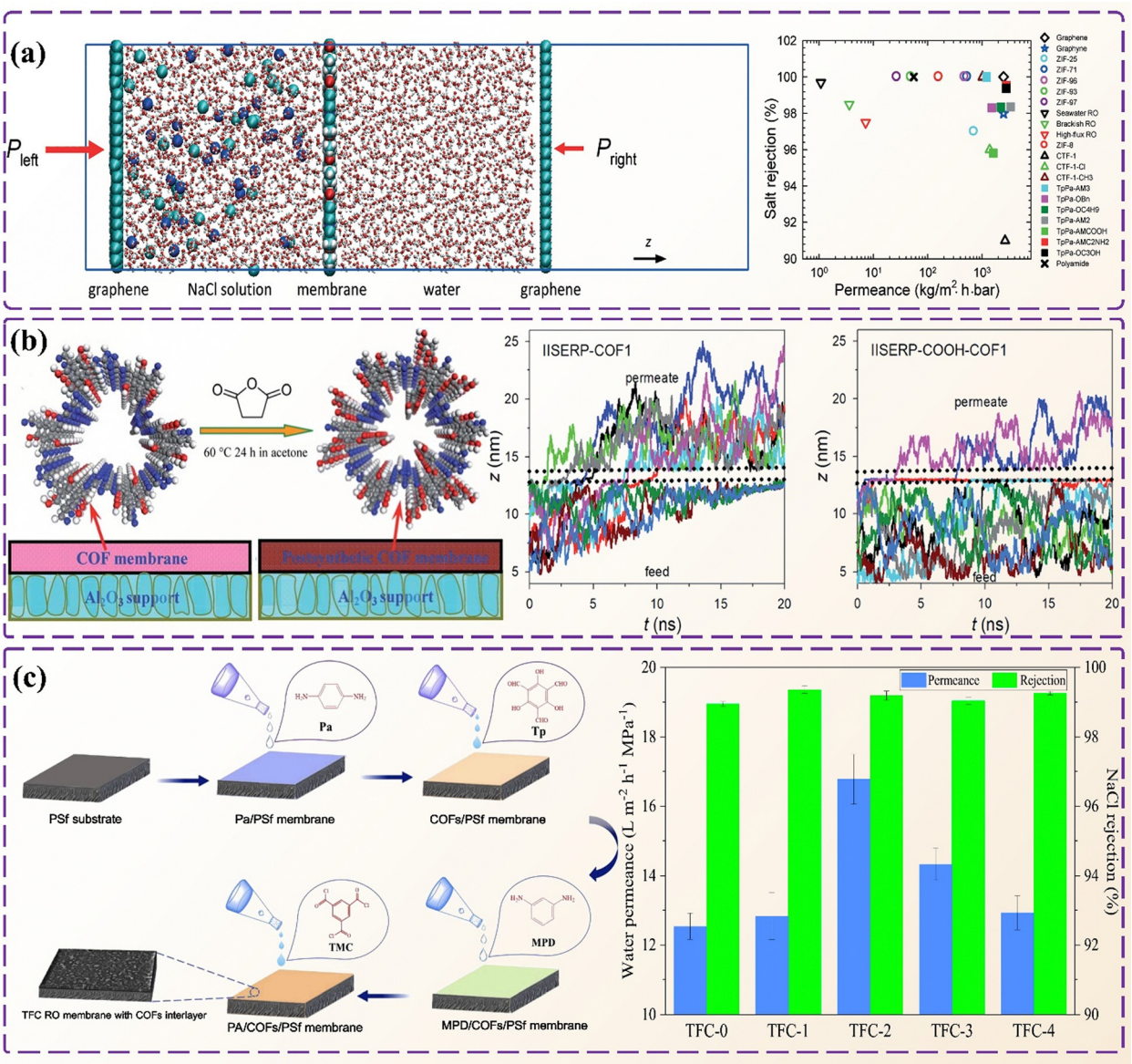


Fig. 15 Application of COFs in water pollution control. (a) Membrane desalination simulation system and performance comparison chart of TpPa-X and other membranes. (b) Trajectories of ions through IISERP-COOH-COF-1 and IISERP-COF-1 membranes. (c) The separation performances of the COF-interlayered reverse osmosis membranes. Reproduced from ref. 223 (Fig. 15a) and ref. 224 (Fig. 15b) with permission from The Royal Society of Chemistry, Copyright 2017 and 2019. Reproduced with permission from ref. 225 (Fig. 15c), Copyright 2020 Elsevier.

electrostatic interaction ability of original COFs, which is highly advantageous for the efficient adsorption of cationic dyes (Fig. 16d).

### 4.3. Heavy metal ion capture

Liquid wastes and high-salt streams containing toxic ions like nickel and cobalt have become a serious environmental hazard.[235] There is a crucial need to remediate heavy metals in industrial wastewater. Since these metals are acidic, highly stable adsorbents are required for remediation.[236] One solution is to use COFs as adsorbents for ion exchange, adsorption, and filtration to capture metal ions from free heavy metal toxic ions.[237] This section discusses the use of COFs to adsorb typical toxic metal ions in water.

Liu *et al.* developed a hollow structure TB-HCOF through an amorphous to crystalline transition strategy, which has the advantages of a large specific surface area and multiple functional sites.[176] The material demonstrates outstanding adsorption capabilities for heavy metal ions and presents the potential for integration with platinum nanoparticles to detect heavy metal ions (Fig. 17a). Li *et al.* utilized amide groups to synthesize COF-TP of aromatic diamines and COF-TE of linear diamines through multi-coordination interactions (Fig. 17b).[238] The fabricated COF-TE exhibited a higher number of amide groups and a stronger capacity for adsorbing $Pb^{2+}$, as it has a

 

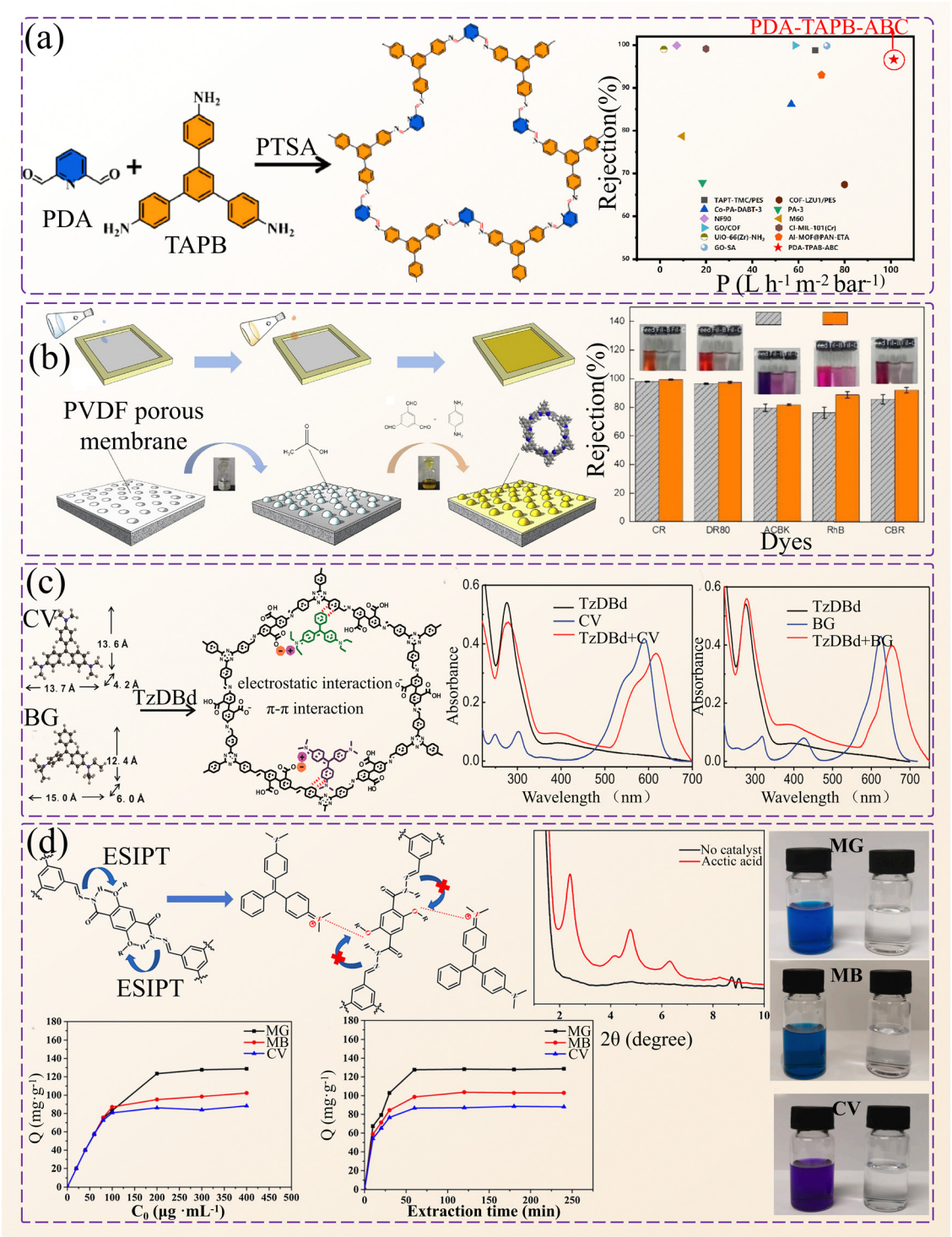


Fig. 16 Application of COFs in water pollution control. (a) Synthesis flow chart of PDA-TAPB-ABC and comparison of water flux and the rejection rate with those of other membranes. (b) The synthesis process of the COF membrane and the water flux and rejection rate of different dyes passing through the COF membrane. (c) Illustration of π–π adsorption and electrostatic interactions between mesoporous TzDBd and CV/BG and the adsorption spectra. (d) Selective mechanism of COF-TPDD-COOH for cationic dyes (CV, MB, and MG), adsorption isotherm model and adsorption kinetic model. Reproduced from ref. 152 (Fig. 16a) and ref. 230 (Fig. 16b) with permission from The Royal Society of Chemistry, Copyright 2017 and 2019. Reproduced with permission from ref. 232 (Fig. 16c), Copyright 2019 American Chemical Society. Reproduced with permission from ref. 72 (Fig. 16d), Copyright 2022 Elsevier.

less aromatic framework, weak π–π stacking structure, and a greater number of internal pores to facilitate the internal diffusion adsorption of $Pb^{2+}$. Cao *et al.* employed a mild solvothermal method to prepare COFs using a Schiff base

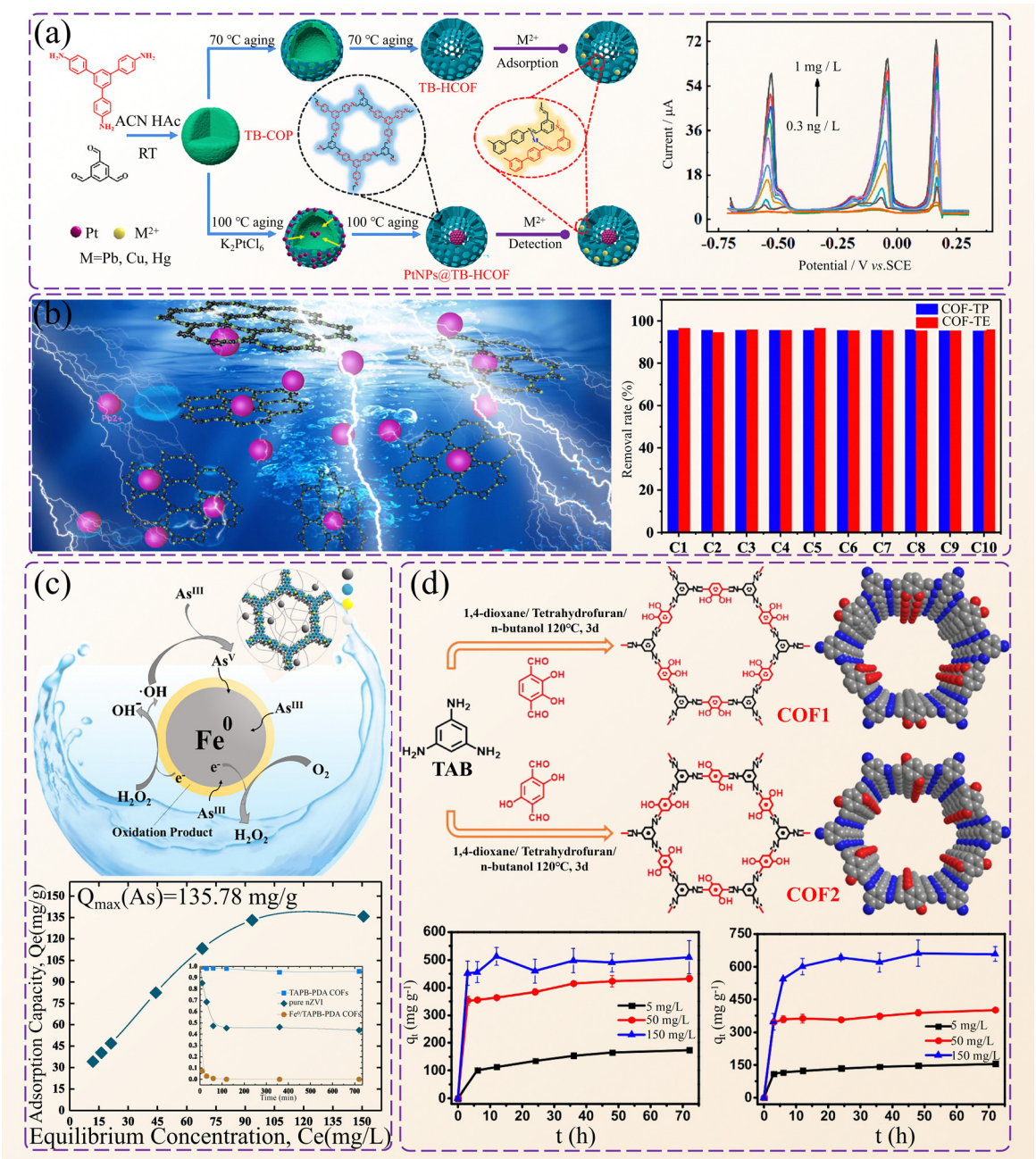


Fig. 17 Application of COFs in water pollution control. (a) The preparation process of TB-HCOF and the adsorption mechanism and efficiency diagram. (b) Schematic diagram of COFs removing $Pb^{2+}$ from solution and their removal rate after regeneration for a few cycles. (c) Mechanism and capture ability of $Fe^0$/COF in removing arsenic from non-ferrous smelting wastewater. (d) Synthesis diagram of COF-1 and COF-2 and a schematic diagram of adsorption kinetics for different Cr(VI). Reproduced from ref. 176 (Fig. 17a), ref. 238 (Fig. 17b), ref. 240 (Fig. 17c) and ref. 241 (Fig. 17d) with permission from Elsevier, Copyright 2024, 2019, 2019 and 2020.

reaction and an imine condensation reaction.[239] The adsorption kinetic curve shows that COF-SH can reach adsorption equilibrium within 48 h, with its adsorption capacity for $Pb^{2+}$ reaching 239 mg $g^{-1}$, exceeding other common adsorbents on the market. In addition, COF-SH also has a high removal rate for other heavy metal ions, the capture capacity of which is equivalent to that of a common single Pb capture adsorbent.

Sun *et al.* recently transformed vinyl-functionalized mesoporous COF (COF-V) into COF-S-SH for the removal of mercury contaminants from water.[168] The microstructure of COF-S-SH shows flexible and dense thiol molecules and thioether chelating arms, which can adsorb 863 and 1350 mg $g^{-1}$ of $Hg^0$ and $Hg^{2+}$, respectively. Huang *et al.* improved the adsorption capacity of COFs for $Hg^{2+}$ by cutting off the disulfide bond based on COF-SH. As a result, a thiol-functionalized magnetic COF

 

(M-COF-SH) with high density and -SH functional groups was obtained.[242] M-COF-SH exhibited an excellent adsorption capacity of up to 383 mg $g^{-1}$ for $Hg^{2+}$, and the adsorption equilibrium could be reached within 10 min. In addition, it was found that M-COF-SH could easily separate the mercury-containing complexes for reuse when rinsed with 0.1% thiourea.

In addition to COF-S-SH, more COFs play a role in heavy metal pollution control. Yu *et al.* combined allyl and hydroxyl functionalized COFs to prepare AH-COF,[243] which showed good removal and detection functions for mercury and $NaBH_4$ solution. The AH-COF can be recycled, hence providing broad application prospects for the practical application of AH-COF. Cui *et al.* integrated the a-based structural unit with a flexible carbohy-drazide linker to obtain a highly luminescent COF (TFPPy-CHYD).[244] The adsorption capacity for $Hg^0$ and $Hg^{2+}$ reached 232 and 758 mg $g^{-1}$. It also has an ultra-low detection limit for mercury and can accurately detect the mercury metal content in water. Wang *et al.* obtained Ag NPs@COF by *in situ* growth of Ag NP carriers through a one-step solution infiltration method,[245] with a removal rate of up to 99% for mercury metal in acidic wastewater and the material can be reused.

Moreover, it is important to consider that the chemical behaviour of arsenic undergoes alteration in water. Liu *et al.* proposed an *in situ* growth strategy to yield $Fe^0$/TAPB-PDA COF composite materials.[240] The porous structure of COFs provides loading sites for $Fe^0$, facilitating arsenic to undergo the oxidation reaction and enhance the adsorption (Fig. 17c) to remove arsenic removal from acidic wastewater.

The functional groups hydroxyl (–OH) and amino ($-NH_2$) are highly effective in capturing chromium(VI). Zhu *et al.* designed a COF that incorporated organic precursors with hydroxyl and amino groups during synthesis.[241] The COF-1 and COF-2 demonstrated a remarkable property to remove Cr(VI) across a wide range of pH values (Fig. 17d). Zhang *et al.* created a novel chitosan-based COF membrane (CM@COF) by introducing hydrazone bonds through ultrasonic treatment and freeze casting.[246] The COF was incorporated into the chitosan film with a unique honeycomb structure, which significantly enhanced the specific surface area of the membrane. At an acidic pH, the CM@COF membrane exhibited an adsorption capacity of 388 mg $g^{-1}$ for Cr(VI).

Da *et al.* prepared cationic covalent organic nanosheets, which were highly effective for absorbing radioactive elements such as $ReO^{4-}$ and $TcO^{4-}$ due to their strong electrostatic attraction and hydrogen bonding properties.[247] The design of these cationic nanosheets provides a high surface area and positive charge distribution, which enhances their interaction with negatively charged radioactive ions. Guo *et al.* used mechanochemical methods to synthesize TpBD nanosheets with many oxygen-containing and nitrogen-containing functional groups to remove uranium (U(VI)) through chemical adsorption and inner sphere surface complexation.[136] It was found that TpBD nanosheets possessed a significantly higher adsorption efficiency for U(VI) than other existing adsorbents.

### 4.4. Removal of organic matter

Organic pollutants result from heavy industrialization activities, manifesting in diverse forms and sources such as industrial wastewater, agricultural runoff, and urban sewage. The treatment of organic contaminants from water can be achieved through four methods: membrane filtration, interfacial adsorption, magnetic solid phase extraction, and solid phase microextraction.[248] Magnetic COFs, combining the advantages of magnetic nanoparticles and COFs, have gained considerable attention for removing organic pollutants from water.[249]

You *et al.* prepared $Fe_3O_4$@COF by a solvothermal method and magnetic separation for adsorbing bisphenols (BPA and BPAF) in water through π–π interactions and the bonding between phenolic substances and COFs.[174] The adsorption rate for bisphenols is comparable to that of commercially available adsorbents in the market (Fig. 18a). Catechol is a toxic chemical compound commonly found in pesticides, electroplating additives, and fragrances. Ji *et al.* prepared phenylboronic acid-functionalized COF (DhaTab-PBA) using a thiol–ene click strategy.[250] DhaTab-PBA effectively removes catechol due to its strong π–π bond interactions and porous structure. Lv *et al.* synthesized $TpMAC_{(1\,mL)}$ and $TpMAC_{(3\,mL)}$ using melamine (MA) and 1,3,5-triformylphloroglucinol (Tp) as raw materials, which demonstrated high efficiency (above 80%) in degrading phenol under photocatalysis, and the efficiency can be retained after five repeated uses.[251] The efficient degradation of phenol by TpMAC underscores its potential application in wastewater treatment and environmental remediation, providing a sustainable solution to mitigate phenolic pollutants.

Polychlorinated biphenyls (PCBs) are highly toxic and hazardous compounds favoured in industrial manufacturing such as insulation, lubricants, and coolants. Many countries have prohibited their utilization due to the adverse effects on human health and the environment.[252] Gan *et al.* prepared ultrathin CONs through monomer condensation polymerization on a large scale.[139] The yielded CONs showed remarkable photocatalytic performance of organic pollutant degradation in the aqueous phase. There are abundant superoxide radicals ($O_2^-$) in CONs, which explains the high organic matter photocatalytic degradation efficiency of CONs. Lu *et al.* reported a 3D TpTAM-COF using 1,3,5-triformylphloroglucinol (Tp) and tetrakis(p-aminophenyl)methane (TAM) as monomers.[253] The 3D-structured COF molecules exhibit good stereoselectivity for PCBs and can perform solid-phase microextraction of PCBs. Compared to commercial PCB extraction agents, TpTAM-COF-coated fibres show higher selectivity for PCBs. Zhou *et al.* used 2,5-dimethoxybenzaldehyde (DB) as a modified raw material to prepare TAPB-DMTP-DB COF, which exhibited excellent enrichment factors (4400–11 360) for polybrominated biphenyls (PBBs) to enable an accurate detection of PBB levels in water(Fig. 18b).[37]

Certain species of marine microalgae produce a toxic substance known as okadaic acid, which humans can consume *via* the food chain and it causes significant harm to human

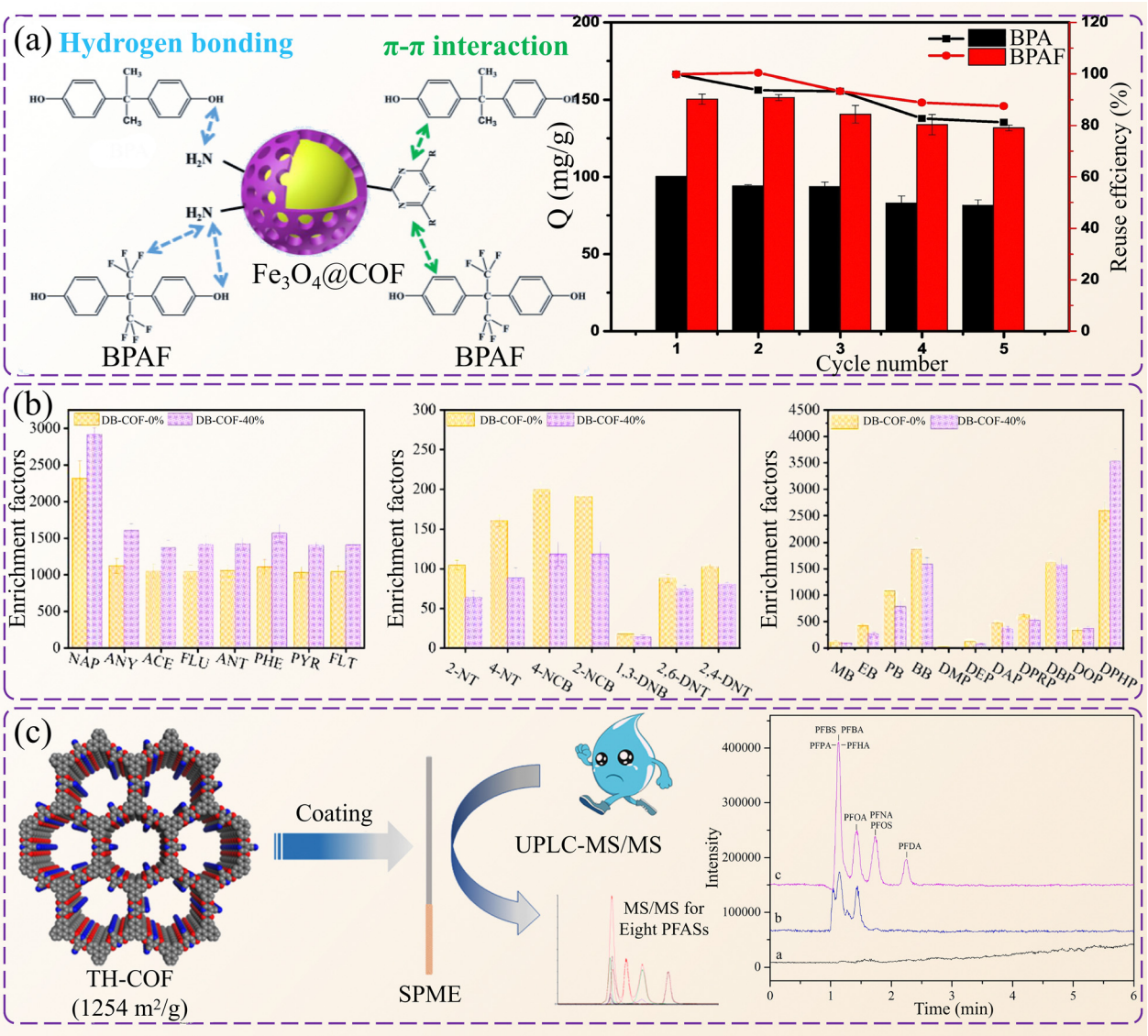


Fig. 18 Application of COFs in water pollution control. (a) The adsorption mechanism and ability of BPAF and BPA on $Fe_3O_4$@COF and the adsorption process of bisphenol on $Fe_3O_4$@COF. (b) Comparison of enrichment performance between the DB-COF-0%-coated fibre and DB-COF-40%-coated fibre for PAHs, nitrobenzenes and PAEs. (c) Synthesis and adsorption mechanism of TH-COF and solid-phase extraction efficiency of PFAS in groundwater. Reproduced from ref. 174 (Fig. 18a), ref. 37 (Fig. 18b), and ref. 131 (Fig. 18c) with permission from Elsevier, Copyright 2020, 2022, and Copyright 2020.

health.[254] Salonen *et al.* developed a highly efficient adsorbent material called TpBD-$Me_2$ COF,[255] which can remove okadaic acid from seawater, even at 19 °C. The TpBD-$Me_2$ COF had a much higher adsorption capacity than other adsorbents, with a capacity of up to 279 mg $g^{-1}$. The desorption process of okadaic acid from TpBD-$Me_2$ COF can be conducted using acetonitrile and 70% ethanol as solvents, which allows the material to be reused effectively.

Perfluorinated and polyfluorinated alkyl substances (PFASs) are commonly utilized in waterproofing agents and foam fire extinguishers. Due to their low reactivity and concentration, eliminating these substances through adsorbent materials or membrane filtration methods can present significant challenges. Ji *et al.* revealed that COFs containing primary amines linked with imine can efficiently and rapidly adsorb PFAS at low concentrations.[256] Besides, Ji *et al.* prepared a TH-COF through microwave-assisted synthesis.[131] This COF material has special intermolecular hydrogen bonds and an ultra-large specific surface area between pyridine N atoms. It was found that hydrogen bonding improves the efficiency of solid-phase microextraction of perfluoroalkyl substances (PFASs). The large specific surface area provides more reaction points for PFAS adsorption, thereby increasing the capacity of solid-phase microextraction (Fig. 18c). The dioxin-linked TH-COF fiber has a wide analytical range and is highly accurate in detecting PFASs.

### 4.5. Drug removal

Pharmaceutical residues in water bodies usually come from medical wastewater discharge, pharmaceutical production wastewater, household pharmaceutical wastewater and other

 

sources.[257] Drug residues in water pose a serious threat to aquatic life.[258,259]

Diclofenac sodium is a commonly used nonsteroidal anti-inflammatory drug (NSAID) that belongs to the fenac class of drugs. Recently, a study conducted by Huang *et al.* revealed that magnetic COF (MCOF) composites can effectively adsorb diclofenac sodium from water.[260] MCOFs had a high specific surface area and magnetic separation ability of magnetic nanoparticles. Once the MCOFs complete the adsorption of diclofenac sodium in water, a magnetic field can be applied to separate it from the water (Fig. 19a). The study also showed that the MCOF demonstrates good repeatability in drug removal.

Sulfonamides (SAs) are synthetic antibacterial drugs with a broad antibacterial spectrum. Ahmed *et al.* used ZIF-8 as a template to prepare highly porous covalent organic polymers with mesopores (MT-MCTP),[261] which contained a mesoporous structure to adsorb SAs through π–π interactions and hydrogen bonding interactions effectively (Fig. 19b). The maximum

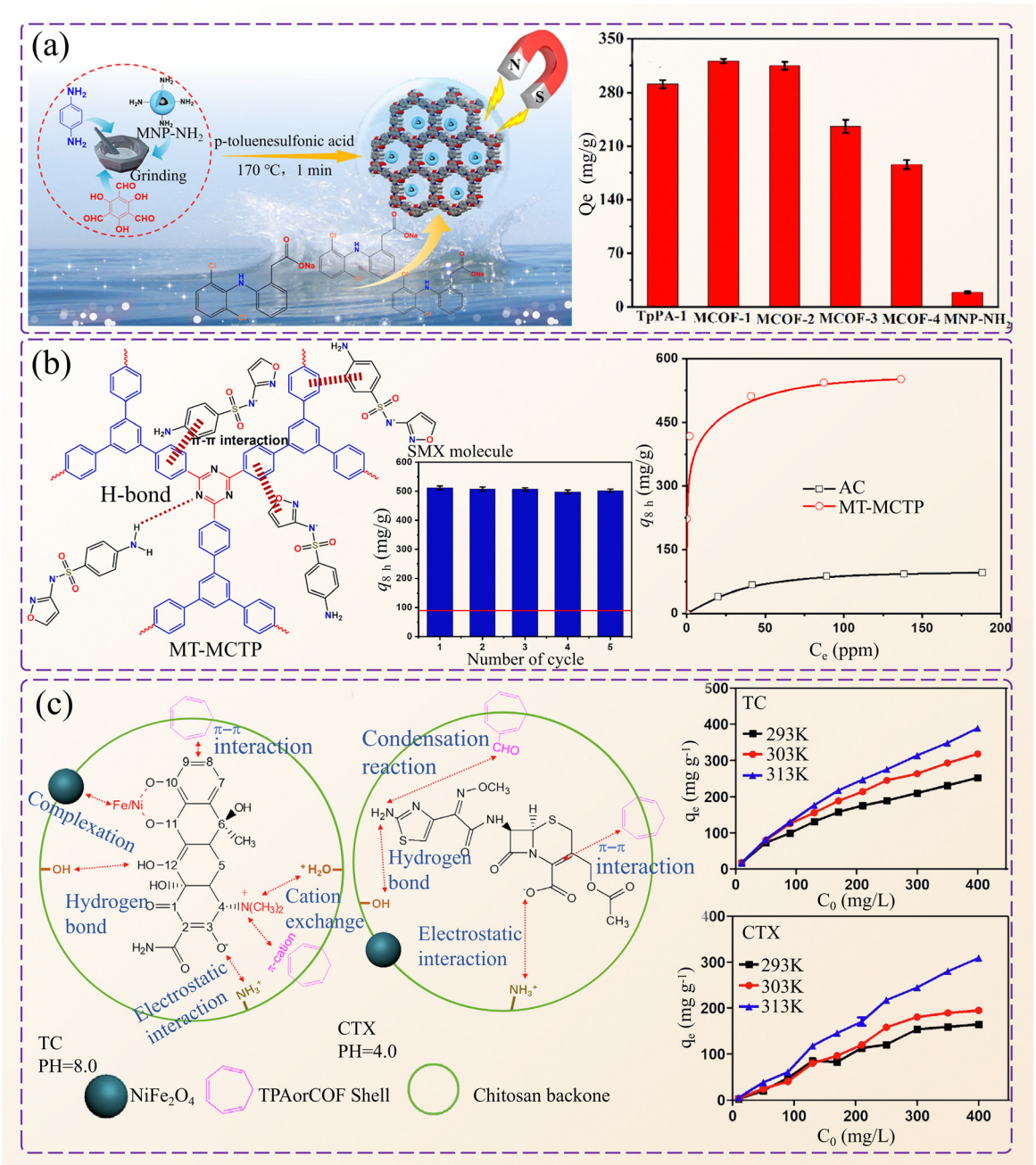


Fig. 19 Application of COFs in water pollution control. (a) Mechanism and ability of magnetic COFs to remove diclofenac sodium from water. (b) Schematic diagram of the SMX adsorption mechanism, AC adsorption efficiency and repeatable service life. (c) Schematic diagram of TC and CTX adsorption on NCCT. Reproduced with permission from ref. 260 (Fig. 19a), Copyright 2019 American Chemical Society. Reproduced from ref. 261 (Fig. 19b) and ref. 262 (Fig. 19c) with permission from Elsevier, Copyright 2024 and Copyright 2019.

Table 6 Application of COFs in water pollution control

| Type | Synthesis method | Application | Feature | Efficiency | Ref. |
|---|---|---|---|---|---|
| TpPa-AMCOOH | Blending method | Desalination | Contains hydrophilic functional groups | Salt removal rate exceeds 98% | 223 |
| IISERP-COOH-COF-1 | Solvothermal method | Desalination, ion retention rate up to 95% | Carboxyl functionalization | Excellent ion rejection | 224 |
| COF DT-Ex | Room temperature synthesis | Seawater desalination | Regularly arranged mesopores and hydrophobic channels | The desalination rate remained at 99.99% after 100 hours of operation | 226 |
| TFC-2 | Self-template method | Seawater desalination | PA thermoselective layer hybridization | NaCl retention rate reaches 99.2% | 225 |
| PDA-TAPB-ABC | Room temperature synthesis | MB is trapped and dye is adsorbed | ABC stacking structure | The stable retention rate of MB is 97.57% | 152 |
| PVDF-COFs | Ultrasonic chemical method | Dye adsorption | Pore diameter 100 nm<br>Multi-cage structure | RhB removal rate 89.7%<br>CR removal rate 99% | 230 |
| CTF/$Fe_2O_3$ | Microwave-assisted synthesis | Removal of organic dyes | Specific surface area is 1149 $m^2\ g^{-1}$<br>Total pore volume is 1.5 $cm^3\ g^{-1}$ | The MO adsorption capacity reached 291 mg $g^{-1}$ | 126 |
| Carboxyl-functionalized COF (TzDBd) | Solvothermal method | Adsorption of CV/BG | Carboxyl functionalization<br>Mesoporous structure | The maximum adsorption capacities for CV and BG were 307.7 and 276.1 mg $g^{-1}$ | 232 |
| MOF-5/COF | Solvothermal method | Removal of cationic dyes | Cubic structure<br>BET is 7.025 $m^2\ g^{-1}$ | The adsorption amounts of AO and RB are 17.95 and 16.18 mg $g^{-1}$ | 231 |
| COF-TPDD-COOH | Ultrasonic chemical method | Monitoring of cationic dye content and adsorption | Glutathione (GSH) functionalization<br>Overlapping stacking structure | LOD is 0.003–0.007 μg $mL^{-1}$<br>Adsorption capacity is 88.02–128.64 mg $g^{-1}$ | 72 |
| TB-HCOF | Soft template method | Detect Pb, Cu and Hg contents with an accuracy of up to 0.11 | Hollow structure<br>BET is 139.9 $m^2\ g^{-1}$ | The maximum adsorption amounts of $Pb^{2+}$, $Cu^{2+}$ and $Hg^{2+}$ were 766.28, 759.32 and 640.83 mg $g^{-1}$ | 176 |
| COF-TE | Mechanochemical synthesis | Capturing $Pb^{2+}$ | Amide group<br>2D sheet | $Pb^{2+}$ saturated adsorption capacity is 185.7 mg $g^{-1}$ | 238 |
| COF-SH | Solvothermal method | Selective capture of relatively soft metal ions | Irregular polymers accumulate into clumps<br>Pore diameter is 1.65 nm | The maximum adsorption capacity of Pb(II) is 239 mg $g^{-1}$ | 239 |
| COF-S-SH | Solvothermal method | Adsorption of $Hg^0$ and $Hg^{2+}$ | Dense chelating groups<br>Specific surface area is 1152 $m^2\ g^{-1}$ | The adsorption capacities of $Hg^{2+}$ and $Hg^0$ were 1350 and 863 mg $g^{-1}$ | 168 |
| M-COF-SH | Room temperature synthesis | Capturing $Hg^{2+}$ | Thiol functionalization<br>Paramagnetic | $Hg^{2+}$ Maximum adsorption capacity is 383 mg $g^{-1}$ | 242 |
| AH-COF | Solvothermal method | Capturing $Hg^{2+}$ | Overlapping structure<br>BET is 753 $m^2\ g^{-1}$ | Hg removal rate over 95% | 243 |
| TFPPy-CHYD | Solvothermal method | Detect mercury content and adsorb $Hg^0$ and $Hg^{2+}$ | Specific surface area is 763 $m^2\ g^{-1}$<br>AA stacking structure | The adsorption capacities of $Hg^0$ and $Hg^{2+}$ are 232 and 758 mg $g^{-1}$ | 244 |
| Ag NPs@COF | One-step *in situ* synthesis | Mercury removal | Silver nanoparticle doping<br>Microporous structure | Mercury removal rate reaches 99% | 245 |
| $Fe^0$/COFs | In situ growth method | Adsorption of As(III) | Spherical stacking structure<br>BET is 131.49 $m^2\ g^{-1}$ | The maximum adsorption capacity of As(III) was 135.78 mg $g^{-1}$ | 240 |
| COF2 | Solvothermal method | Adsorption of Cr(VI) | AA stacking mode<br>BET is 28.79 $m^2\ g^{-1}$<br>Decomposes at 225 °C | Cr(VI) adsorption capacity reaches 649.35 mg $g^{-1}$ | 241 |
| CM@COF | Ultrasonic chemical method | Adsorption of Cu(II) and Cr(VI) | Hierarchical porous structure<br>π–π stacked continuous layer structure | The adsorption capacities of Cu(II) and Cr(VI) were 144 and 388 mg $g^{-1}$ | 246 |
| iCON | Solvothermal method | Absorb radioactive elements | Corrosion resistance<br>AA stacking mode<br>Cationic soft acid guanidine group | The adsorption capacity of $ReO4^-$ reached 437 mg $g^{-1}$ | 247 |
| TpBD nanosheets | Mechanochemical synthesis | Removal of U(VI) | BET is 139 $m^2\ g^{-1}$ and pore size is 14 Å | Adsorption equilibrium is reached within 0.5 hours, and the adsorption capacity is 167 mg $g^{-1}$ | 136 |
| $Fe_3O_4$ @COF | Blending method | Adsorption of bisphenol | Saturation magnetization is as high as 49.6 emu $g^{-1}$<br>BET is 335.2 $m^2\ g^{-1}$ | The maximum adsorption capacity of BPA and BPAF reached 140 and 290.4 mg $g^{-1}$ | 174 |

 

Table 6 (*continued*)

| Type | Synthesis method | Application | Feature | Efficiency | Ref. |
|---|---|---|---|---|---|
| COF DhaTab-PBA | Solvothermal method | Adsorption and removal of catechol | Phenylboronic acid functionalized<br>AA model structure | The maximum adsorption of catechol was 133.3–151.5 mg $g^{-1}$ | 250 |
| TpMA | Solvothermal method | Photocatalytic degradation of organic pollutants | Thin ribbon structure<br>High crystallinity | The photodegradation rate still reaches 87.6% after multiple cycles | 251 |
| CON | Ultrasonic chemical method | Photocatalytic degradation of organic pollutants | BET is 972 $m^2$ $g^{-1}$<br>High number of active functional groups | The photodegradation efficiency of MB is as high as 99.8% | 139 |
| TpTAM-COF | Solvothermal method | Solid phase extraction of PCB | β-Ketoamine framework<br>BET is 537.2 $m^2$ $g^{-1}$ | The recovery rate of PCBs was 84.8 ± 7.8% | 253 |
| TAPB-DMTP-DB COF | Room temperature synthesis | Accurate quantification of polybrominated biphenyls | Layered stacking structure<br>Good hydrophobicity<br>Many methoxy functional groups | PBB enrichment factor is 4400–11 360<br>Detection limit is as low as 0.04–0.28 ng $L^{-1}$ | 37 |
| TpBD-$Me_2$ COF | Solvothermal method | Okadaic acid adsorption | BET is 468 $m^2$ $g^{-1}$<br>Pore size is only 2 nm<br>Linear structure | The maximum adsorption capacity of okadaic acid is 61 mg $g^{-1}$ | 255 |
| X%[$NH_2$]−COFs | Solvothermal method | PFAS Removal | Many amine functional groups<br>Two-dimensional ultra-thin structure | Removed more than 90% of 12 of 13 PFAS | 256 |
| TH-COF | Microwave-assisted synthesis | PFAS Removal | BET is 1254 $m^2$ $g^{-1}$<br>Network structure<br>AA stacking mode | The recovery rate is 89.5%–105%<br>Detection precision error ≤7.9% | 131 |
| MCOF-2 | Blending method | Removal of DS from water | Non-porous magnetic nanoparticles aggregate<br>Saturation magnetization value is 21.7 emu $g^{-1}$ | DS removal efficiency >97%<br>Adsorption equilibrium is reached within 20 minutes | 260 |
| MT-MCTP | Hard template method | Sulfonamide adsorption | Microporous structure<br>Amorphous structure | The adsorption capacity for sulfonamides is 534–557 mg $g^{-1}$ | 261 |
| $NiFe_2O_4$-COF-chitosan-terephthalaldehyde (NCCT) | Ultrasonic chemical method | Adsorbed antibiotics | Grafted chitosan molecules<br>Ordered single-crystal structure | The maximum adsorption capacities of TC and CTX were 388.52 and 309.26 mg $g^{-1}$ | 262 |
| RT-iCOF | Room temperature synthesis | Adsorption of diclofenac sodium | ABC staggered stacking structure<br>BET is 69 $m^2$ $g^{-1}$ | The adsorption efficiency of DCF after multiple cycles is still higher than 90% | 154 |

adsorption capacities for sulfamethoxazole and sulfachlorpyridazine are 557 and 534 mg $g^{-1}$, respectively. MT-MCTP can be recycled after use and will not cause additional harm to the environment. Akhzari *et al.* used molecular dynamics to simulate the adsorption capacity of a functionalized COF (F-COF) for antibiotic drugs and proved that COFs with a pore-based structure have higher pollutant removal capacity.[263]

Antibiotics such as tetracycline and cefotaxime are widely used to cure infections. However, improper disposal of antibiotics in water bodies can develop drug-resistant microorganisms, posing serious risks to ecology and human health.[264,265] To address this issue, Li *et al.* developed a novel nanocomposite membrane made of $NiFe_2O_4$-COF-chitosan-terephthalaldehyde (NCCT) to eradicate antibiotics from water.[262] The adsorption mechanism of antibiotics on NCCT is based on cation exchange between the protonated amino group in the antibiotic and the π electrons on NCCT (Fig. 19c), allowing complete separation of antibiotics in 2 seconds. Li *et al.* recently studied a room temperature-induced COF (RT-iCOF) as an adsorbent for diclofenac sodium (DCF).[154] The researchers used ion exchange, hydrogen bonding, electrostatic force, and π–π interactions to adsorb DCF into the RT-iCOF pore structure. Compared to traditional adsorbents, the RT-iCOF has the highest adsorption rate for DCF and retains over 90% adsorption efficiency after five cycles (Table 6).

# 5. Applications of COFs and their derivatives in the treatment of soil pollution

Soil pollution can adversely affect plant growth and development, ultimately leading to decreased yields and a diminished quality of agricultural production. Pollutants can also penetrate groundwater or be washed into rivers and lakes by rain, thereby causing water source pollution.[266–268] This section discusses the use of COFs to absorb and degrade organic pollutants and remove heavy metals and radioactive elements.[269,270]

## 5.1. Adsorption and degradation of organic pollutants

There are various types of toxic organic pollutants in soil, including but not limited to pesticides,[271] chlorinated organic

compounds,[272] volatile organic compounds,[273] polycyclic aromatic hydrocarbons,[274] phenolic compounds,[275] and phthalates.[276] Koonani *et al.* utilized melamine-based COFs and zinc-based MOFs to develop a new adsorbent (Zn-MOF/COF),[73] with a high extraction efficiency in extracting and enriching polycyclic aromatic hydrocarbons from contaminated soil. This hybrid material combines the advantages of COF tunable pore structures and MOF high surface area, resulting in a synergistic effect that enhances adsorption capabilities. The recovery rate of soil after using this fibre reached approximately 10%, indicating significant remediation potential for PAH-contaminated environments. The 3D TpTAM-COF developed by Lu *et al.* performed a microextraction of PCBs in soil and water with an extraction rate of 93%.[253] Fig. 20a shows that TpTAM-COF extracts PCBs through interactions such as spatial selectivity, hydrophobicity, halogen bonds, and π–π conjugation. PAE as an important organic pollutant in plastics shows a great impact on human endocrine. Wang *et al.* constructed three different CTFs through a simple Friedel–Crafts reaction.[277] The high specific surface area and porosity of CTFs facilitated their use as solid phase microextraction (SPME) coatings to extract PAE and yield positive outcomes (Fig. 20b). Compared to commercial fibres, the extraction rate improved by 100% and the extraction efficiency remained consistent even after more than 100 reuses.

### 5.2. Removal of radioactive elements and heavy metals

Radioactive elements like uranium, thorium, and potassium-40 can release harmful radioactive rays through natural radioactive decay.[280,281] The radiation contamination of these substances can significantly damage the environment and human health. The consequences of radiation-contaminated land can be irreversible, posing a long-lasting threat.[282,283]

Li *et al.* synthesized a new amide-based COF material (COF-TH) by a solvothermal method,[278] which showed significant selectivity for Pb among heavy metals in the soil, with a maximum Pb adsorption capacity of 189 mg $g^{-1}$. Pot experiments confirmed that only a dosage of 2% was needed to significantly reduce the risk of heavy metal leaching from sludge while promoting plant growth and maintaining microbial diversity (Fig. 20c).

Liu *et al.* modified a MCOF with a new deep eutectic solvent (DES) to obtain a new material (MCOF-DES),[284] which can selectively separate and determine $Cu^{2+}$ in complex matrices in soil. The $Cu^{2+}$ recovery rate reached 90.6%. Zhou *et al.* prepared FeO@COF@SH with the help of a thiol-alkyne "click" reaction,[279] and achieved good anti-interference ability for complex matrices such as soil. The contents of Cd, Hg, Pb and Bi in soil samples of Jianghan University detected were 0.17, 0.06, 24.6 and 0.35 μg $g^{-1}$, respectively. These findings demonstrate a higher accuracy level than those of traditional measurement methods, indicating significant potential for the precise analysis of trace heavy metals in complex environmental samples (Fig. 20d and Table 7).

## 6. The advances in big data and machine learning empowered exploration of COFs

The rapid development of computing technology has facilitated the amassing of large amounts of big data. The discovery of novel materials serves as a critical impetus for societal development, as well as scientific and technological innovation.[285] Artificial intelligence (AI) is a recently evolved technical science that focuses on studying and developing data systems and computing technologies. Machine learning (ML) has emerged in materials research with the advent of the big data era and is recognized as a valuable tool for exploring new materials.[286,287] Fig. 21a shows a commonly used ML algorithm in materials science. The application fields of ML algorithms include reverse design of materials, multi-objective optimization, process optimization, phase change research, phase diagram construction, auxiliary microscopic characterization, identification and classification, and material property prediction.[29,288,289] In this section, we will elaborate on the impact of big data on COF research in three parts.

### 6.1. Data enhanced structural optimization of COFs

COFs possess predictable and customizable structural frameworks. Ball *et al.* synthesized a phenanthroline-based COF (PACOF) to be used as cathode material for rechargeable zinc-ion batteries (ZIBs), where the electronic structure was analyzed by density functional theory (DFT).[290] They combined previous findings to predict a new type of COF (QPACOF) with phenanthroline and quinone structures (Fig. 21b). By leveraging ML to study COF structures, insights can be gained into producing optimal cathode materials for ZIB applications. Pakhira *et al.* conducted first-principles calculations and discovered that incorporating the first row transition metal elements into a COF structure can rectify its electronic imbalance issue.[291] By intercalating various transition metal (TM) elements with triazine COF, 31 types of distinct COF materials (COF-TM-*x*) were predicted using computer simulations. Fig. 21c displays the optimized crystal structure and energy band structure of the initial COFs. Upon evaluating its properties, it was observed that the band gap and density of states (DOS) of COF-TM-*x* can be manipulated by modifying the type and concentration of the inserted transition element. By forecasting the binding energy of COF-TM-*x*, all 31 COF-TM-*x* variations with a high density of active metal sites and stable structures were prepared.

### 6.2. Performance prediction of COFs

COFs and other porous materials such as MOFs and porous polymer networks (PPNs) have been widely used as molecular building blocks.[293] There is a significant focus on developing COF databases to predict their performance. Park *et al.* introduced the PMT transformer (Fig. 21d), a multi-modal transfer learning model that uses pre-training on more than 1.9 million models in its database and fine-tuning to achieve state-of-the-art performance in predicting various properties of porous

 

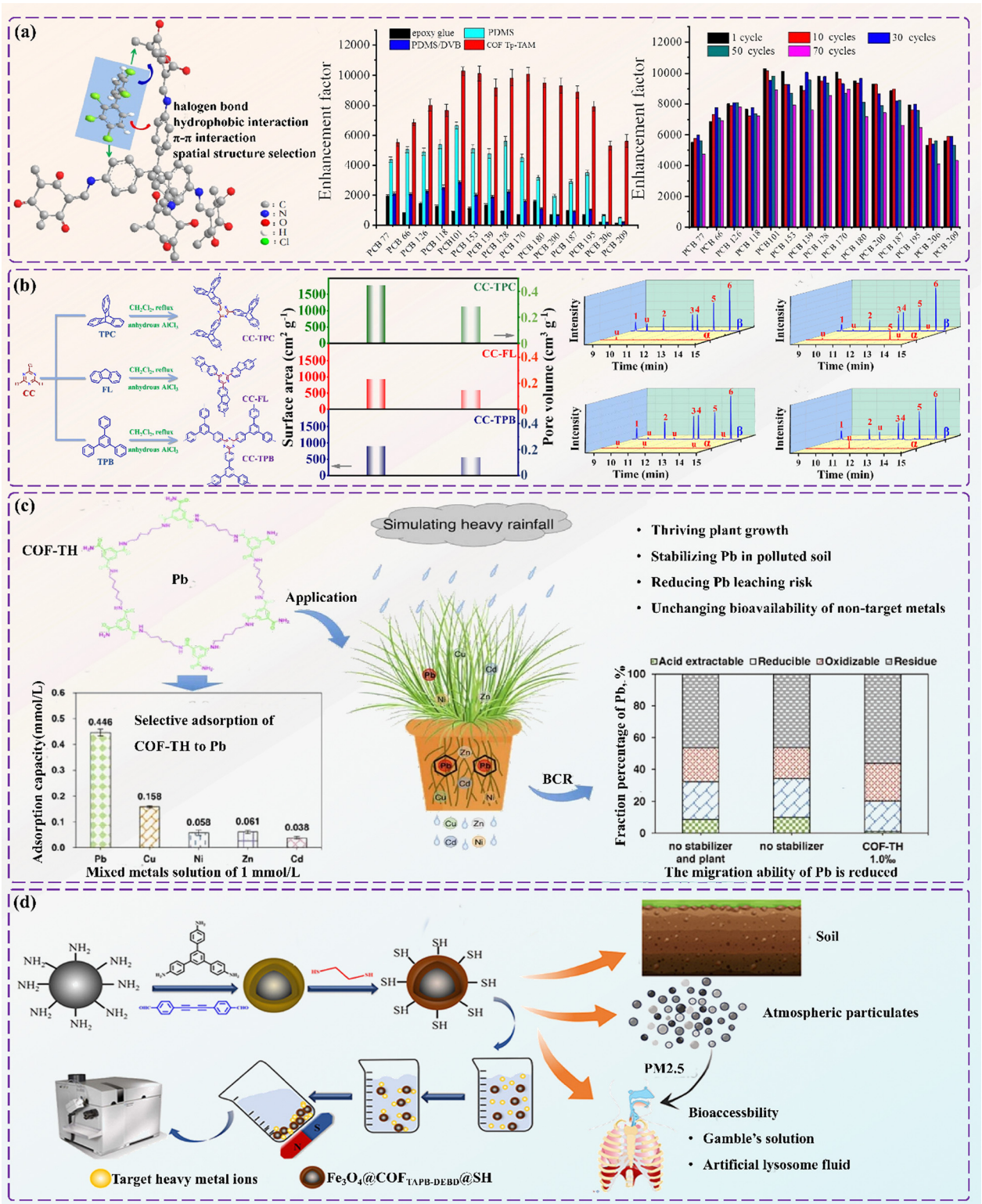


Fig. 20 Application of COFs in soil pollution control. (a) Various action mechanisms of PCB in TpTAM-COF solid-phase microextraction, extraction effects and extraction cycle times. (b) Schematic diagram of the synthesis and pore volume of CTFs and typical chromatograms of PAEs in different samples. (c) COF-TH exhibits obvious selectivity for Pb in soil and promotes active plant growth. (d) The ability of $Fe_3O_4$@$COF_{TAPB\text{-}DEBD}$@SH to tolerate complex matrices and its detection accuracy. Reproduced from ref. 253 (Fig. 20a), ref. 277 (Fig. 20b), ref. 278 (Fig. 20c) and ref. 279 (Fig. 20d) with permission from Elsevier, Copyright 2022, 2022, 2024 and Copyright 2024.

Table 7 Application of COFs in soil pollution control

| Type | Synthesis method | Application | Feature | Efficiency | Ref. |
|---|---|---|---|---|---|
| Zn-MOF/COF | Solvothermal method | Solid phase microextraction of PAH | Many imine groups<br>Rhombus structure arrangement<br>BET is 51.37 $m^2$ $g^{-1}$ | Relative recoveries for soil samples were 91.1–110.2% | 73 |
| CTF | Ultrasonic chemical method | Solid phase microextraction (PAE) | BET is 1768 $m^2$ $g^{-1}$<br>Water contact angle is 102 °C<br>Uniform porous structure | PAE enrichment factors (978–2210), low detection limits (0.027–0.10 ng $g^{-1}$) | 277 |
| COF-TH | Ultrasonic chemical method | Selective adsorption of Pb in soil | With amide functional groups<br>Flake-like stacking structure | The maximum adsorption capacity of Pb is 189 mg $g^{-1}$ | 278 |
| MCOF-DES | Ultrasonic chemical method | Selective separation and determination of $Cu^{2+}$ in soil | The specific surface area is 71.22 $m^2$ $g^{-1}$<br>Pore diameter is 17.58 nm | The enrichment factor of $Cu^{2+}$ was 30 and the detection limit was 0.16 μg $L^{-1}$ | 284 |
| FeO@COF@SH | Solvothermal method | Quantification of trace heavy metals in soil | Particle size is about 200 nm<br>Obvious core-–shell structure | The test results of Cd, Hg, Pb and Bi contents in soil samples were 0.17, 0.06, 24.6 and 0.35 μg $g^{-1}$ | 279 |

materials.[292] Utilizing a rich database of MOFs, Park *et al.* applied density functional theory (DFT) to predict the band gap values of COFs. Their findings revealed that the band gap values of COFs are directly proportional to the size of their atoms and the attention scores they receive. Hou *et al.* converted COF-300 into eCOF-300 through an interpenetrating cyclization reaction based on extensive quantum chemical calculations and molecular dynamics (Fig. 22a).[294] This finding significantly advanced the research in expanding the application range of COF materials in higher-temperature environments.

ML plays a key role in applying COFs to control air pollution. Wang *et al.* calculated the interaction force between $SO_2$ and COF through DFT and found that the adsorption of $SO_2$ by COF-105 with the addition of TBPS would be greatly enhanced.[215] Lu *et al.* used DFT analysis and confirmed that the transition metal is mainly fixed between the interlayer quinone oxygen atoms,[196] explaining why DQTP has the highest photocatalytic efficiency for $CO_2$. Yang *et al.* calculated the pore size distribution of $[HOOC]_X$-COF using NL-DFT and confirmed the high capture ability of $[HOOC]_{17}$-COF for ammonia through the adsorption theoretical model.[205] Han *et al.* also used a first principle approach along with regular Monte Carlo simulations to predict the hydrogen ($H_2$) absorption characteristics of six COFs (Fig. 22b).[295] The prediction results showed similarities to the $H_2$ absorption characteristics of COF-5, which is the only COF with experimental data available.

In addition, ML is also being gradually applied to predict the control effect of COFs on pollutants in soil and water environments. Li *et al.* used quenched solid phase density functional theory (QSDFT) to fit nitrogen adsorption–desorption and obtained the pore size distribution of TzDBd to be around 4.0 nm.[232] The adsorption capacity of CV and BG simulated using the Langmuir adsorption model was consistent with the actual data, confirming that the mesoporous structure increased the adsorption capacity of the dye. Li *et al.* used pseudo-first-order, pseudo-second-order and Weber–Morris models to simulate the adsorption process of $Pb^{2+}$ by COF-TH.[278] The theoretical simulation results were consistent with the actual results, confirming that COF-TH mainly chemically adsorbs $Pb^{2+}$.

## 6.3. Reverse design of COFs

COFs are highly customizable members of the porous organic material family.[298] Reverse design relies on intelligent algorithms to input expected parameters and reversely solve the structure. Haldar *et al.* modelled COFs and conducted *ex situ*/*in situ* mechanism research to determine the COF structure which transfers electrons more efficiently by adding strong redox groups (*e.g.* nitroxyl and viologen).[299] The interaction between metal ions and COF substrates can be effectively evaluated through advanced methodologies. A deeper understanding of the mechanisms underlying guest ion behaviour in batteries can be achieved by leveraging big data calculations. The integration of comprehensive databases with ML techniques has proven to be a powerful strategy for accelerating the synthesis and design of COF-based electrodes.[300]

Altintas *et al.* combined molecular simulations and ML to extract quantitative structure–property relationships from molecular simulation results and provide new guidelines for the reverse design of new COFs.[301] GCMC simulation is a highly effective technique that can be used to calculate the adsorption of $H_2$ by COFs, along with their heat of adsorption and transport capacity. Porphyrin COFs, 2D materials with strong π conjugated bonds and remarkable electrical and thermal stability, have attracted significant attention for various applications. Currently, researchers are focusing on the magnetic and electrical aspects of these materials.[302]

Wu *et al.* proposed a new type of 2D porphyrin COF semiconductor material using first-principles calculations, ML fitting potentials, and solving the phonon Boltzmann

 

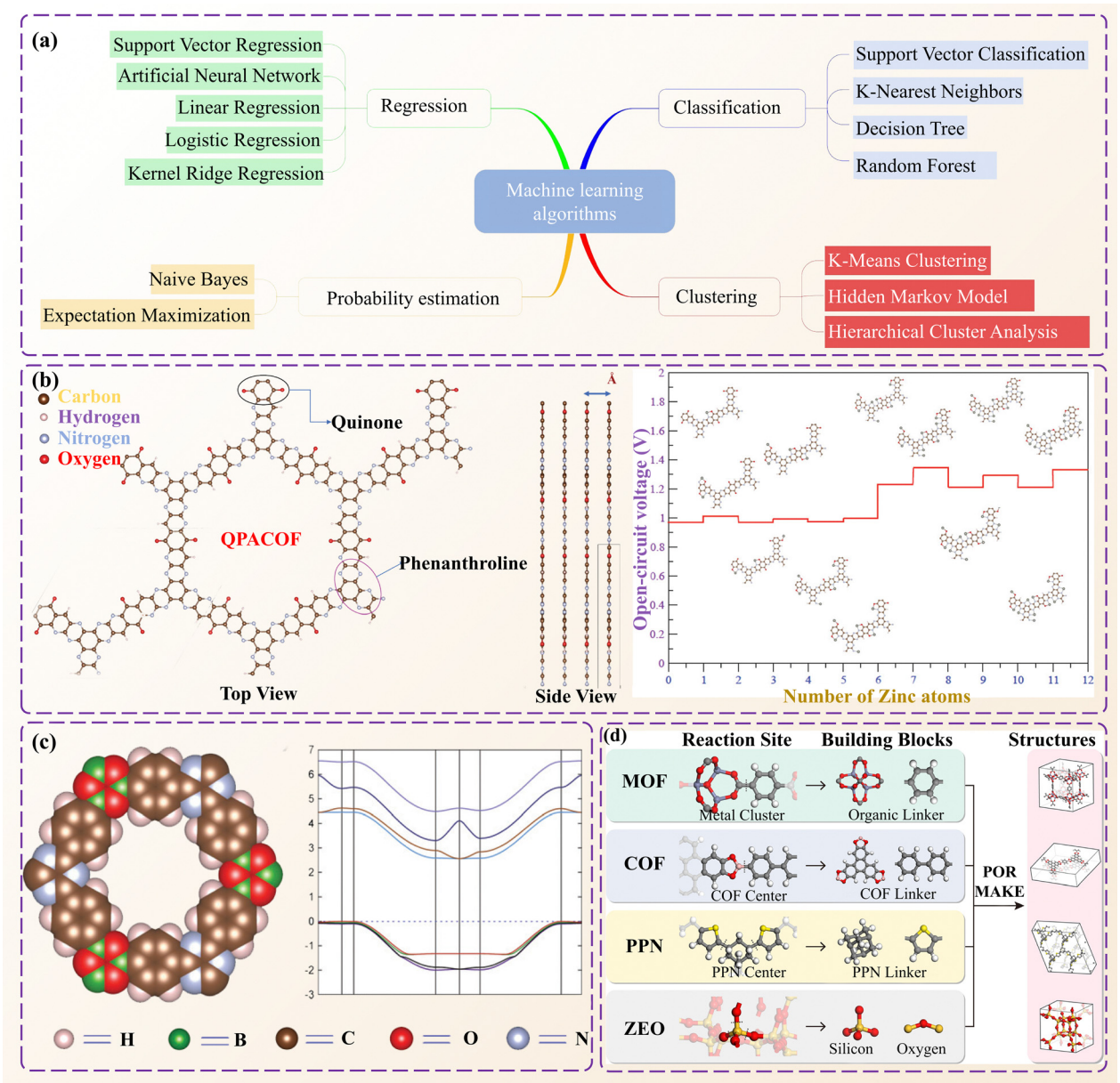


Fig. 21 The impact of ML and AI on COFs. (a) Commonly used ML algorithms in materials science. (b) Top and side views of the optimized geometric structure of the QPACOF super unit cell and a voltage distribution diagram showing the gradual insertion of zinc atoms into the unit cell. (c) Optimized crystal structure and energy band structure of the original COFs. (d) A diverse and large pre-training dataset of porous materials. Reproduced with permission from ref. 288 (Fig. 21a), Copyright 2021 Elsevier. Reproduced from ref. 290 (Fig. 21b) and ref. 291 (Fig. 21c) with permission from The Royal Society of Chemistry, Copyright 2021 and Copyright 2019. Reproduced with permission from ref. 292 (Fig. 21d), Copyright 2023 American Chemical Society.

transport equation.[297] The impact of various transition metal elements on the thermal conductivity of porphyrin COF was studied (Fig. 22c). It was proved that inserting Pt into a 2D porphyrin COF can make it a semiconductor material with excellent performance. Pakhira *et al.* inserted Fe atoms into the organic layer of boroxine and triazine COFs based on the hybrid DFT design of van der Waals dispersion correction.[296] Fig. 22d shows the optimized crystal structures of Fe-intercalated COF-Fe-5 and pristine COF-Fe-0 materials. Iron-intercalated COFs possess unique band gap values from 1.12 to 1.97 eV, making them promising candidates for semiconductor applications. Transition element intercalated COFs have expanded the scope and complexity of nanoporous COFs, paving the way for their wider applications in various fields.

## 7. LCA assessment of COFs and policy impact

### 7.1. LCA evaluation of COFs

Life cycle assessment (LCA) is a method of assessing the environmental impact of a product or service throughout its

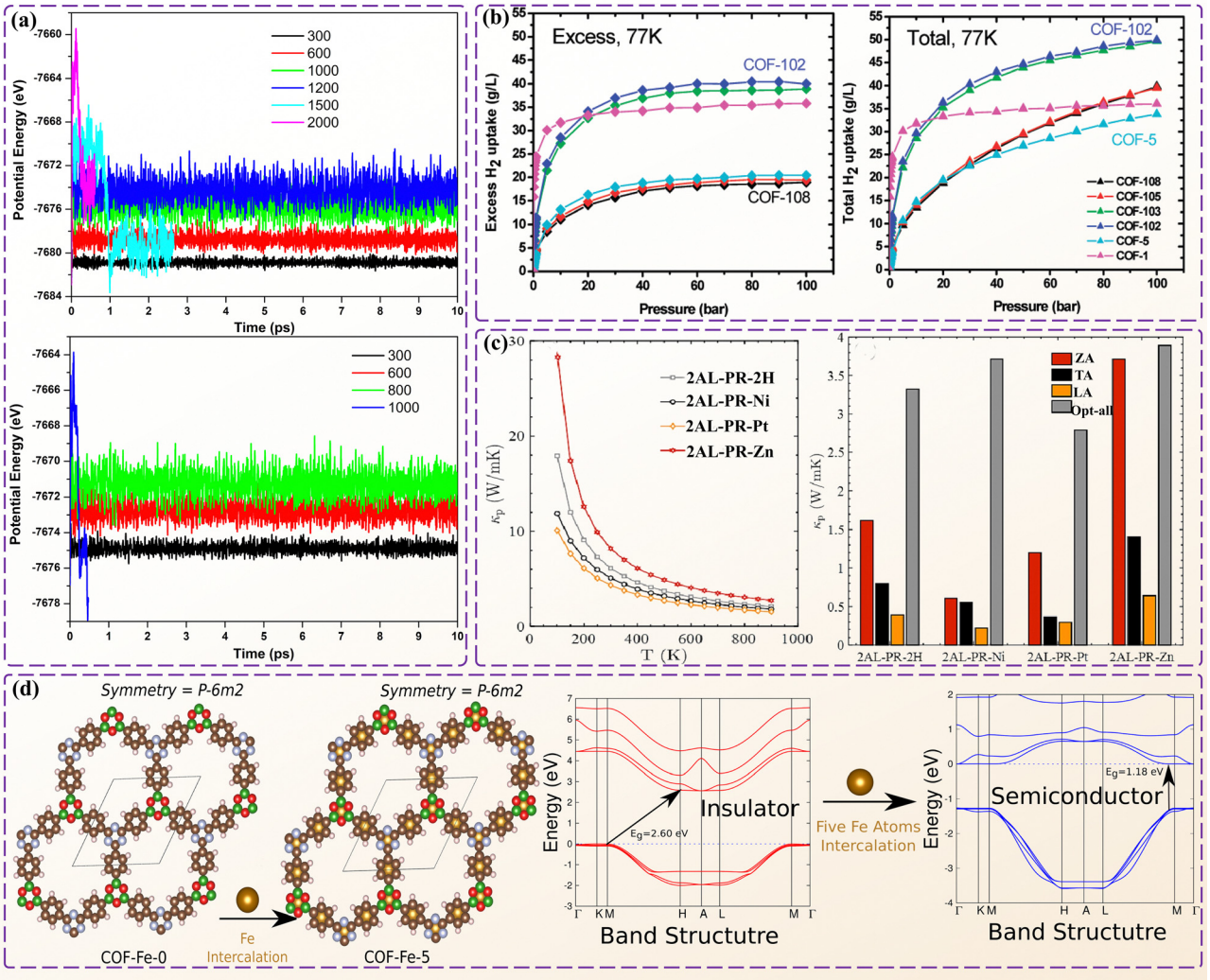


Fig. 22 The impact of ML and AI on COFs. (a) Time potential energy of eCOF-300a and eCOF-300b from MD simulations. (b) $H_2$ adsorption isotherm simulated by COFs in density (g $L^{-1}$) at 77 K. (c) The lattice thermal conductivity and lattice thermal conductivity of 2AL-PR-X of the single phonon mode. (d) Optimized crystal structures of pristine COF-Fe-0 and Fe-intercalated COF-Fe-5 COF materials. Reproduced with permission from ref. 294 (Fig. 22a), Copyright 2021 Wiley. Reproduced from ref. 295 (Fig. 22b) and ref. 296 (Fig. 22d) with permission from the American Chemical Society, Copyright 2008 and Copyright 2017. Reproduced with permission from ref. 297 (Fig. 22c), Copyright 2023 Elsevier.

life cycle, from birth to death.[303] For COFs, LCA assessment is usually carried out in four aspects: production stage, use stage, maintenance stage, and disposal stage. Table 8 shows the LCA evaluation of some COFs.[304]

The production of COFs involves the linkage of organic molecules through covalent bonds. This process typically requires large amounts of petroleum resources, leading to indirect increases in greenhouse gas emissions. The synthesis of COFs often requires high-temperature conditions and substantial energy consumption.[305] Additionally, subsequent washing, filtration, and other steps also consume a large amount of flammable and toxic organic solvents such as acetone and tetrahydrofuran, which creates certain safety risks for the production process of COFs. In order to address the challenges above, researchers are currently investigating mechanochemical methods that eliminate the need for organic solvents, photochemical methods with gentle synthesis conditions, and room-temperature synthesis techniques for producing COFs.[306]

COFs, with porous and flexible nature, can remove or transform environmental pollutants such as harmful gases, heavy metal ions, and organic dyes through physical or chemical adsorption. In this process, different environmental impacts may be caused by the different solvents and machines used. Espada *et al.* used inkjet printing and 3D printing to print RT-COF-1. The results showed that 3D printing has less impact on the environment.[307] The spatial structure of the COF is extremely stable, the COF exhibited good physical integrity and chemical stability, and it required little maintenance during use.[308] In addition, most COF materials currently available on the market can be recycled and the absorption rate of harmful substances can remain above 95% of the raw materials after repeated use.

 

Table 8 LCA evaluation of some COFs

| Material | Resolve resolution | Units of measurement | Environmental impact of the synthesis process | | | Environmental impact of use process | | |
|---|---|---|---|---|---|---|---|---|
| | | | Global warming potential (GWP) | Stratospheric ozone depletion (ODP) | Human toxicity potential (HTP) | Global warming potential (GWP) | Stratospheric ozone depletion (ODP) | Human toxicity potential (HTP) |
| W-MIL-47@CNT | Solvothermal method | Kg | $7.47 \times 10^{0}$ | $3.85 \times 10^{-6}$ | $5.72 \times 10^{-1}$ | $1.40 \times 10^{0}$ | $3.82 \times 10^{-7}$ | $3.69 \times 10^{-2}$ |
| RT-COF-1 (TAPB) | Bottom-up synthesis | g | $1.09 \times 10^{-2}$ | $5.93 \times 10^{-10}$ | $3.27 \times 10^{-3}$ | $6.15 \times 10^{-2}$ | $1.51 \times 10^{-2}$ | $5.86 \times 10^{-8}$ |
| RT-COF-1 (BTCA) | Bottom-up synthesis | g | $2.89 \times 10^{-2}$ | $5.56 \times 10^{-8}$ | $5.85 \times 10^{-3}$ | $4.89 \times 10^{-2}$ | $9.96 \times 10^{-3}$ | $5.65 \times 10^{-8}$ |



Traditional COFs contain organic ligands that can not be easily degraded, leading to chemical residues in soil and water bodies, which can harm the environment. Incineration of COFs may release harmful gases and particulate matter, causing air pollution and threatening ecosystems. Researchers are investigating the use of biodegradable organic ligands, non-heavy metal catalysts, and environmentally benign synthesis methods to mitigate these issues. These advancements ensure that discarded COFs do not cause long-term environmental damage.[309] After fulfilling their pollution control missions, COFs can be safely returned to the natural environment through decomposition. Researchers also employ physical or chemical methods to repurpose discarded COFs as additives to low-value materials or to modify them for novel functions, thereby extending their utility. Recycling not only diminishes the necessity for new material synthesis but also lessens the environmental impact of discarded materials. This further advances the sustainable development and environmental protection of COF materials.[310]

### 7.2. The impact of national policies on the development of COFs

From fundamental research to industrialization to market application, policy guidance and support are indispensable. The Sustainable Development Goals (SDGs) were adopted by the United Nations in 2015 as an important call to action to end poverty, protect the planet and ensure that all people enjoy peace and prosperity by 2030. Over 100 countries have incorporated the SDGs into their national development plans.

To fulfil the SDGs aimed at reducing carbon emissions, developed nations that have ratified the United Nations Framework Convention have pledged to mobilize $100 billion annually from various funding sources by 2020. This financial commitment is intended to support developing countries in their endeavours. COFs are highly porous and have adjustable pore sizes. It can remove $SO_x$, separate $CH_4$ and $CO_2$ in the air, and catalytically convert atmospheric $CO_2$ into valuable chemicals. As a clean, renewable and environmentally friendly material, it has received widespread attention from governments worldwide. Governments of various countries attach great importance to climate governance issues and provide a large amount of financial support and policies to reduce greenhouse gas emissions. These have promoted the fundamental research and application development of COFs in clean energy technology.

Currently, more than 3 billion people worldwide rely on marine and coastal biodiversity for their livelihoods, and the industrial value created by the ocean accounts for 5% of global GDP every year. The United Nations invests approximately $400 million annually in small island developing states to improve their marine environments and reduce debt vulnerability. The United Nations World Water Development Report, proposed by the global water partnership (GWP), emphasizes the complex relationship between sustainable water management, prosperity, and peace. It highlights the need to address new water pollutants such as PFASs and antibacterial agents and offers recommendations for sustainable water resources management. Water-related partnerships and cooperation projects are very common in the EU. For example, the Aarhus Convention emphasizes the need for cooperation and participation of all parties involved. In the Paris Agreement, over 80% of countries listed freshwater resources as a key concern. COFs with a layered structure have fast mass transfer and high adsorption capacity, showing good pollutant removal performance and excellent chemical stability in environmental remediation. COFs can also be used in seawater desalination technology to utilize its structural diversity and adjustability through the membrane desalination process to increase freshwater production and seawater desalination efficiency.

Approximately thirteen million hectares of forest are lost and desertification disproportionately impacts poor communities. The SDGs outline the initiative to combat desertification, restore degraded land and soil affected by desertification, drought, and floods, and strive for a neutral world regarding land degradation by 2030. By modifying the structure and synthesis methods of COFs, their adsorption capacity and selectivity for specific pesticides can be enhanced. The utilization of COFs has been found to significantly enhance the metabolic activity of soil microorganisms, thereby playing a critical role in the decomposition and conversion of organic matter. This substantially impacts the soil carbon cycle and carbon storage, consequently aiding in climate change mitigation through soil carbon sequestration. The inherent stability and long-lasting nature of COFs make them particularly fitting for soil environments that necessitate repetitive treatment and prolonged use. Moreover, ongoing research on the post-use

disposal phase of COFs has further diminished their environmental impact.

## 8. Prospects of COFs and their derivatives in environmental pollution control

In the past decade, COF research has witnessed unprecedented progress with a focus on structural design, innovative synthesis with different functions, surface modification and functionalization, and grafting functional groups onto active sites to leverage the advantages of other materials. COFs have been proven effective adsorption agents for capturing harmful gases in air pollution, metal ions and dyes in water, and organic pollutants and heavy metals in soil. They function as catalysts to facilitate the oxidation–reduction reactions of gaseous pollutants, thereby reducing their toxicity and pollution. COFs can also serve as filter membranes to selectively filter toxic substances from water or air, facilitating centralized processing of hazardous substances. Furthermore, COFs can be utilized as detection tools to measure environmental pollutants in air and soil. Their application in monitoring these pollutants is highly promising. The associated chemical and physical enhancements in the structure–property relationship of COFs for these purposes have gained significant interest. As a result, substantial efforts and investments will be dedicated to advancing these research areas.

Specifically, the introduction of active groups or metal atoms into the COF skeleton structure can enhance the adsorption capacity and efficiency of these materials for specific metal ions such as uranyl ions and mercury or gaseous pollutants like $SO_2$. This can be achieved through various methods, including bottom-up, post-synthesis, and blending techniques. Surface functionalization of COFs can also improve their catalytic effect by introducing active transition metal atoms (*e.g.*, Co) to convert $CO_2$ into CO and $H_2$. COFs are characterized by a nanoscale-ordered pore structure, and some COFs feature a hydrophobic skeleton structure with customizable pore size, thus offering alternative pathways for molecular sieving. These attributes make COFs well-suited for use as effective filtration membranes in gas separation and water treatment applications.

COFs have excellent luminescence activity, making them potential candidates for deployment as chemical sensors. Their luminescence characteristics change when COFs interact with target ions, molecules, and particulate substances. As such, COFs are expected to detect a wide range of ions, molecules, and particulate matter in the environment. However, research on structurally stable luminescent COFs is limited. The use of COFs in detection instruments is still in its infancy, and extensive research is required to exploit their potential fully as chemical sensors. The challenges that COFs face in environmental pollution governance are outlined as follows:

First, the structural properties such as specific surface area and pore size, of covalent organic frameworks (COFs) are intrinsically connected to performance during mass transfer, adsorption, separation, and catalysis. Novel COFs are developed by strategically designing regular pore structures to optimise their functions. The strategy makes it possible to create COFs with high densities of active sites within the framework. A hierarchical structure that combines micropores with mesopores can increase the availability of such active sites. Another way to improve the efficiency of adsorption is by designing COFs in such a way that their porous structure can efficiently adsorb target pollutants. For example, mesoporous COFs will be good for large molecules, and microporous ones will be good for small ones. The incorporation of functional groups that have selective interaction with the target pollutants can considerably enhance performance. For example, coordination bonds formed through amine groups exhibit enhanced capturing of heavy metals, while hydrophobic groups lead to the adsorption of organic pollutants. However, a further understanding of the mechanisms for removing particular pollutants is lacking, which would support more advanced improvements in their efficiency. An important aspect here is the design of experimental studies and advanced characterisation techniques to clarify the reaction mechanisms. This would allow targeted functional modifications of COFs, with a corresponding enhancement in the performance of COFs and a promising future in environmental engineering.

Secondly, one should also consider that the functionalities of COFs in environmental governance have not yet been fully realized. The introduction of many functional properties such as adsorption affinity and luminescence is still in the infancy of development. For instance, structural disorder attributed to the intrinsic porous backbone of COFs may drastically obstruct the filtration efficiency of COF-based membrane filtration in many water treatment or gas separation processes. This disorder is liable to result in uneven pore size and distribution, which affects the selective permeability in COFs and general performance. These issues could be alleviated and developed into more reliable and effective environmental applications with higher crystallinity and uniformity in COF structures. A COF design with high structural orderliness and unique structure-property relationship is highly desired (Fig. 23).

Third, although COFs are far more stable than many MOFs, COFs have to remain stable after functionalization in a particular environment for their regenerative and sustainable long term operation. Pore structure and stability must therefore be key to the rational design of COF-based materials for targeted applications, strong covalent bonds and stable linkers could enhance the durability of COFs, environmental conditions (pH, temperature, and the presence of solvents) should also be taken into account in which COFs are deployed and stable building blocks should also be chosen accordingly.

Fourth, tremendous strides in the rational design of COFs have been made to tune their physical and chemical properties, yet their industrial potential is very much in the rudimentary stage. High costs related to the production of COF materials have always been a significant issue against their application in environmental remediation. In this regard, future development should focus on simplified processes of synthesizing COFs,

 

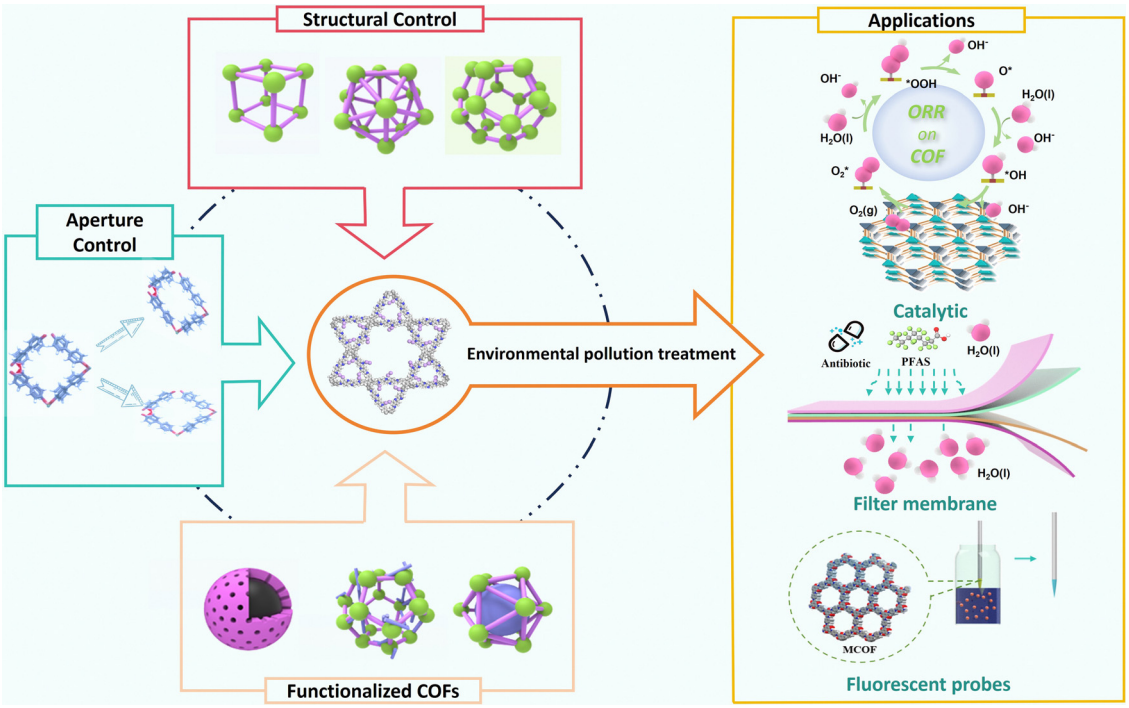


Fig. 23 Prospects of COFs in environmental pollution control.

which require low energy in the synthesis process and substitute expensive reagents with more economical ones. Such an approach will decrease the cost of production and prevent expensive synthesis equipment, leading to large-scale production.

The current literature has not considered the environmental impact of COFs and their synthesis process through various chemicals. In this respect, the overall scope of COFs causing human health and environmental hazards is unclear. Also, effective removal from soil and water bodies must be considered to prevent secondary pollution. Considering these concerns, it is very important to look for some alternative and green methods for synthesising COFs to have a clear picture of their effects on environment.

## Data availability

All data are available online or upon request to the author(s).

## Conflicts of interest

The authors declare no conflicts of interest. They have no known competing financial interests or personal relationships that could have appeared to influence the work reported in this paper.

## Acknowledgements

S. G. R. H., B. B. X. and J. J. developed the scope. S. G., K. W., W. P., R. H. and X. Z. performed literature search and completed the analysis. S. G., K. W., W. P., R. H., E. A., H. X., M. S., X. Z. and B. B. X. processed the figures and visualizations. The work was supervised by S. G., R. H., B. B. X. and J. J. The manuscript was written and revised by S. G., E. A., R. H., X. H., X. Z., B. B. X. and J. J., with contributions from all authors. The authors thank the National Natural Science Foundation of China (32201491), Young Elite Scientists Sponsorship Program by CAST (2023QNRC001), Key Research and Development Program of Jiangsu Province (BE2023361), and Strategic Research and Consulting Project of Chinese Academy of Engineering (2024-XZ-49). B. B. X. is grateful for the support from the Engineering and Physical Sciences Research Council (EPSRC, UK) RiR grant – RIR18221018-1.

## References

1 L. Zhu, H. Zhu, L. Wang, J. Lei and J. Liu, *J. Energy Chem.*, 2023, **82**, 198–218.
2 L. Guo, J. Zhang, Q. Huang, W. Zhou and S. Jin, *Chin. Chem. Lett.*, 2022, **33**, 2856–2866.
3 N. Contreras-Pereda, S. Pané, J. Puigmartí-Luis and D. Ruiz-Molina, *Coord. Chem. Rev.*, 2022, **460**, 214459.
4 J. Sun, Y. Xu, Y. Lv, Q. Zhang and X. Zhou, *CCS Chem.*, 2023, **5**, 1259–1276.
5 X.-L. Hu, H.-G. Li and B.-E. Tan, *Chin. J. Polym. Sci.*, 2020, **38**, 673–684.
6 S. Xu, J. Wu, X. Wang and Q. Zhang, *Chem. Sci.*, 2023, **14**, 13601–13628.
7 R. Iqbal, G. Yasin, M. Hamza, S. Ibraheem, B. Ullah, A. Saleem, S. Ali, S. Hussain, T. Anh Nguyen, Y. Slimani and R. Pathak, *Coord. Chem. Rev.*, 2021, **447**, 214152.

8 S. Li, J. Zou, L. Tan, Z. Huang, P. Liang and X. Meng, *Chem. Eng. J.*, 2022, **446**, 137148.
9 J. Sun, Y. Fei, H. Tang, J. Bao, Q. Zhang and X. Zhou, *ACS Appl. Energy Mater.*, 2023, 7(18), 7592–7602.
10 W. Wang, W. Zhao, H. Xu, S. Liu, W. Huang and Q. Zhao, *Coord. Chem. Rev.*, 2021, **429**, 213616.
11 R. E. Mow, G. A. Russell-Parks, G. E. B. Redwine, B. E. Petel, T. Gennett and W. A. Braunecker, *Chem. Mater.*, 2024, **36**, 1579–1590.
12 Q. Liu, Y. Zou, Y. Yang, L. Wang, L. Li, M. Wang, M. Tian, J. Wang, Y. Tao, D. Wang and D. Gao, *Mater. Today Chem.*, 2023, **34**, 101810.
13 S. Zhao, C. H. Jiang, J. C. Fan, S. S. Hong, P. Mei, R. X. Yao, Y. L. Liu, S. L. Zhang, H. Li, H. Q. Zhang, C. Sun, Z. B. Guo, P. P. Shao, Y. H. Zhu, J. W. Zhang, L. S. Guo, Y. H. Ma, J. Q. Zhang, X. Feng, F. C. Wang, H. A. Wu and B. Wang, *Nat. Mater.*, 2021, **20**, 1551.
14 Y. Yang, C. Tu, H. Yin, J. Liu, F. Cheng and F. Luo, *Molecules*, 2022, **27**, 9045.
15 H. Wang, Y. Yang, X. Yuan, W. Liang Teo, Y. Wu, L. Tang and Y. Zhao, *Mater. Today*, 2022, **53**, 106–133.
16 S. Ghosh, A. Nakada, M. A. Springer, T. Kawaguchi, K. Suzuki, H. Kaji, I. Baburin, A. Kuc, T. Heine, H. Suzuki, R. Abe and S. Seki, *J. Am. Chem. Soc.*, 2020, **142**(21), 9752–9762.
17 R. Chormare and M. A. Kumar, *Chemosphere*, 2022, **302**, 134836.
18 H. Ma, S. Pu, S. Liu, Y. Bai, S. Mandal and B. Xing, *Environ. Pollut.*, 2020, **261**, 114089.
19 Y. Xiang, L. Jiang, Y. Zhou, Z. Luo, D. Zhi, J. Yang and S. S. Lam, *J. Hazard. Mater.*, 2022, **422**, 126843.
20 H. Zang, J. Zhou, M. R. Marshall, D. R. Chadwick, Y. Wen and D. L. Jones, *Soil Biol. Biochem.*, 2020, **148**, 107926.
21 S. Khoshnevis Yazdi and B. Khanalizadeh, *Econ. Res.-Ekon. Istraz*, 2017, **30**, 1181–1190.
22 S. Zheng, Y. Yang, C. Wen, W. Liu, L. Cao, X. Feng, J. Chen, H. Wang, Y. Tang, L. Tian, X. Wang and F. Yang, *Environ. Int.*, 2021, **154**, 106555.
23 Y. Jin, S. Wu, Z. Zeng and Z. Fu, *Environ. Pollut.*, 2017, **222**, 1–9.
24 C. Sun, Y. Wang and Z. Zhu, *Environ. Sci. Pollut. Res.*, 2023, **30**, 67820–67838.
25 S.-H. Yang and J.-M. Chen, *Process Saf. Environ. Prot.*, 2022, **159**, 992–995.
26 M. L. Eder, L. Oliva-Teles, R. Pinto, A. P. Carvalho, C. M. R. Almeida, R. Hornek-Gausterer and L. Guimarães, *J. Hazard. Mater.*, 2021, **417**, 125980.
27 T.-B. Nguyen, K. Sherpa, X.-T. Bui, V.-T. Nguyen, T.-D.-H. Vo, H.-T.-T. Ho, C.-W. Chen and C.-D. Dong, *Environ. Pollut.*, 2023, **337**, 122571.
28 C. Xing, C. Liu, Q. Hong, H. Liu, H. Wu, J. Lin, Y. Song, Y. Chen, T. Liu, Q. Hu, W. Tan and H. Lin, *J. Environ. Manage.*, 2022, **319**, 115721.
29 M. Chen, J. Liu, P. Li, H. Gharavi, Y. Hao, J. Ouyang, J. Hu, L. Hu, C. Hou, I. Humar, L. Wei, G.-Z. Yang and G. Tao, *Innovation*, 2022, **3**, 100340.
30 Y. Zou, X. Liu, T. Zhu, M. Tian, M. Cai, Z. Zhao and H. Wu, *ACS Omega*, 2019, **4**, 21091–21099.
31 H. Lee, R.-s Park, H. W. Lee, Y. Hong, Y. Lee, S. H. Park, S.-C. Jung, K.-S. Yoo, J.-K. Jeon and Y.-K. Park, *Carbon lett.*, 2016, **19**, 79–88.
32 Z. Meddeb, H. Hajjem, A. Mabrouk, N. Hajjaji and N. Hajji, *Int. J. Hydrogen Energy*, 2017, **42**, 8602–8610.
33 R. Li, Y. Rao and Y. Huang, *Chin. Chem. Lett.*, 2023, **34**, 108000.
34 L. Tomassetti, D. Di Giuseppe, A. Zoboli, V. Paolini, M. Torre, E. Paris, E. Guerriero, F. Petracchini and A. F. Gualtieri, *J. Cleaner Prod.*, 2020, **268**, 122179.
35 Y. Zhao, S. Das, T. Sekine, H. Mabuchi, T. Irie, J. Sakai, D. Wen, W. Zhu, T. Ben and Y. Negishi, *Angew. Chem., Int. Ed.*, 2023, 62.
36 Y. Gong, S. Huang, Z. Lei, L. Wayment, H. Chen and W. Zhang, *Chem. - Eur. J.*, 2023, 29.
37 S. Zhou, Y. Kuang, Y. Shi, Y. Hu, L. Chen, J. Zheng and G. Ouyang, *Chem. Eng. J.*, 2023, **453**, 139743.
38 J. Dong, X. Han, Y. Liu, H. Li and Y. Cui, *Angew. Chem., Int. Ed.*, 2020, **59**, 13722–13733.
39 J. Xiu, Y. Bian, Z. Ali, Y. Chen and G. Wang, *Spectrochim. Acta, Part A*, 2024, **306**, 123577.
40 C. Xia, X. Li, Y. Wu, S. Suharti, Y. Unpaprom and A. Pugazhendhi, *Environ. Res.*, 2023, **222**, 115318.
41 L. Gao, X. Li, M. Li, A. Zamyadi and Q. Wang, *Process Saf. Environ. Prot.*, 2023, **171**, 132–135.
42 F. Biancullo, N. F. F. Moreira, A. R. Ribeiro, C. M. Manaia, J. L. Faria, O. C. Nunes, S. M. Castro-Silva and A. M. T. Silva, *Chem. Eng. J.*, 2019, **367**, 304–313.
43 R. Li, S. Alomari, T. Islamoglu, O. K. Farha, S. Fernando, S. M. Thagard, T. M. Holsen and M. Wriedt, *Environ. Sci. Technol.*, 2021, **55**, 15162–15171.
44 M. Ding, H. Xu, A. Wang, C. Yao, A. Wang and L. Gao, *Sep. Purif. Technol.*, 2023, **305**, 122466.
45 Z. Xia, Y. Zhao and S. B. Darling, *Adv. Mater. Interfaces*, 2020, 8.
46 R. Castro-Muñoz, L. L. González-Melgoza and O. García-Depraect, *Chemosphere*, 2021, **270**, 129421.
47 T. Bonny, M. Kashkash and F. Ahmed, *Desalination*, 2022, **522**, 115443.
48 T. Wang, W. Liu, L. Chen and X. Li, *Chem. Eng. J.*, 2023, **475**, 146044.
49 X. Song, Z. Zhao, D. Si, X. Wang, F. Zhou, M. Zhang, Y. Shi and C. Hao, *J. Mol. Model.*, 2019, 25.
50 S. Manwani, P. Devi, T. Singh, C. S. Yadav, K. K. Awasthi, N. Bhoot and G. Awasthi, *Environ. Sci. Pollut. Res.*, 2022, **30**, 71940–71956.
51 J. L. Goldfarb, G. Dou, M. Salari and M. W. Grinstaff, *ACS Sustainable Chem. Eng.*, 2017, **5**, 3046–3054.
52 B. Wang, B. Gao and J. Fang, *Crit. Rev. Environ. Sci. Technol.*, 2018, **47**, 2158–2207.
53 Z. Bao, C. Shi, W. Tu, L. Li and Q. Li, *Environ. Pollut.*, 2022, **313**, 120184.
54 C. Zhao, Y. Dong, Y. Feng, Y. Li and Y. Dong, *Chemosphere*, 2019, **221**, 841–855.

 

55 J. Liu, H. Zhang, Z. Yao, X. Li and J. Tang, *Chemosphere*, 2019, **220**, 1041–1046.
56 F. I. Khan, T. Husain and R. Hejazi, *J. Environ. Manage.*, 2004, **71**, 95–122.
57 X. Chen, X. Zhou, P. Geng, Y. Zeng, F. Hu, P. Sun, G. Zhuang and A. Ma, *Chem. Eng. J.*, 2023, **475**, 146142.
58 H. Zhang, D. Ma, R. Qiu, Y. Tang and C. Du, *Chem. Eng. J.*, 2017, **313**, 157–170.
59 C. A. Aggelopoulos, C. D. Tsakiroglou, S. Ognier and S. Cavadias, *Int. J. Environ. Sci. Technol.*, 2014, **12**, 1011–1020.
60 A. P. Côté, A. I. Benin, N. W. Ockwig, M. O'Keeffe, A. J. Matzger and O. M. Yaghi, *Science*, 2005, **310**, 1166–1170.
61 H. M. El-Kaderi, J. R. Hunt, J. L. Mendoza-Cortés, A. P. Côté, R. E. Taylor, M. O'Keeffe and O. M. Yaghi, *Science*, 2007, **316**, 268–272.
62 N. L. Campbell, R. Clowes, L. K. Ritchie and A. I. Cooper, *Chem. Mater.*, 2009, **21**, 204–206.
63 X. L. Zou, G. Zhou, W. H. Duan, K. Choi and J. Ihm, *J. Phys. Chem. C*, 2010, **114**, 13402–13407.
64 A. Nagai, Z. Guo, X. Feng, S. Jin, X. Chen, X. Ding and D. Jiang, *Nat. Commun.*, 2011, 2.
65 M. Gooyit, M. Lee, V. A. Schroeder, M. Ikejiri, M. A. Suckow, S. Mobashery and M. Chang, *J. Med. Chem.*, 2011, **54**, 6676–6690.
66 T. Sick, A. G. Hufnagel, J. Kampmann, I. Kondofersky, M. Calik, J. M. Rotter, A. Evans, M. Döblinger, S. Herbert, K. Peters, D. Böhm, P. Knochel, D. D. Medina, D. Fattakhova-Rohlfing and T. Bein, *J. Am. Chem. Soc.*, 2017, **140**, 2085–2092.
67 S. Chandra, D. Roy Chowdhury, M. Addicoat, T. Heine, A. Paul and R. Banerjee, *Chem. Mater.*, 2017, **29**, 2074–2080.
68 Z.-F. Cai, G. Zhan, L. Daukiya, S. Eyley, W. Thielemans, K. Severin and S. De Feyter, *J. Am. Chem. Soc.*, 2019, **141**, 11404–11408.
69 E. Hamzehpoor, A. Jonderian, E. McCalla and D. F. Perepichka, *J. Am. Chem. Soc.*, 2021, **143**, 13274–13280.
70 L. K. Ritchie, A. Trewin, A. Reguera-Galan, T. Hasell and A. I. Cooper, *Microporous Mesoporous Mater.*, 2010, **132**, 132–136.
71 S. D. Brucks, D. N. Bunck and W. R. Dichtel, *Polymer*, 2014, **55**, 330–334.
72 S. Liu, L. Yang, T. Quan, L. Deng, D. Wang, K. Zhang, L. Wang, J. Wang, F. Ke, X. Li and D. Gao, *Sep. Purif. Technol.*, 2022, **288**, 120673.
73 S. Koonani and A. Ghiasvand, *Talanta*, 2024, **267**, 125236.
74 R. R. Liang, S. Y. Jiang, A. Ru-Han and X. Zhao, *Chem. Soc. Rev.*, 2020, **49**, 3920–3951.
75 S. Xue, X. Ma, Y. Wang, G. Duan, C. Zhang, K. Liu and S. Jiang, *Coord. Chem. Rev.*, 2024, **504**, 215659.
76 M. P. Moghadasnia, B. J. Eckstein, H. R. Martin, J. U. Paredes and C. M. McGuirk, *Cryst. Growth Des.*, 2024, **24**, 2304–2321.
77 X. Chen, K. Geng, R. Liu, K. T. Tan, Y. Gong, Z. Li, S. Tao, Q. Jiang and D. Jiang, *Angew. Chem., Int. Ed.*, 2019, **59**, 5050–5091.
78 N. Huang, L. Zhai, D. E. Coupry, M. A. Addicoat, K. Okushita, K. Nishimura, T. Heine and D. Jiang, *Nat. Commun.*, 2016, 7.
79 J. Wang and S. Zhuang, *Coord. Chem. Rev.*, 2019, **400**, 213046.
80 X. Wang, L. Zhang, X. Wang, T. Cheng, M. Xue, Q. Dong, Y. Peng and Q. Zhang, *Adv. Funct. Mater.*, 2024, DOI: **10.1002/adfm.202401362**.
81 J. Yang, F. Kang, X. Wang and Q. Zhang, *Mater. Horiz.*, 2022, **9**, 121–146.
82 K. Geng, T. He, R. Liu, S. Dalapati, K. T. Tan, Z. Li, S. Tao, Y. Gong, Q. Jiang and D. Jiang, *Chem. Rev.*, 2020, **120**, 8814–8933.
83 M. S. Lohse and T. Bein, *Adv. Funct. Mater.*, 2018, 28.
84 E. Jin, J. Li, K. Geng, Q. Jiang, H. Xu, Q. Xu and D. Jiang, *Nat. Commun.*, 2018, 9.
85 H. Yang, Y. Du, S. Wan, G. D. Trahan, Y. Jin and W. Zhang, *Chem. Sci.*, 2015, **6**, 4049–4053.
86 S.-Q. Xu, T.-G. Zhan, Q. Wen, Z.-F. Pang and X. Zhao, *ACS Macro Lett.*, 2015, **5**, 99–102.
87 Z.-F. Pang, S.-Q. Xu, T.-Y. Zhou, R.-R. Liang, T.-G. Zhan and X. Zhao, *J. Am. Chem. Soc.*, 2016, **138**, 4710–4713.
88 J. W. Crowe, L. A. Baldwin and P. L. McGrier, *J. Am. Chem. Soc.*, 2016, **138**, 10120–10123.
89 G. Lin, H. Ding, R. Chen, Z. Peng, B. Wang and C. Wang, *J. Am. Chem. Soc.*, 2017, **139**, 8705–8709.
90 Y. Xiao, Y. Ling, K. Wang, S. Ren, Y. Ma and L. Li, *J. Am. Chem. Soc.*, 2023, **145**, 13537–13541.
91 Q. Zhu, X. Wang, R. Clowes, P. Cui, L. J. Chen, M. A. Little and A. I. Cooper, *J. Am. Chem. Soc.*, 2020, **142**, 16842–16848.
92 H. Li, F. Q. Chen, X. Y. Guan, J. L. Li, C. Y. Li, B. Tang, V. Valtchev, Y. S. Yan, S. L. Qiu and Q. R. Fang, *J. Am. Chem. Soc.*, 2021, **143**, 2654–2659.
93 H. Li, J. H. Ding, X. Y. Guan, F. Q. Chen, C. Y. Li, L. K. Zhu, M. Xue, D. Q. Yuan, V. Valtchev, Y. S. Yan, S. L. Qiu and Q. R. Fang, *J. Am. Chem. Soc.*, 2020, **142**, 13334–13338.
94 Z. L. Li, L. Sheng, C. H. Hsueh, X. L. Wang, H. Cui, H. Q. Gao, Y. Z. Wu, J. L. Wang, Y. P. Tang, H. Xu and X. M. He, *Chem. Mater.*, 2021, **33**, 9618–9623.
95 X. Y. Xu, P. Y. Cai, H. Z. Chen, H. C. Zhou and N. Huang, *J. Am. Chem. Soc.*, 2022, **144**(40), 18511–18517.
96 Y. Z. Liu, J. W. Li, J. Lv, Z. T. Wang, J. Q. Suo, J. X. Ren, J. C. Liu, D. Liu, Y. J. Wang, V. Valtchev, S. L. Qiu, D. L. Zhang and Q. R. Fang, *J. Am. Chem. Soc.*, 2023, **145**, 9679–9685.
97 F. Z. Jin, E. Lin, T. H. Wang, S. B. Geng, T. Wang, W. S. Liu, F. H. Xiong, Z. F. Wang, Y. Chen, P. Cheng and Z. J. Zhang, *J. Am. Chem. Soc.*, 2022, **144**, 5643–5652.
98 W. B. Liu, L. Gong, Z. X. Liu, Y. C. Jin, H. H. Pan, X. Y. Yang, B. Q. Yu, N. Li, D. D. Qi, K. Wang, H. L. Wang and J. Z. Jiang, *J. Am. Chem. Soc.*, 2022, **144**, 17209–17218.
99 Y. Qin, X. Zhu and R. Huang, *Biomater. Sci.*, 2023, **11**, 6942–6976.
100 F. J. Uribe-Romo, J. R. Hunt, H. Furukawa, C. Klöck, M. O'Keeffe and O. M. Yaghi, *J. Am. Chem. Soc.*, 2009, **131**, 4570.

101 Q. Fang, S. Gu, J. Zheng, Z. Zhuang, S. Qiu and Y. Yan, *Angew. Chem., Int. Ed.*, 2014, **53**, 2878–2882.
102 X. Wang, M. Bahri, Z. Fu, M. A. Little, L. Liu, H. Niu, N. D. Browning, S. Y. Chong, L. Chen, J. W. Ward and A. I. Cooper, *J. Am. Chem. Soc.*, 2021, **143**, 15011–15016.
103 Y. Z. Liu, Y. H. Ma, Y. B. Zhao, X. X. Sun, F. Gandara, H. Furukawa, Z. Liu, H. Y. Zhu, C. H. Zhu, K. Suenaga, P. Oleynikov, A. S. Alshammari, X. Zhang, O. Terasaki and O. M. Yaghi, *Science*, 2016, **351**, 365–369.
104 S. Das, H. Mabuchi, T. Irie, K. Sasaki, M. Nozaki, R. Tomioka, D. Wen, Y. Zhao, T. Ben and Y. Negishi, *Small*, 2024, **20**, 2307666.
105 L. Guo, W. Chen, Y. Li, Z. Wei, F. Li and C. Li, *Mater. Chem. Phys.*, 2023, **301**, 127645.
106 L. Cusin, H. Peng, A. Ciesielski and P. Samorì, *Angew. Chem., Int. Ed.*, 2021, **60**, 14236–14250.
107 W. Gong, Y. Dong, C. Liu, H. Shi, M. Yin, W. Li, Q. Song and C. Zhang, *Dyes Pigm.*, 2022, **204**, 110464.
108 F. J. Uribe-Romo, C. J. Doonan, H. Furukawa, K. Oisaki and O. M. Yaghi, *J. Am. Chem. Soc.*, 2011, **133**, 11478–11481.
109 S. Dalapati, S. Jin, J. Gao, Y. Xu, A. Nagai and D. Jiang, *J. Am. Chem. Soc.*, 2013, **135**, 17310–17313.
110 T. Huo and Y. He, *ACS Appl. Mater. Interfaces*, 2024, **16**, 21233–21241.
111 K. Wang, T.-M. Geng, H. Zhu and C. Guo, *Microporous Mesoporous Mater.*, 2024, **363**, 112794.
112 M. Liu, Q. Huang, S. Wang, Z. Li, B. Li, S. Jin and B. Tan, *Angew. Chem., Int. Ed.*, 2018, **57**, 11968–11972.
113 S. Mitra, H. S. Sasmal, T. Kundu, S. Kandambeth, K. Illath, D. Díaz Díaz and R. Banerjee, *J. Am. Chem. Soc.*, 2017, **139**, 4513–4520.
114 E. Q. Jin, M. Asada, Q. Xu, S. Dalapati, M. A. Addicoat, M. A. Brady, H. Xu, T. Nakamura, T. Heine, Q. H. Chen and D. L. Jiang, *Science*, 2017, **357**, 673–676.
115 J. L. Shi, R. Chen, H. Hao, C. Wang and X. Lang, *Angew. Chem., Int. Ed.*, 2020, **59**, 9088–9093.
116 C. Zhu, A. J. Kalin and L. Fang, *Acc. Chem. Res.*, 2019, **52**, 1089–1100.
117 X. Ji and L. Fang, *Polym. Chem.*, 2021, **12**, 1347–1361.
118 Y. Yang, M. Ratsch, A. M. Evans and K. Börjesson, *J. Am. Chem. Soc.*, 2023, **145**, 18668–18675.
119 X.-G. Li, J. Li, J. Chen, L. Rao, L. Zheng, F. Yu, Y. Tang, J. Zheng and J. Ma, *Biomater. Sci.*, 2024, **12**, 2766–2785.
120 A. Hayat, S. Raza, M. A. Amin, Z. Ajmal, M. M. Alghamdi, A. A. El-Zahhar, H. Ali, D. Ghernaout, Y. Al-Hadeethi, M. Sohail and Y. Orooji, *Mater. Sci. Eng., R*, 2024, **157**, 100771.
121 Y. Su, M. Qin, J. Kong, Q. Zhai, D. Yuan, Z. Liu and Y. Fang, *Adv. Funct. Mater.*, 2024, **34**, 2400433.
122 F. Hamdi, M. Roushani, M. Nasibipour and S. J. Hoseini, *Anal. Chim. Acta*, 2024, **1291**, 342235.
123 A. Ghosh, A. Ghosh, A. Bhattacharyya, R. Mitra, B. B. Das and A. Bhaumik, *Dalton Trans.*, 2024, **53**, 3010–3019.
124 S. Xiong, X. Cui, J. Guo, C. Hua, J. Chu, R. Zhang, Y. Dang and N. Yan, *J. Electroanal. Chem.*, 2023, **942**, 117563.
125 Z. Su, J. Huang, R. Wang, Y. Zhang, L. Zeng, Y. Zhang and H. Fan, *J. Colloid Interface Sci.*, 2023, **639**, 7–13.
126 W. Zhang, F. Liang, C. Li, L.-G. Qiu, Y.-P. Yuan, F.-M. Peng, X. Jiang, A.-J. Xie, Y.-H. Shen and J.-F. Zhu, *J. Hazard. Mater.*, 2011, **186**, 984–990.
127 X.-H. Han, J.-Q. Chu, W.-Z. Wang, Q.-Y. Qi and X. Zhao, *Chin. Chem. Lett.*, 2022, **33**, 2464–2468.
128 H. Lavillunière, T.-N. Pham-Truong, T.-K.-L. Nguyen, C. Vancaeyzeele and P.-H. Aubert, *ACS Appl. Energy Mater.*, 2024, **7**, 1723–1734.
129 Z. Alsudairy, Q. Zheng, N. Brown, R. Behera, C. Yang, M. Hanif Uddin, A. Saintlima, L. Middlebrooks, J. Li, C. Ingram and X. Li, *Chem. Eng. J.*, 2024, **485**, 149135.
130 C. Ching Lau, M. Kemal Bayazit, P. J. T. Reardon and J. Tang, *Chem. Rec.*, 2018, **19**, 172–187.
131 W. Ji, Y.-S. Guo, H.-M. Xie, X. Wang, X. Jiang and D.-S. Guo, *J. Hazard. Mater.*, 2020, **397**, 122793.
132 S. T. Emmerling, L. S. Germann, P. A. Julien, I. Moudrakovski, M. Etter, T. Friščić, R. E. Dinnebier and B. V. Lotsch, *Chem*, 2021, **7**, 1639–1652.
133 T. Friscic, C. Mottillo and H. M. Titi, *Angew. Chem., Int. Ed.*, 2020, **59**, 1018–1029.
134 B. P. Biswal, S. Chandra, S. Kandambeth, B. Lukose, T. Heine and R. Banerjee, *J. Am. Chem. Soc.*, 2013, **135**, 5328–5331.
135 Y. Yang, W. Zhao, H. Niu and Y. Cai, *ACS Appl. Mater. Interfaces*, 2021, **13**, 42035–42043.
136 W. Guo, L. Yan, J. Qian, C. Luo, Y. Ren, W. Xie, J. Cai, J. Ding, M. Qiu and B. Hu, *J. Environ. Chem. Eng.*, 2023, **11**, 109763.
137 Y. Hu, W.-K. Han, Y. Liu, R.-M. Zhu, X. Yan, H. Pang and Z.-G. Gu, *ACS Mater. Lett.*, 2023, **5**, 2534–2541.
138 S.-T. Yang, J. Kim, H.-Y. Cho, S. Kim and W.-S. Ahn, *RSC Adv.*, 2012, **2**, 10179.
139 S.-X. Gan, C. Jia, Q.-Y. Qi and X. Zhao, *Chem. Sci.*, 2022, **13**, 1009–1015.
140 J. Fan, X. Suo, T. Wang, Z. Wang, C.-L. Do-Thanh, S. M. Mahurin, T. Kobayashi, Z. Yang and S. Dai, *J. Mater. Chem. A*, 2022, **10**, 14310–14315.
141 J. Hu, Z. Huang and Y. Liu, *Angew. Chem., Int. Ed.*, 2023, 62.
142 S. Asgharzadehahmadi, A. A. Abdul Raman, R. Parthasarathy and B. Sajjadi, *Renewable Sustainable Energy Rev.*, 2016, **63**, 302–314.
143 T. M. Masson, S. D. A. Zondag, M. G. Debije and T. Noël, *ACS Sustainable Chem. Eng.*, 2022, **10**, 10712–10717.
144 S. Kim, C. Park, M. Lee, I. Song, J. Kim, M. Lee, J. Jung, Y. Kim, H. Lim and H. C. Choi, *Adv. Funct. Mater.*, 2017, 27.
145 S. Kim, H. Lim, J. Lee and H. C. Choi, *Langmuir*, 2018, **34**, 8731–8738.
146 C.-J. Wu, X.-Y. Li, T.-R. Li, M.-Z. Shao, L.-J. Niu, X.-F. Lu, J.-L. Kan, Y. Geng and Y.-B. Dong, *J. Am. Chem. Soc.*, 2022, **144**, 18750–18755.
147 T. Jadhav, Y. Fang, C.-H. Liu, A. Dadvand, E. Hamzehpoor, W. Patterson, A. Jonderian, R. S. Stein and D. F. Perepichka, *J. Am. Chem. Soc.*, 2020, **142**, 8862–8870.
148 B. An, B. Zheng, Z. Liu, Z. Wu, M. Wu and W. Wu, *Curr. Opin. Green Sustainable Chem.*, 2023, **41**, 100798.

 

149 C. J. Wu, M. Z. Shao, Y. Geng and Y. B. Dong, *ChemCatChem*, 2023, 15.
150 F. G. Fabozzi, N. Severin, J. P. Rabe and S. Hecht, *J. Am. Chem. Soc.*, 2023, **145**, 18205–18209.
151 H.-Z. Li, C. Yang, H.-L. Qian, S.-T. Xu and X.-P. Yan, *Anal. Chem.*, 2024, **96**, 3561–3568.
152 J. Wang, J. Wang, S. Qiao, N. Li and Z. Guo, *Polymer*, 2024, **300**, 126998.
153 D. D. Medina, J. M. Rotter, Y. Hu, M. Dogru, V. Werner, F. Auras, J. T. Markiewicz, P. Knochel and T. Bein, *J. Am. Chem. Soc.*, 2015, **137**, 1016–1019.
154 H.-Z. Li, C. Yang, H.-L. Qian and X.-P. Yan, *Sep. Purif. Technol.*, 2023, **306**, 122704.
155 L. Guo, Q. Y. Zhang, Z. Yu, R. Krishna and F. Luo, *Chem. Mater.*, 2023, **35**, 5648–5656.
156 X. Wang, N. Wang, H. Ni, T. Liu and Q.-F. An, *J. Membr. Sci.*, 2023, **665**, 121129.
157 J. He, X. Jiang, F. Xu, C. Li, Z. Long, H. Chen and X. Hou, *Angew. Chem., Int. Ed.*, 2021, **60**, 9984–9989.
158 H. Jyoti Bora, P. Jyoti Boruah, P. Kalita, G. Gogoi, H. Bailung, N. Sen Sarma and A. Kalita, *Chem. - Eur. J.*, 2023, 29.
159 G. Zhan, Z.-F. Cai, M. Martínez-Abadía, A. Mateo-Alonso and S. De Feyter, *J. Am. Chem. Soc.*, 2020, **142**, 5964–5968.
160 M. Zhang, J. Chen, S. Zhang, X. Zhou, L. He, M. V. Sheridan, M. Yuan, M. Zhang, L. Chen, X. Dai, F. Ma, J. Wang, J. Hu, G. Wu, X. Kong, R. Zhou, T. E. Albrecht-Schmitt, Z. Chai and S. Wang, *J. Am. Chem. Soc.*, 2020, **142**, 9169–9174.
161 X. Zhao, S. Shang, H. Liu, C. Peng and J. Hu, *Chemosphere*, 2024, **356**, 141947.
162 J. M. Rotter, S. Weinberger, J. Kampmann, T. Sick, M. Shalom, T. Bein and D. D. Medina, *Chem. Mater.*, 2019, **31**, 10008–10016.
163 B. Sun, Z. Sun, Y. Yang, X. L. Huang, S. C. Jun, C. Zhao, J. Xue, S. Liu, H. K. Liu and S. X. Dou, *ACS Nano*, 2023, **18**, 28–66.
164 L. Xiao, Z. Wang and J. Guan, *Adv. Funct. Mater.*, 2023, 34.
165 J. L. Segura, S. Royuela and M. Mar Ramos, *Chem. Soc. Rev.*, 2019, **48**, 3903–3945.
166 H. Ding, A. Mal and C. Wang, *Mater. Chem. Front.*, 2020, **4**, 113–127.
167 Q. Yan, H. Xu, X. Jing, H. Hu, S. Wang, C. Zeng and Y. Gao, *RSC Adv.*, 2020, **10**, 17396–17403.
168 Q. Sun, B. Aguila, J. Perman, L. D. Earl, C. W. Abney, Y. Cheng, H. Wei, N. Nguyen, L. Wojtas and S. Ma, *J. Am. Chem. Soc.*, 2017, **139**, 2786–2793.
169 W. Zhou, X. Wang, W. Zhao, N. Lu, D. Cong, Z. Li, P. Han, G. Ren, L. Sun, C. Liu and W.-Q. Deng, *Nat. Commun.*, 2023, 14.
170 J. Liu, T. Cheng, L. Jiang, H. Zhang, Y. Shan and A. Kong, *Electrochim. Acta*, 2020, **363**, 137280.
171 F. Jin, E. Lin, T. Wang, S. Geng, T. Wang, W. Liu, F. Xiong, Z. Wang, Y. Chen, P. Cheng and Z. Zhang, *J. Am. Chem. Soc.*, 2022, **144**, 5643–5652.
172 M. Zhang, M. Yuan, X. Zhao, J. Chen, L. He, Q. Gao, J. Hu, G. Wu, Z. Chai and S. Wang, *Sci. China: Chem.*, 2023, **66**, 1781–1787.
173 C. Guo, F. Duan, S. Zhang, L. He, M. Wang, J. Chen, J. Zhang, Q. Jia, Z. Zhang and M. Du, *J. Mater. Chem. A*, 2022, **10**, 475–507.
174 L. You, K. Xu, G. Ding, X. Shi, J. Li, S. Wang and J. Wang, *J. Mol. Liq.*, 2020, **320**, 114456.
175 Y. Ji, Y. He, R. Chen, C. Zhong, H. Li, Y. Wu and Z. Lin, *J. Mater. Chem. B*, 2022, **10**, 6507–6513.
176 J. Liu, X. Zhong, Q.-E. Zhang, L. Deng, L. Hou, J. Zou, S. Liu, Y. Gao, L. Wang and L. Lu, *Microchem. J.*, 2024, **201**, 110603.
177 L. Huang, J. Yang, Y. Asakura, Q. Shuai and Y. Yamauchi, *ACS Nano*, 2023, **17**, 8918–8934.
178 B. Sun, D. Wang and L. Wan, *Sci. China: Chem.*, 2017, **60**, 1098–1102.
179 Y. Tang, W. Li, Y. Muhammad, S. Jiang, M. Huang, H. Zhang, Z. Zhao and Z. Zhao, *Chem. Eng. J.*, 2021, **421**, 129743.
180 S. Kandambeth, V. Venkatesh, D. B. Shinde, S. Kumari, A. Halder, S. Verma and R. Banerjee, *Nat. Commun.*, 2015, 6.
181 T.-Y. Zhou, F. Lin, Z.-T. Li and X. Zhao, *Macromolecules*, 2013, **46**, 7745–7752.
182 T. Li, Y. Pan, B. Shao, X. Zhang, T. Wu, Q. He, M. He, L. Ge, L. Zhou, S. Liu, X. Zheng, J. Ye and Z. Liu, *Adv. Funct. Mater.*, 2023, 33.
183 Y. L. Chen, Y. Xie, X. Sun, Y. Wang and Y. Wang, *Sens. Actuators, B*, 2021, 331.
184 K. Hu, J. Cheng, W. Zhang, T. Pang, X. Wu, Z. Zhang, Y. Huang, W. Zhao and S. Zhang, *Anal. Chim. Acta*, 2020, **1140**, 132–144.
185 R. Li, L. Xing, A. Chen, X. Zhang, A. Kong and Y. Shan, *Ionics*, 2019, **26**, 927–937.
186 W. Sun, X. Tang, Q. Yang, Y. Xu, F. Wu, S. Guo, Y. Zhang, M. Wu and Y. Wang, *Adv. Mater.*, 2019, 31.
187 C. Gao, Q. Meng, K. Zhao, H. Yin, D. Wang, J. Guo, S. Zhao, L. Chang, M. He, Q. Li, H. Zhao, X. Huang, Y. Gao and Z. Tang, *Adv. Mater.*, 2016, **28**, 6485–6490.
188 Z. Jiang, W. Wan, H. Li, S. Yuan, H. Zhao and P. K. Wong, *Adv. Mater.*, 2018, 30.
189 M. Liu, Q. Xu and G. Zeng, *Angew. Chem., Int. Ed.*, 2024, **63**, e202404886.
190 Y. Huang, X. Hao, S. Ma, R. Wang and Y. Wang, *Chemosphere*, 2022, **291**, 132795.
191 C. Zhang, Y. Yang, X. Liu, M. Mao, K. Li, Q. Li, G. Zhang and C. Wang, *Innovation*, 2023, **4**, 100518.
192 Y. Zeng, R. Zou and Y. Zhao, *Adv. Mater.*, 2016, **28**, 2855–2873.
193 C. Kessler, R. Schuldt, S. Emmerling, B. V. Lotsch, J. Kästner, J. Gross and N. Hansen, *Microporous Mesoporous Mater.*, 2022, **336**, 111796.
194 Y. Zhao, X. Tao, J. Lin and S. Lin, *Adv. Funct. Mater.*, 2023, 33.
195 E. H. Wolpert, A. Tarzia and K. E. Jelfs, *Chem. Commun.*, 2023, **59**, 6909–6912.
196 M. Lu, Q. Li, J. Liu, F.-M. Zhang, L. Zhang, J.-L. Wang, Z.-H. Kang and Y.-Q. Lan, *Appl. Catal., B*, 2019, **254**, 624–633.

197 M. Lu, M. Zhang, C. G. Liu, J. Liu, L. J. Shang, M. Wang, J. N. Chang, S. L. Li and Y. Q. Lan, *Angew. Chem., Int. Ed.*, 2021, **60**, 4864–4871.
198 W.-L. Peng, X. Kan, W. Chen, J. Mi, G. Zhang, Y. Xiao, W. Liu, F. Liu and A. Zheng, *ACS Appl. Mater. Interfaces*, 2021, **13**, 34124–34133.
199 P. Wang, F. Zhou, C. Zhang, S.-Y. Yin, L. Teng, L. Chen, X.-X. Hu, H.-W. Liu, X. Yin and X.-B. Zhang, *Chem. Sci.*, 2018, **9**, 8402–8408.
200 M. Wang, D. Chen and J. Lu, *Sep. Purif. Technol.*, 2024, **343**, 126917.
201 X. Y. D. Soo, J. J. C. Lee, W.-Y. Wu, L. Tao, C. Wang, Q. Zhu and J. Bu, *J. CO2 Util.*, 2024, **81**, 102727.
202 D. L. White, S. C. Burkert, S. I. Hwang and A. Star, *Nano Lett.*, 2019, **19**, 2824–2831.
203 M. Zhang, H. Wang, B. Fan, C. Liu, M. Wang and Q. Liu, *J. Environ. Chem. Eng.*, 2024, **12**, 112306.
204 D. W. Kang, S. E. Ju, D. W. Kim, M. Kang, H. Kim and C. S. Hong, *Adv. Sci.*, 2020, 7.
205 Y. Yang, M. Faheem, L. Wang, Q. Meng, H. Sha, N. Yang, Y. Yuan and G. Zhu, *ACS Cent. Sci.*, 2018, **4**, 748–754.
206 L. Jiang, Y. Tian, T. Sun, Y. Zhu, H. Ren, X. Zou, Y. Ma, K. R. Meihaus, J. R. Long and G. Zhu, *J. Am. Chem. Soc.*, 2018, **140**, 15724–15730.
207 L. He, L. Chen, X. Dong, S. Zhang, M. Zhang, X. Dai, X. Liu, P. Lin, K. Li, C. Chen, T. Pan, F. Ma, J. Chen, M. Yuan, Y. Zhang, L. Chen, R. Zhou, Y. Han, Z. Chai and S. Wang, *Chem*, 2021, **7**, 699–714.
208 G.-Y. Lee, J. Lee, H. T. Vo, S. Kim, H. Lee and T. Park, *Sci. Rep.*, 2017, 7.
209 A. Mangotra and S. K. Singh, *J. Biotechnol.*, 2024, **382**, 51–69.
210 Z. Zhang, W. Chen, L. Ding, M. Wu and S. Wei, *J. Environ. Chem. Eng.*, 2024, **12**, 112749.
211 M. Gharaylou, N. Pegahfar and O. Alizadeh, *Earth Space Sci.*, 2024, 11.
212 A. Guo, H. Liu, Y. Li, Y. Luo, D. Ye, J. Jiang and P. Chen, *Catal. Today*, 2023, **422**, 114212.
213 A. R. Sánchez-Rodríguez, E. Gómez-Álvarez, J. M. Méndez, U. M. Skiba, D. L. Jones, D. R. Chadwick, M. C. del Campillo, R. B. A. Fernandes, J. Kleffmann and V. Barrón, *Chemosphere*, 2023, **338**, 139576.
214 Y. Gao, *IOP Conf. Ser.: Mater. Sci. Eng.*, 2021, **692**, 032014.
215 J. Wang, J. Wang, W. Zhuang, X. Shi and X. Du, *J. Chem.*, 2018, 1–8.
216 Z. Meng, R. M. Stolz and K. A. Mirica, *J. Am. Chem. Soc.*, 2019, **141**, 11929–11937.
217 C. Zamora-Ledezma, D. Negrete-Bolagay, F. Figueroa, E. Zamora-Ledezma, M. Ni, F. Alexis and V. H. Guerrero, *Environ. Technol. Innovation*, 2021, **22**, 101504.
218 S. Bochynska, A. Duszewska, M. Maciejewska-Jeske, M. Wrona, A. Szeliga, M. Budzik, A. Szczesnowicz, G. Bala, M. Trzcinski, B. Meczekalski and R. Smolarczyk, *Maturitas*, 2024, **185**, 107981.
219 S. P. S. Fernandes, V. Romero, B. Espiña and L. M. Salonen, *Chem. - Eur. J.*, 2019, **25**, 6461–6473.
220 A. R. Bagheri, N. Aramesh, F. Sher and M. Bilal, *Chemosphere*, 2021, **270**, 129523.
221 X. Liu, H. Pang, X. Liu, Q. Li, N. Zhang, L. Mao, M. Qiu, B. Hu, H. Yang and X. Wang, *Innovation*, 2021, **2**, 100076.
222 T. Rasheed, *Sci. Total Environ*, 2022, **833**, 155279.
223 K. Zhang, Z. He, K. M. Gupta and J. Jiang, *Environ. Sci.: Water Res. Technol.*, 2017, **3**, 735–743.
224 C. Liu, Y. Jiang, A. Nalaparaju, J. Jiang and A. Huang, *J. Mater. Chem. A*, 2019, **7**, 24205–24210.
225 C. Li, S. Li, J. Zhang, C. Yang, B. Su, L. Han and X. Gao, *J. Membr. Sci.*, 2020, **604**, 118065.
226 S. Zhao, C. Jiang, J. Fan, S. Hong, P. Mei, R. Yao, Y. Liu, S. Zhang, H. Li, H. Zhang, C. Sun, Z. Guo, P. Shao, Y. Zhu, J. Zhang, L. Guo, Y. Ma, J. Zhang, X. Feng, F. Wang, H. Wu and B. Wang, *Nat. Mater.*, 2021, **20**, 1551–1558.
227 B. Hosseini Monjezi, K. Kutonova, M. Tsotsalas, S. Henke and A. Knebel, *Angew. Chem., Int. Ed.*, 2021, **60**, 15153–15164.
228 M. F. Chowdhury, S. Khandaker, F. Sarker, A. Islam, M. T. Rahman and M. R. Awual, *J. Mol. Liq.*, 2020, **318**, 114061.
229 Z. U. Zango, A. M. Binzowaimil, O. A. Aldaghri, M. H. Eisa, A. Garba, N. M. Ahmed, J. W. Lim, H.-S. Ng, H. Daud, K. Jumbri, K. S. Khoo and K. H. Ibnaouf, *Chemosphere*, 2023, **343**, 140223.
230 C. Wu, X. Wang, T. Zhu, P. Li and S. Xia, *Chemosphere*, 2020, **261**, 127580.
231 M. Firoozi, Z. Rafiee and K. Dashtian, *ACS Omega*, 2020, **5**, 9420–9428.
232 Y. Li, C.-X. Yang, H.-L. Qian, X. Zhao and X.-P. Yan, *ACS Appl. Nano Mater.*, 2019, **2**, 7290–7298.
233 M. Wang, R. Yan, M. Shan, S. Liu and H. Tang, *Chemosphere*, 2024, **352**, 141363.
234 S. P. Padinhattath, J. Govindaraj and R. L. Gardas, *J. Water Process. Eng*, 2024, **58**, 104921.
235 M. Wang, X. Li, W. Hua, L. Shen, X. Yu and X. Wang, *ACS Appl. Mater. Interfaces*, 2016, **8**, 23995–24007.
236 H. Deng, W. Wei, L. Yao, Z. Zheng, B. Li, A. Abdelkader and L. Deng, *Adv. Sci.*, 2022, **9**, e2203189.
237 C. Wu, L. Xia, S. Xia, B. Van der Bruggen and Y. Zhao, *Small*, 2022, 19.
238 G. Li, J. Ye, Q. Fang and F. Liu, *Chem. Eng. J.*, 2019, **370**, 822–830.
239 Y. Cao, X. Hu, C. Zhu, S. Zhou, R. Li, H. Shi, S. Miao, M. Vakili, W. Wang and D. Qi, *Colloids Surf., A*, 2020, **600**, 125004.
240 X. Liu, H. Xu, L. Wang, Z. Qu and N. Yan, *Chem. Eng. J.*, 2020, **381**, 122559.
241 D. Zhu, S. Zhou, Z. Zhou, R. Li, J. Ye, X. Ziyu, S. Lan, Y. Zhang, S. Miao and W. Wang, *Colloids Surf., A*, 2020, **600**, 124910.
242 L. Huang, R. Shen, R. Liu and Q. Shuai, *J. Hazard. Mater.*, 2020, **392**, 122320.
243 Y. X. Yu, G. L. Li, J. H. Liu and D. Q. Yuan, *Chem. Eng. J.*, 2020, 401.
244 W. R. Cui, W. Jiang, C. R. Zhang, R. P. Liang, J. W. Liu and J. D. Qiu, *ACS Sustainable Chem. Eng.*, 2020, **8**, 445–451.

 

245 L. L. Wang, H. M. Xu, Y. X. Qiu, X. S. Liu, W. J. Huang, N. Q. Yan and Z. Qu, *J. Hazard. Mater.*, 2020, 389.
246 L. Zhang, Y. Li, Y. Wang, S. Ma, J. Ou, Y. Shen, M. Ye and H. Uyama, *J. Hazard. Mater.*, 2021, **407**, 124390.
247 H.-J. Da, C.-X. Yang and X.-P. Yan, *Environ. Sci. Technol.*, 2019, **53**, 5212–5220.
248 G. Devendrapandi, X. Liu, R. Balu, R. Ayyamperumal, M. Valan Arasu, M. Lavanya, V. R. Minnam Reddy, W. K. Kim and P. C. Karthika, *Environ. Res.*, 2024, **249**, 118404.
249 J. Yang, L. Huang, J. You and Y. Yamauchi, *Small*, 2023, 19.
250 S.-L. Ji, H.-L. Qian, C.-X. Yang, X. Zhao and X.-P. Yan, *ACS Appl. Mater. Interfaces*, 2019, **11**, 46219–46225.
251 H. Lv, X. Zhao, H. Niu, S. He, Z. Tang, F. Wu and J. P. Giesy, *J. Hazard. Mater.*, 2019, **369**, 494–502.
252 C. Wu, X. Du, H. Liu, X. Chen, K. Ge, R. Meng, Z. Zhang and H. Zhang, *Sci. Total Environ*, 2024, **918**, 170543.
253 F. Lu, M. Wu, C. Lin, X. Lin and Z. Xie, *J. Chromatogr. A*, 2022, **1681**, 463419.
254 V. Romero, S. P. S. Fernandes, L. Rodriguez-Lorenzo, Y. V. Kolen'ko, B. Espiña and L. M. Salonen, *Nanoscale*, 2019, **11**, 6072–6079.
255 L. M. Salonen, S. R. Pinela, S. P. S. Fernandes, J. Louçano, E. Carbó-Argibay, M. P. Sarriá, C. Rodríguez-Abreu, J. Peixoto and B. Espiña, *J. Chromatogr. A*, 2017, **1525**, 17–22.
256 W. Ji, L. Xiao, Y. Ling, C. Ching, M. Matsumoto, R. P. Bisbey, D. E. Helbling and W. R. Dichtel, *J. Am. Chem. Soc.*, 2018, **140**, 12677–12681.
257 Y. Tang, Z. Liang, G. Li, H. Zhao and T. An, *Chemosphere*, 2021, **283**, 131224.
258 I. Ahmed, G. Lee, H. J. Lee and S. H. Jhung, *Chem. Eng. J.*, 2024, **488**, 151022.
259 A. T. P. Hoang, M. C. Do and K.-W. Kim, *Chemosphere*, 2024, **356**, 141973.
260 L. Huang, N. Mao, Q. Yan, D. Zhang and Q. Shuai, *ACS Appl. Nano Mater.*, 2019, **3**, 319–326.
261 I. Ahmed, M. Yoon and S. H. Jhung, *Chem. Eng. J.*, 2024, **484**, 149578.
262 Z. Li, Y. Liu, S. Zou, C. Lu, H. Bai, H. Mu and J. Duan, *Chem. Eng. J.*, 2020, **382**, 123008.
263 S. Akhzari, H. Raissi and A. Ghahari, *npj Clean Water*, 2024, 7.
264 Y. Ben, C. Fu, M. Hu, L. Liu, M. H. Wong and C. Zheng, *Environ. Res.*, 2019, **169**, 483–493.
265 A. Kumar Mehata, M. N. Lakshmi Suseela, P. Gokul, A. Kumar Malik, M. Kasi Viswanadh, C. Singh, J. Selvin and M. S. Muthu, *Microchem. J.*, 2022, **179**, 107573.
266 L. Beesley and M. Hardman, *Cities*, 2024, **149**, 104971.
267 H. Luo, L. Yang, C. Zhang, X. Xiao and X. Lyu, *Ecol. Indic.*, 2024, **160**, 111908.
268 M. Xu, R. He, G. Cui, J. Wei, X. Li, P. Shi, Z. Lu and Y. Xie, *Water, Air, Soil Pollut.*, 2024, 235.
269 T. Skorjanc, D. Shetty and A. Trabolsi, *Chem*, 2021, **7**, 882–918.
270 R. Ajay Rakkesh, T. B. Naveen, D. Durgalakshmi and S. Balakumar, *Chemosphere*, 2024, **346**, 140655.
271 A. Franco, D. Vieira, L. A. Clerbaux, A. Orgiazzi, M. Labouyrie, J. Köninger, V. Silva, R. van Dam, E. Carnesecchi, J. Dorne, J. Vuaille, J. L. Vicente and A. Jones, *Integr. Environ. Assess. Manage.*, 2024, **20**, 1639–1653.
272 Z. Chen, Z. Chen, Y. Li, R. Zhang, Y. Liu, A. Hui, W. Cao, J. Liu, H. Bai and J. Song, *J. Ind. Eng. Chem.*, 2024, **133**, 112–121.
273 S. Wang, L. Song, H. He and W. Zhang, *Coatings*, 2024, **14**, 270.
274 S. Gholami, A. Behnami, M. Hesami Arani and R. Rezaei Kalantary, *Environ. Chem. Lett.*, 2024, **22**, 889–918.
275 X. Wu, H. Yang, H. Lyu, H. Chen, X. Dang and X. Liu, *J. Hazard. Mater.*, 2023, **453**, 131382.
276 J. Tian, Y. Qian, X. He, R. Qi, J. Lei, Q. Wang and C. Feng, *Chemosphere*, 2024, **357**, 142041.
277 Z. Wang, X. Y. Zhang, Q. Yang, S. H. Zhang, G. F. Chang, X. H. Zang, C. Wang and Z. Wang, *J. Chromatogr. A*, 2022, 1681.
278 F. L. Li, C. Chen, H. Jin, T. Z. Ding, J. R. Feng, W. T. Qiu and Q. L. Wang, *J. Hazard. Mater.*, 2024, 478.
279 X. Zhou, Z. K. Wu, B. B. Chen, Z. Zhou, Y. Liang, M. He and B. Hu, *Talanta*, 2024, 276.
280 M. Taharia, D. Dey, K. Das, U. Sukul, J.-S. Chen, P. Banerjee, G. Dey, R. K. Sharma, P.-Y. Lin and C.-Y. Chen, *Ecotoxicol. Environ. Saf.*, 2024, **271**, 115990.
281 A. S. Shilpa, T. D. Thangadurai, G. M. Bhalerao and S. Maji, *Talanta*, 2024, **272**, 125783.
282 G. Wei, W. Han, X. Shu, F. Luo, H. Tang, S. Chen, L. Wang, Y. Xie and X. Lu, *J. Hazard. Mater.*, 2021, **405**, 124273.
283 S. Rout, A. Patra, S. Yadav, S. Wagh, V. Pulhani, I. V. Saradhi and A. V. Kumar, *Sci. Total Environ.*, 2024, **907**, 167899.
284 Y. Liu, X. F. Yang, J. Y. Hu, N. Lu, D. C. He, H. J. Chi, Y. Liu, S. C. Yang and X. D. Wen, *Anal. Chim. Acta*, 2024, 1290.
285 J. Fang, M. Xie, X. He, J. Zhang, J. Hu, Y. Chen, Y. Yang and Q. Jin, *Mater. Today Commun.*, 2022, **33**, 104900.
286 Q. Gou, J. Liu, H. Su, Y. Guo, J. Chen, X. Zhao and X. Pu, *iScience*, 2024, **27**, 109452.
287 J. Cai, X. Chu, K. Xu, H. Li and J. Wei, *Nanoscale Adv.*, 2020, **2**, 3115–3130.
288 Y. Juan, Y. Dai, Y. Yang and J. Zhang, *J. Mater. Sci. Technol.*, 2021, **79**, 178–190.
289 H. Ma, Y. Y. Jiao, W. P. Guo, X. C. Liu, Y. W. Li and X. D. Wen, *Innov.-Organ. Manag.*, 2024, 5.
290 B. Ball and P. Sarkar, *Phys. Chem. Chem. Phys.*, 2021, **23**, 12644–12653.
291 S. Pakhira and J. L. Mendoza-Cortes, *Phys. Chem. Chem. Phys.*, 2019, **21**, 8785–8796.
292 A. Cesaretti, P. Foggi, C. G. Fortuna, F. Elisei, A. Spalletti and B. Carlotti, *J. Phys. Chem. C*, 2020, **124**, 15739–15748.
293 H.-C. Zhou, J. R. Long and O. M. Yaghi, *Chem. Rev.*, 2012, **112**, 673–674.
294 H. Hou and B. Wang, *Int. J. Quantum Chem.*, 2021, 121.
295 S. S. Han, H. Furukawa, O. M. Yaghi and W. A. Goddard, *J. Am. Chem. Soc.*, 2008, **130**, 11580.

296 S. Pakhira, K. P. Lucht and J. L. Mendoza-Cortes, *J. Phys. Chem. C*, 2017, **121**, 21160–21170.
297 C.-W. Wu, F. Li, Y.-J. Zeng, H. Zhao, G. Xie, W.-X. Zhou, Q. Liu and G. Zhang, *Appl. Surf. Sci.*, 2023, **638**, 157947.
298 C. S. Diercks and O. M. Yaghi, *Science*, 2017, 355.
299 S. Haldar, A. Schneemann and S. Kaskel, *J. Am. Chem. Soc.*, 2023, **145**, 13494–13513.
300 S. S. Han, W. Q. Deng and W. A. Goddard, *Angew. Chem.*, 2007, **119**, 6405–6408.
301 C. Altintas and S. Keskin, *Mater. Today Energy*, 2023, **38**, 101426.
302 S. Thomas, H. Li, R. R. Dasari, A. M. Evans, I. Castano, T. G. Allen, O. G. Reid, G. Rumbles, W. R. Dichtel, N. C. Gianneschi, S. R. Marder, V. Coropceanu and J.-L. Brédas, *Mater. Horiz.*, 2019, **6**, 1868–1876.
303 Y. H. Shi, R. Y. Ni and Y. Zhao, *Energy Fuels*, 2023, **37**, 6365–6381.
304 B. Maleki, H. Esmaeili, Y. K. Venkatesh and M. Yusuf, *Process Saf. Environ. Prot.*, 2024, **187**, 903–925.
305 J. L. Woodliffe, R. S. Ferrari, I. Ahmed and A. Laybourn, *Coord. Chem. Rev.*, 2021, **428**, 213578.
306 H. A. Maitlo, G. Maitlo, X. Song, M. Zhou and K. H. Kim, *Sci. Total Environ.*, 2022, **822**, 153428.
307 J. J. Espada, R. Rodríguez, A. de la Peña, M. Ramos, J. L. Segura and E. M. Sánchez-Carnerero, *J. Cleaner Prod.*, 2023, **395**, 136381.
308 J. Yang, H. Tian, Y. Li, H. Li, S. Li, H. Yang, M. Ding, X. Wang and P.-Y. Chen, *Energy Storage Mater.*, 2022, **53**, 352–362.
309 C. Filosa, X. Gong, A. Bavykina, A. D. Chowdhury, J. M. R. Gallo and J. Gascon, *Acc. Chem. Res.*, 2023, **56**, 3492–3503.
310 B. Zhang, Z. Zhu, X. Wang, X. Liu and F. Kapteijn, *Adv. Funct. Mater.*, 2023, **34**, 2304788.